COMPUTATIONALLY EFFICIENT FIR DIGITAL FILTERS

YANG CHUNZHU

NATIONAL UNIVERSITY OF SINGAPORE

2004

COMPUTATIONALLY EFFICIENT FIR DIGITAL FILTERS

YANG CHUNZHU

(*M. Eng.*)

A THESIS SUBMITTED

FOR THE DEGREE OF DOCTOR OF PHILOSOPHY

DEPARTMENT OF ELECTRICAL & COMPUTER ENGINEERING

NATIONAL UNIVERSITY OF SINGAPORE

2004

Acknowledgements

First of all, I would like to express my gratitude to my supervisor, Dr. Lian Yong, who has done much more than merely advise me. I am particularly grateful for his guidance, valuable suggestions and patience in all aspects of my research work from the beginning to the end. His confidence, understanding, and friendship made this challenging task possible.

I would like to thank all the members in the VLSI lab of NUS for many enlightening conversations and help over the years. They have shared their fun and experience with me from time to time. They have been more than colleagues, but good friends as well.

My special thanks go to my friends, Yu Yajun, Qiu Wenjie, Mao Zhi, Zou Yuquan and Deng Jiewen for their encouragements and helping hands.

Most importantly, I would like to take this opportunity to thank my parents, Yang Tanyuan and Hu Lirong, and my sister, Yang Jianmei, for their love and trust.

Finally, I also wish to thank National University of Singapore, for the financial support for this research work.

Contents

Abbreviations

BPCs	Bandpass cascade cosine functions
BS	Bandage shaping
CCOSs	Cascade of cosine functions
CMOS	Complementary metal-oxide silicon
DSP	Digital signal processing
FIR	Finite impulse response
FRM	Frequency-response Masking
IFIR	Interpolated finite impulse response
IIR	Infinite impulse response
RHF	Recursive Hartley filters
RRS	Recursive running sum
SPT	Signed-power-of-two
SFFM	Single filter frequency masking
VLSI	Very large scale integration

Summary

With the advancement of CMOS technology, finite impulse response (FIR) filters are getting increasingly popular in many applications such as speech recognition systems, biomedical instrumentations, and read/write channels due to the linear-phase property and guaranteed stability. However, the very large scale integration (VLSI) implementation cost of an FIR filter is generally higher than that of the infinite impulse response (IIR) filters with the same transition bandwidth requirement, especially when the required transition-band is very narrow. The main purposes of this research work are to develop computationally efficient techniques for the design of FIR filters.

In this thesis, new techniques and methods are proposed to design computationally efficient FIR filters. First, a modified frequency-response masking (FRM) approach is proposed to decouple the masking filters from the bandedge shaping filter in an FRM filter. The proposed structure adds more flexibility in selection of the interpolation factors for the bandedge shaping filter and the masking filters. Second, two methods are presented to reduce the arithmetic complexity of FRM filters. One of the methods utilizes a prefilter-equalizer to replace one masking filter in an FRM based filter. Novel multiplication-free prefilters are developed for the design of prefilter-equalizer

pairs. The other method incorporates the single filter frequency masking technique into the FRM approach. The resulting structures make use of the cascade of the same model filter with different interpolation factors to perform the bandedge shaping and the masking tasks. With simple modifications, the proposed structures can be used to design FIR filters with varying specifications. Third, new masking filter structures are developed to design narrowband and wideband IFIR filters. The new masking filters are multiplication free. Finally, novel non-uniform linear-phase digital filter banks are proposed for digital audio applications. The filter banks have very low hardware cost.

List of Figures

List of Tables

Chapter 1

Introduction

Digital signal processing (DSP) is one of the most powerful technologies that will shape engineering in the twenty-first century. DSP technology has found its applications in a broad range of fields such as communication, medical imaging, radar & sonar, multimedia systems, high fidelity music reproduction, and oil prospecting, to name just a few. In DSP systems, there are basically two types of digital filters, namely, finite impulse response (FIR) digital filters and infinite impulse response (IIR) digital filters. FIR filters have some very desirable features like guaranteed stability, linear-phase and low coefficient sensitivity. However, the computational complexity in terms of multiplication and addition of an FIR filter is generally higher than that of IIR filters when the same magnitude response specification is required. This problem is particularly acute in implementation of FIR filters demanding narrow transition bands. Thus, it is important to find ways to reduce the computational complexity of FIR filters.

1.1 Literature Review

Let a linear-phase lowpass FIR filter $H(z)$ be designed with the following specifications,

$$\begin{aligned} 1-\delta_p \le \left|H\left(e^{j\omega}\right)\right| \le 1+\delta_p, \quad \text{for } \omega \in \left[0, \omega_p\right] \\ -\delta_s \le \left|H\left(e^{j\omega}\right)\right| \le \delta_s, \quad \text{for } \omega \in \left[\omega_s, \pi\right] \end{aligned} \tag{1.1}$$

where $H(e^{j\omega})$ is the frequency response of $H(z)$, ω_p and ω_s refer to the passband and stopband cutoff frequencies, respectively, δ_p and δ_s denote the maximum passband ripple and the minimum stopband attenuation, respectively. The length, *N*, of a minimax optimum linear-phase lowpass filter satisfying (1.1) can be estimated by [1]

$$N = \frac{-20\log_{10}\sqrt{\delta_p \delta_s} - 13}{14.6(\omega_s - \omega_p)/2\pi} + 1. \tag{1.2}$$

It is clear from (1.2) that *N* is inversely proportional to the filter transition-width $(\omega_s - \omega_p)$. For this reason, if the transition-width is narrow, the length of the filter will be quite long. Since the number of multipliers in the direct form implementation of a linear-phase FIR filter is approximately half of the length of the impulse response sequence, and the number of adders is approximately the same as the impulse response length, the hardware implementation of a long FIR filter is costly.

To reduce the arithmetic operations of FIR filters with narrow transition-width, many efficient approaches were proposed in the past two decades. In general, there are three techniques for the design of computationally efficient FIR filters:

- The "prefilter plus equalizer" approach [2–9],
- Interpolated finite impulse response (IFIR) technique [10–20],

- The frequency-response masking technique [21–74].

1.1.1 "Prefilter Plus Equalizer" Approach

In [2, 3], a method called "prefilter plus equalizer" was proposed for the design of low computational complexity FIR filters. Fig. 1.1 shows a realization structure of the "prefilter-equalizer" approach where two FIR sections are cascaded to synthesize an FIR filter. In Fig. 1.1, $P(z)$ is a prefilter which provides some stopband attenuation with minimum number of multipliers and adders, and $E(z)$ is an equalizer designed to compensate the passband errors and provide the rest of stopband attenuation. The prefilter relieves the stopband attenuation requirement for the equalizer, which leads to the arithmetic operation reduction of the equalizer. As a result, the overall computational complexity of the desired filter is reduced compared with an equivalent conventional FIR filter.

Figure 1.1 A structure for "prefilter plus equalizer" method.

Some efficient prefilter structures were proposed for the design of prefilters [3–9]. Adams and Willson [3] proposed the single and dual recursive running sum (RRS) structures which have only shift/adders and provide rather good stopband attenuation. The prefilter produces several zeros on the unit circle without any multiplications, while the amplitude equalizer is used to make the overall filter meet the specifications. The RRS structure proposed in [3] can not be applied to bandpass filters. In [4], an

extension to design bandpass filters was introduced with a different design concept from the design of lowpass (highpass) filters.

Vaidyanathan and Beiman [5] introduced another prefilter structure which is based on the Dolph-Chebyshev functions. The equal-ripple stopband behavior of the Dolph-Chebyshev function provides the largest possible stopband attenuation for a given order, leading to the computational reduction of the prefilter. However, this method is still rather complicated because the prefilter consists of substructures involving multipliers. Based on cyclotomic polynomials and a mirror-image quadratic polynomial, and by adopting the interpolation concept, Kikuchi et al. [6] proposed three types of prefiltering for lowpass, highpass and bandpass FIR filter design. These prefiltering techniques alleviate the burden on the equalizer leading to the reduction of the number of multipliers in implementation. Tai and Lin [7] developed two prefitler structures on the basis of the cascade of cosine functions (CCOSs). The CCOSs prefilter is multiplication free and suitable for the design of lowpass and highpass FIR filters. For the design of bandpass filters, the CCOSs prefilter is modified to bandpsss filters (BPCs) which require two multipliers. Both the CCOSs and BPCs can achieve some savings in the number of multipliers and adders in FIR filter design. Liu et al. [8] proposed an efficient prefilter structure called recursive Hartley filter (RHF) which has the ability to design lowpass, bandpass and highpass digital filters simultaneously. Another interesting efficient prefilter structure was introduced by Lian [9] which is a combination of a 4^{th} order multiplication-free FIR filter. This prefilter is suitable for the design of narrowband lowpass filters to some extent.

1.1.2 Interpolated Finite Impulse Response Filters

The "prefilter plus equalizer" technique [2, 3] can achieve moderate savings in the number of multipliers and adders over the conventional FIR filters at the expense of a small increase in the number of delays. To further reduce the arithmetic operations for implementation of FIR filters, Neuvo et al. [10] introduced a technique called interpolated finite impulse response (IFIR) filter. The IFIR technique is very suitable for narrowband and wideband lowpass (highpass) as well as narrowband bandpass FIR filter design. To synthesize an IFIR filter, two cascaded subfilters are required as shown in Fig. 1.2. One subfilter is a bandedge shaping filter $H_M(z^M)$ obtained from a model filter $H_M(z)$ by replacing each delay element of $H_M(z)$ with M delay elements. $H_M(z^M)$ has periodic frequency response. The other one is a masking filter (or interpolator) $G(z)$ used to remove the unwanted passbands of $H_M(z^M)$. Since $H_M(z^M)$ has a sparse coefficient vector with every M^{th} coefficient value being nonzero and $G(z)$ can be designed with only few arithmetic operations, the overall implementation of an IFIR filter requires less multipliers and adders compared with an equivalent conventional FIR filter.

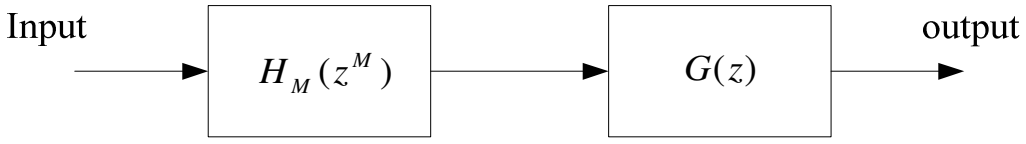

Figure 1.2 An IFIR filter.

In [10], simple interpolator was proposed to design $G(z)$ which may not be effective for some stringent filter specifications. To solve this problem, Saramäki et al. [11, 12]

utilized the Remez multiple exchange algorithm to optimize the interpolation factor M, the bandedge shaping filter $H_M(z^M)$ and the interpolator $G(z)$ simultaneously, which leads to considerable savings in the number of multipliers, adders and delays over the conventional FIR filters. In their method, further reduction of multipliers and adders is possible by using RRS based interpolators [12]. Kikuchi et al. [14] proposed a set of efficient and practical interpolators based on the cyclotomic polynomials which are multiplication free. The interpolators can be applied to lowpass, highpass and bandpass filter design. Similarly, Cabezas and Diniz [15] developed a general method to design efficient prefilters in which some interpolated RRS filters are cascaded with non-recursive filters. Large stopband attenuation is achieved by cascading the prefilters properly. Combining the prefilter-equalizer and IFIR concepts together, the cascade of prefilters is followed by an interpolated equalizer to meet the overall filter specification. This technique is applicable to the design of bandpass filters.

For the design of moderately wideband FIR filters, Jing and Fam [16] proposed a generalized IFIR technique in which the overall filter is decomposed into a set of subfilters with much less stringent specifications. This method can achieve some savings in the number of multipliers at the cost of increasing the length of the overall filter significantly. Gustafsson et al. [17–19] introduced another structure in which several identical filters with different interpolation factors are cascaded to design narrowband and wideband FIR filters. Since only one model filter is utilized in this method, much reduction of multipliers and adders can be achieved at the expense of a large number of delay elements.

By adopting the IFIR concept, Lian and Lim [20] introduced an efficient structure to synthesize FIR filters with narrow and moderately wide transition-width. The proposed structure utilizes two prototype filters which are interpolated by even number factors and have even and odd number orders. They are arranged in parallel to perform the bandedge shaping which can relieve the task of the interpolator. Much reduction in the number of multipliers can be achieved, especially, when the desired transition-width is very narrow.

1.1.3 Frequency-Response Masking Approach

The IFIR method is applicable to FIR filters with narrow or wide passband. It is difficult to design FIR filters with arbitrary bandwidths using the IFIR approach. Lim [21] proposed an efficient method to design sharp lowpass and highpass FIR filters with arbitrary bandwidths. This method is called frequency-response masking (FRM) approach. The basic idea behind the FRM technique is to compose a sharp FIR filter using several short subfilters as shown in Fig. 1.3. Two sectors are required to synthesize a single-stage FRM filter. The first sector uses the delay-complementary concept to form the sharp transition-band and arbitrary bandwidth by a pair of complementary interpolated bandedge shaping filters, $H_a(z^M)$ and $z^{-\frac{M(N-1)}{2}} - H_a(z^M)$, where N is length of $H(z)$ and M is an interpolation factor. The second sector removes undesired periodic frequency components from the bandedge shaping filters by using two masking filters $G_1(z)$ and $G_2(z)$ to form the overall filter. The FRM technique can significantly decrease the required number of multipliers and adders for implementation of FIR filters. If the coefficient values of FRM filters are constrained

to be the sums of signed-power-of-two (SPT) terms [75–77], the computational complexity of FRM filters can be further reduced.

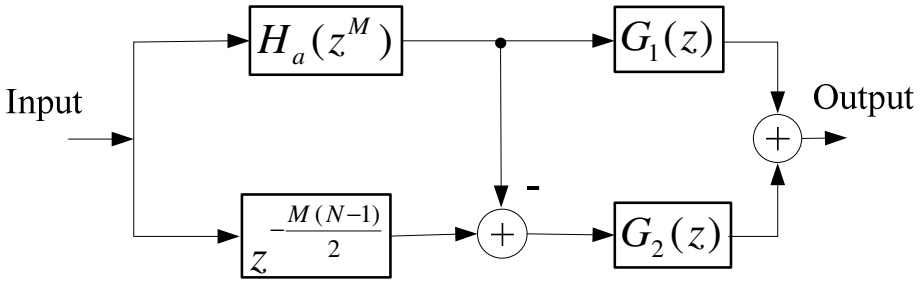

Figure 1.3 A realization structure of the FRM approach.

Many developments and improvements [22–37] have been made to the FRM technique since the inception of this method. A major contribution to the FRM technique was introduced by Lim and Lian [23] which generalized the optimum multi-stage FRM structures. It was reported in [23] that

(1) as the number of frequency-response masking stages increases, the impulse response up-sampling ratio approaches *e* (the base of the natural logarithm).

(2) the FRM technique is useful when the normalized transition-width is less than 1/16.

(3) in *K*-stage FRM design, the overall complexity is inversely proportional to the $(K+1)^{th}$ root of the transition-width.

Yang et al. [22] proposed a modified FRM structure to reduce the computational complexities of the two masking filters in the narrowband lowpass case. This technique uses the IFIR concept to interpolate the two masking filters by a factor of *N* which results in an *N* factor reduction in the computational complexity of the two masking filters. Another technique to improve the masking filter design was proposed

by Lim and Lian [24] which focused on reducing the implementation costs of the two masking filters by factoring a common subfilter from the two original masking filters. Besides the improvement [24] to FRM filters, Lian proposed another interesting approach to achieve savings in the number of multipliers by designing one of the masking filters as a half-band FIR filter [25]. To further reduce the computational complexity of FRM filters introduced in [24], Saramäki and Yli-Kaakinen [33] proposed an optimization algorithm to design all the subfilters simultaneously.

In [27, 28], an "IFIR-FRM" structure was proposed to reduce the computational workload of the bandedge shaping filter, where the bandedge shaping filter is replaced by an IFIR filter. Some savings in the number of multipliers can be achieved with a slight increase in the number of delays over the original FRM filters. Using the concept of prefilter-equalizer, Lian [30, 31] introduced a modified FRM structure in which the computational complexity of the bandedge shaping filter or one of the masking filters is reduced by designing one of them as a prefilter-equalizer based filter.

Saramäki and Lim [26] introduced a technique to improve the design algorithm of the original FRM filters [21]. In their method, the Remez algorithm was utilized to design FRM filters resulting in a time-saving procedure better than the linear programming approach. In [29], Saramäki and Johansson proposed an improved design technique for FRM filters, in which subfilters are optimized simultaneously. This method reduces the arithmetic complexity of the original FRM filter. Other optimization approaches for the design of FRM filters can be found in [34–37].

There are many literatures dealing with the employment of the FRM technique. Saramaki et al. [38] modified the original FRM structure to design half-band FIR filters with narrow transition-widths. The approach achieves considerable savings in terms of multiplication. Lian [39] used the multi-stage FRM approach to optimize the design of half-band FIR filters. The design of bandpass and bandstop filters based on the FRM technique can be found in [40–42]. The FRM technique is also suitable for the synthesis of multi-rate filters [43–46], filter banks [47–54], two-dimensional filters [55–58], IIR filters [59–68], filters with short delay [69, 70], long FIR filters [71] and discrete valued coefficient FIR filters [72]. Efficient methods for the implementation of FRM filters can be found in [73, 74].

1.2 Research Objectives

The above three main approaches and their corresponding extensions for the design of FIR filters with narrow transition-width can achieve computational efficiency under certain conditions. However, there is still room for the improvement and development in the design of sharp FIR filters. The main research objective is to find ways to reduce the computational complexity of sharp FIR filters further.

1.3 Outline

The thesis consists of the following parts:

1. Chapter one is a review of some efficient methods for FIR filter design with low computational complexity.
2. In Chapter two, the IFIR-FRM approach is generalized to develop a novel structure to synthesize very sharp FIR filters. The proposed structure decouples

the masking filters from the bandedge shaping filter. With the introduction of an additional decoupling stage, the computational complexity of the overall filter can be greatly reduced. Examples show that more than 40% savings in the number of multipliers and adders can be achieved compared with the original FRM approach.

3. In Chapter three, by using the concept of FRM technique, two classes of new structures for the design of sharp lowpass and highpass FIR filters are presented. The proposed structures utilize a prefilter-equalizer to replace one masking filter in FRM-based filters. Novel prefilters are developed to design the prefilter-equalizer. Design examples show that the new method can yield considerable savings in the number of multipliers and adders while keeping the group delay of the overall filter in check, compared with other computationally efficient methods.
4. In Chapter four, the single filter frequency masking filter structure is extended to design arbitrary bandwidth sharp filters using the FRM technique. The presented structures make use of one identical model filter (except for the periods) repeatedly to perform the bandedge shaping and the masking purposes, which reduces the computational complexity significantly. Based on the proposed structures, new single filter design structures are developed which have much flexibility to design FIR filters with different specifications.
5. In Chapter five, a new type of masking filters for the design of narrowband and wideband lowpass/highpass IFIR filters as well as narrowband bandpass IFIR filters are proposed. The proposed structures are multiplication free. It is shown, by means of examples, that great savings in the number of multipliers and adders are achieved when the new masking filters are adopted in the IFIR

technique. Another advantage of this method is that the total number of delay elements of the designed filter is less than those of other equivalent computationally efficient filters.

6. In Chapter six, the design of linear-phase digital filter banks based on the FRM approach for digital audio systems is proposed. The proposed structures can be used to synthesize non-uniform filter bank with very narrow transition-bands. Equalization for each subband can be easily achieved. The implementation of the new filter banks is simple.
7. In Chapter seven, conclusions are presented for the thesis along with some ideas for future research works.

1.4 Major Contributions of the Thesis

The following is claimed to be the contributions of the thesis.

1. A new FRM structure is developed that decouples the dependency between the bandedge shaping filter and the two masking filters (Chapter 2).
2. Two novel structures based on the FRM approach to design computationally efficient sharp FIR filters are introduced. (Chapter 3).
3. An extension of the single filter frequency masking filter for the design of arbitrary bandwidth sharp FIR filters using the FRM technique is presented (Chapter 4).
4. Three new masking filter structures are proposed for the design of narrowband and wideband sharp lowpass and highpass FIR filters as well as narrowband bandpass filters (Chapter 5).

5. New linear-phase digital filter banks for digital audio applications are proposed (Chapter 6).

1.5 List of Publications

Part of the research works reported in this thesis is published or to be submitted for publication as follows.

[1] Y. Lian and C. Z. Yang, "Complexity reduction by decoupling the masking filters from bandedge shaping filter in the frequency-response masking technique," *Journal of Circuits, Systems, Signal processing*, vol. 22, No. 2, pp. 115–135, 2003.

[2] C. Z. Yang and Yong Lian, "A new digital filter bank for digital audio applications," in *Proc.* 7th *Int. Symp. Signal Processing Its Applications*, vol. 2, pp. 267–270, Paris, France, July 1-4, 2003.

[3] C. Z. Yang and Y. Lian, "Reduce the complexity of frequency-response masking filter using multiplication free filter," in *Proc. IEEE Int. Symp. Circuits Syst*., ISCAS 2003, vol. 4, pp. 181–184, Bangkok, Thailand, May 25-28, 2003.

[4] C. Z. Yang and Y. Lian, "Efficient prefilter structure for narrow-band bandpass FIR filter design," in *Proc. IEEE* TENCON'02, Vol. 2, pp. 893–896, Beijing, China, Oct. 29- Nov. 01, 2002.

[5] C. Z. Yang and Y. Lian, "A modified structure for the design of sharp FIR filters using frequency-response masking technique," in *Proc. IEEE Int. Symp. Circuits Syst*., ISCAS 2002, vol. 3, pp. 237–240, Phoenix, USA, May, 2002.

[6] Y. Lian and C. Z. Yang, "A new structure for design narrow band lowpass FIR filters," in *Proc. IEEE* TENCON'01, Vol. 1, pp. 274–277, Singapore, Aug. 2001.

[7] Y. Lian and C. Z. Yang, "The design of computationally efficient narrowband sharp FIR filters," to be submitted to *IEEE Trans. on Signal Processing*.

Chapter 2

Decoupling the Masking Filters from the Bandedge Shaping Filter in the FRM Technique

2.1 Introduction

The FRM technique [21] is very efficient for the design of arbitrary bandwidth FIR filters with narrow transition-width. It is a well-known fact that the lengths of subfilters in the FRM approach depend largely on the interpolation factor M. This is because the sum of the transition-widths of both masking filters $G_1(z)$ and $G_2(z)$ is inversely proportional to M. When M is very large, $G_1(z)$ and $G_2(z)$ themselves become sharp filters. The IFIR-FRM approach [27, 28] was proposed to reduce the complexities of the bandedge shaping filter and one of the masking filters by replacing the bandedge shaping filter with an interpolated finite impulse response (IFIR) filter [10]. The drawback is that the filter length of the other masking filter becomes excessively long due to the fact that the transition-band of this masking filter has the same width as the highly compressed passband of the IFIR filter. To address this problem, two improvements are made to the IFIR-FRM technique in this chapter. First,

the IFIR-based bandedge shaping filter is generalized to an IFIR alike filter. Second, an additional filtering stage is inserted between the bandedge shaping filter and the masking filters to decouple the masking filters from the bandedge shaping filter. Hence, the complexity of the overall filter is reduced significantly.

This chapter is organized as follows. The FRM and the IFIR-FRM approach are introduced in Section 2.2. A new structure to decouple the masking filters from the bandedge shaping filter is presented in Section 2.3. Following that design equations are given in Section 2.4. The optimization of interpolation factors and the design procedure are discussed in Section 2.5 and 2.6, respectively. Section 2.7 is dedicated to examples. A summary is given in Section 2.8.

2.2 Backgrounds of the FRM and the IFIR-FRM Techniques

2.2.1 The Frequency-Response Masking Approach

To illustrate the FRM technique, let us consider the design of a lowpass FIR filter. Three subfilters are required in a single-stage FRM approach, i.e., a model filter $H_a(z)$, two masking filters $G_1(z)$ and $G_2(z)$. The frequency responses of the three subfilters are shown in Fig. 2.1. $H_a(z)$ is an odd length symmetric lowpass filter with passband and stopband edges at θ_a and ϕ_a, respectively, as shown in Fig. 2.1(a). $H_c(z)$ is a complementary filter of $H_a(z)$, i.e., $\left|H_a(e^{j\omega}) + H_c(e^{j\omega})\right| = 1$, where $H_a(e^{j\omega})$ and $H_c(e^{j\omega})$ are the frequency responses of $H_a(z)$ and $H_c(z)$, respectively. If $H_a(z)$ is

interpolated by a factor of *M*, i.e., replacing each delay element of $H_a(z)$ by *M* delay elements, the frequency response of $H_a(z^M)$ becomes a compressed version of $H_a(z)$ with a period of $\frac{2\pi}{M}$ as shown in Fig. 2.1(b). The complementary filter of $H_a(z^M)$ becomes $H_c(z^M)$. Each band of $H_a(z^M)$ is a replica of $H_a(z)$ scaled by a factor of $\frac{1}{M}$ at the frequency axis. Though the transition-width of each band of $H_a(z^M)$ is $\frac{1}{M}$ of the transition-width of $H_a(z)$, the complexity of $H_a(z^M)$ in terms of multiplication and addition is the same as that of $H_a(z)$. Let the passband and stopband edges of the desired filter $H(z)$ be ω_p and ω_s, respectively. The FRM technique requires that one of the transition-bands of $H_a(z^M)$ or $H_c(z^M)$ falls on ω_p and ω_s, as shown in Figs. 2.1(d) or 2.1(f), respectively. This can be done by properly selecting the bandedges of $H_a(z)$ and the interpolation factor. To form the arbitrary bandwidth, two masking filters $G_1(z)$ and $G_2(z)$ are cascaded to $H_a(z^M)$ and $H_c(z^M)$, respectively, to remove the undesired bands as shown in Figs. 2.1(c) or 2.1(e), respectively. The outputs of $G_1(z)$ and $G_2(z)$ are added together to form the overall filter.

Fig. 2.2 shows a typical realization structure of the FRM approach. The *z*-transform transfer function of an FRM filter is constructed as follows:

$$H(z) = D\left(N_{G_2}, N_{G_1}\right) H_a\left(z^M\right) G_1(z) + D\left(N_{G_1}, N_{G_2}\right) H_c\left(z^M\right) G_2(z) \tag{2.1}$$

where $H_c(z^M)$ is given by

$$H_c\left(z^M\right) = z^{-\frac{M(N_a-1)}{2}} - H_a\left(z^M\right). \tag{2.2}$$

N_a is the filter length of $H_a(z)$ and it must be odd. N_{G_1} and N_{G_2} are the filter lengths of $G_1(z)$ and $G_2(z)$, respectively. $D(L_1, L_2)$ is defined as

$$D(L_1, L_2) = \begin{cases} z^{-\frac{L_1 - L_2}{2}} & L_1 \geq L_2, L_1 \text{ and } L_2 \text{ are either even or odd.} \\ 1 & L_1 < L_2 \end{cases} \tag{2.3}$$

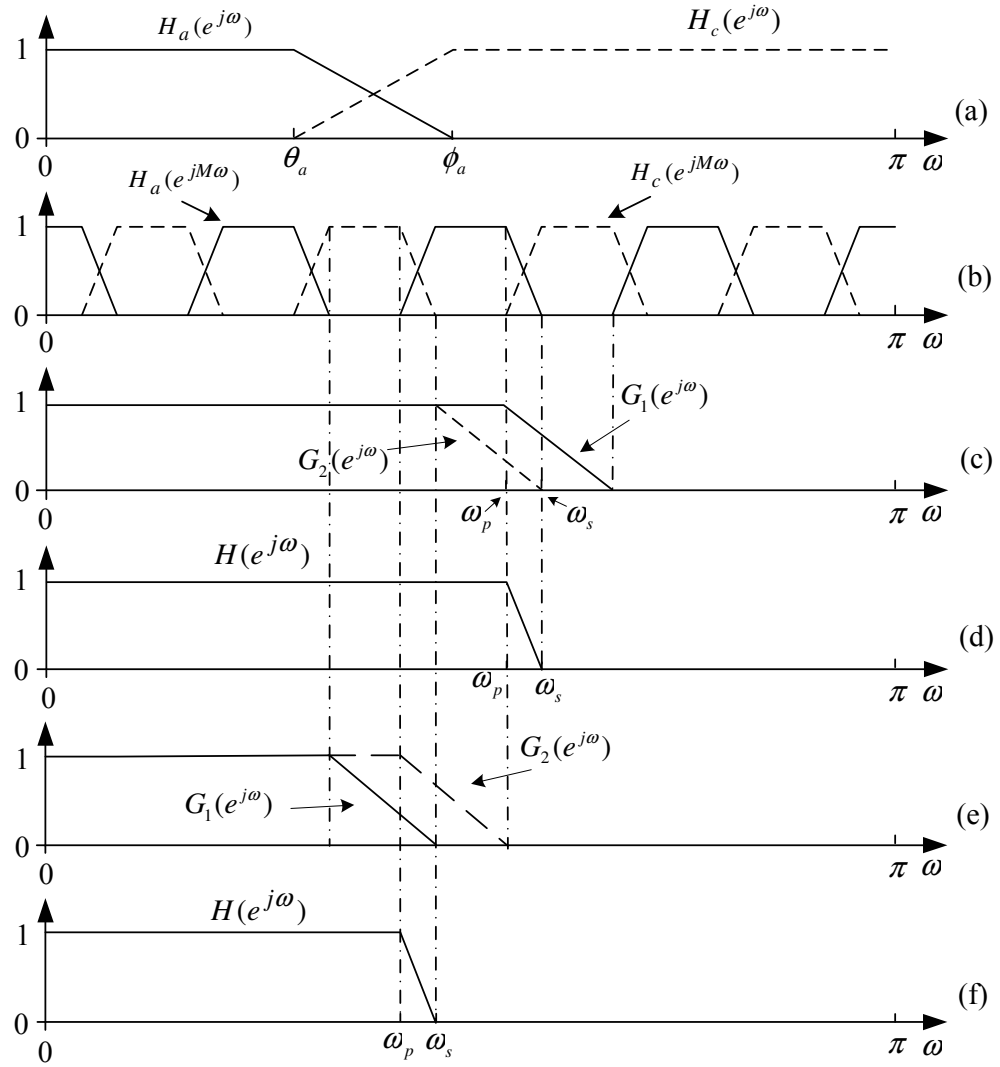

Figure 2.1 Frequency responses for the design of a lowpass FRM filter**.**

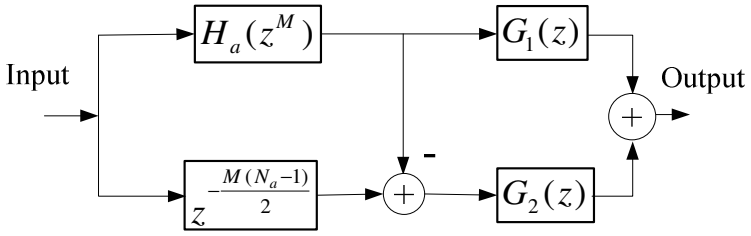

Figure 2.2 A realization structure of the FRM technique.

The equation (2.3) makes sure that the group delays in the two masking branches in Fig. 2.2 are the same.

2.2.2 The IFIR-FRM Approach

In the FRM approach, the transition-bands of the two masking filters are mainly determined by M and the passband and stopband edges of $H_a(z)$. The sum of the transition-widths of the two masking filters equals to $\frac{2\pi}{M}$ [23]. It is this constraint that makes it difficult for the FRM approach to increase M while keeping the complexity of the masking filters in check. One alternative way to solve this problem is to use an IFIR filter to replace the original bandedge shaping filter in order to form a so-called IFIR-FRM approach [27, 28]. The structure of an IFIR-FRM filter is shown in Fig. 2.3, where k and l are two integers and $H_a(z^l)H_g(z)$ forms an IFIR filter. The transfer function of an IFIR-FRM filter is given by

$$H(z) = D\left(N_{G_2}, N_{G_1}\right) H_a\left(z^{kl}\right) H_g\left(z^k\right) G_1(z) + D\left(N_{G_1}, N_{G_2}\right) H_c\left(z^k\right) G_2(z) \quad (2.4)$$

where $H_c(z^k)$ is written as

$$H_c\left(z^k\right) = z^{-\frac{(N_a-1)kl}{2} - \frac{(N_g-1)k}{2}} - H_a\left(z^{kl}\right) H_g\left(z^k\right) \quad (2.5)$$

where N_g is the length of $H_g(z)$. It was shown in [28] that the replacement of $H_a(z)$ by an IFIR filter is possible if a large k is selected that guarantees $H_a(z)$ to be a narrowband filter.

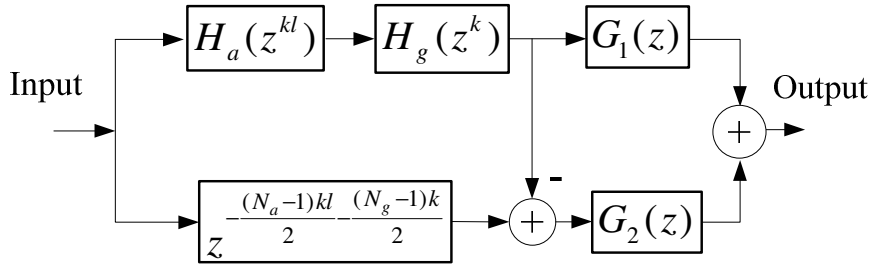

Figure 2.3 The IFIR-FRM approach.

The efficiency of the IFIR-FRM approach is close to a two-stage FRM structure in some cases and its design procedure is simpler than that of a two-stage FRM filter. The benefit of an IFIR-FRM structure comes from the large interpolation factor kl and an interpolated masking filter $H_g(z^k)$ which lower the complexity of the bandedge shaping filter and one of the masking filters. The negative impact is an increase in complexity of the other masking filter whose transition-width is about the same as the passband of the highly compressed bandedge shaping filter. It was shown in example of [28] that one of the masking filters is four times longer than that of the other masking filter. To solve this problem, a new structure is proposed in the next section.

2.3 A New Structure

From the structure point of view, the IFIR-FRM technique is not an optimal solution. This is because the minimum complexity is achieved only when the transition-widths

(or complexities) of the two masking filters are equal according to [23]. By using the IFIR-based bandedge shaping filter, it forces one of the masking filters to be a sharp filter and creates an unbalanced pair of masking filters. The complexity reduction in the IFIR-FRM approach is not a result of a structural optimization. Rather it is due to the computational efficiency of an IFIR filter. Actually, the IFIR-FRM approach can be considered as a special case of the two-stage FRM approach where the second stage becomes a narrowband filter with the help of a large interpolation factor. This results in the omission of the complementary branch in the FRM approach. It is reasonable to believe that the overall complexity can be further reduced when the transition-widths of the two masking filters are brought as close to each other as possible. To this end, a modified FRM structure is proposed which inserts an additional subfilter $M_c(z)$ between the bandedge shaping filter and the masking filters in the original FRM structure. The modified FRM structure is shown in Fig. 2.4, where $H_a(z)$ and $M_a(z)$ form a bandedge shaping filter, $M_c(z)$ is a decoupling filter with its role explained late, and $G_C(z)$ and $G_D(z)$ are the two masking filters. The z-transform transfer function of the overall filter is given by

$$H(z) = C(z)G_C(z) + D(z)G_D(z) \tag{2.6}$$

where

$$C(z) = \left[z^{\frac{-L_a(N_{H_a}-1)-L_M(N_{M_a}-1)}{2}} - H_a(z^{L_a})M_a(z^{L_M}) \right] M_c(z^{L_C}), \tag{2.7}$$

$$D(z) = z^{\frac{-L_a(N_{H_a}-1)-L_M(N_{M_a}-1)-L_C(N_{M_c}-1)}{2}} - C(z) \tag{2.8}$$

where L_a, L_M, and L_C are integers, whereas N_{H_a}, N_{M_a}, and N_{M_c} are the lengths of $H_a(z)$, $M_a(z)$ and $M_c(z)$, respectively.

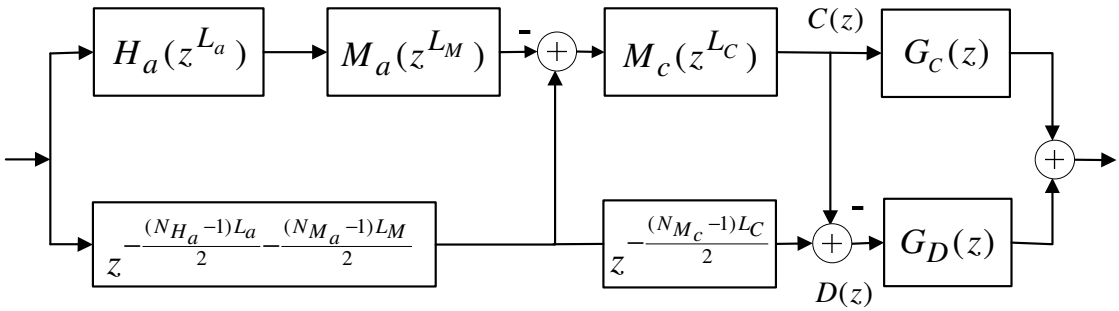

Figure 2.4 A modified FRM structure.

To understand the role of each subfilter in Fig. 2.4, the frequency responses of all subfilters are sketched as shown in Figs. 2.5 and 2.6. In Fig. 2.4, $H_a(z)$ and $M_a(z)$ will form an IFIR filter if L_a is a multiple of L_M, as shown in Figs. 2.5(b) and 2.5(c). In this case, the role of $H_a(z)$ and $M_a(z)$ are exactly the same as the one in the IFIR-FRM approach. It is obvious that restricting L_a to be a multiple of L_M will narrow the selection of L_a and L_M to a small set of values. Hence, the selected interpolation factors may not lead to a design with minimum complexity. This prompts us to loose the restriction on the selection of L_a and L_M, i.e., let $H_a(z)$ and $M_a(z)$ to form a non-IFIR (or aperiodic) filter. The question is whether a non-IFIR filter performs comparably with an IFIR filter. According to ripple analysis described in [21], the role played by the bandedge shaping filter is to form the sharp transition-band of the overall filter and to contribute to the ripple compensation effect in the vicinity of the transition-band. This requirement can be easily satisfied if at least one period of $H_a(z^{L_a})$ is kept undistorted when it is masked by $M_a(z^{L_M})$, as indicated by the shaded areas in Figs. 2.5(c) and 2.6(a). To simplify the notation, let us denote the cascade combination of $H_a(z^{L_a})$ and $M_a(z^{L_M})$ by $A(z)$ and its complement by B(z), as shown

in Figs. 2.5(c), 2.5(d), 2.6(b), and 2.6(c). It is clear that the relaxation on L_a and L_M will create extra ripples in the passband and stopband of $A(z)$ and $B(z)$. These extra ripples will be corrected by the two masking filters if a proper design procedure is adopted as will be presented in Section 2.6.

With the generalization of the IFIR-FRM approach, it gives designers more freedom to choose L_a and L_M, which in turn may achieve additional savings in terms of arithmetic operations. But the savings will not be significant if the problem related to the unbalanced complexity in the two masking filters is not addressed. In fact, the design may worsen if a much larger L_a is adopted as a result of relaxation of L_a and L_M. Moreover, a pair of unbalanced masking filters will increase the implementation cost as a large number of D flip-flops have to be inserted into a short filter to equalize the group delays. It is these two drawbacks that motivate the introduction of a so-called decoupling filter $M_c(z^{L_c})$, as shown in Fig. 2.4. The decoupling filter is expected to play the following two roles. First, it minimizes the impact of the bandedge shaping filter on the masking filters such that the masking filters have less dependency on L_a. Second, it balances the complexity of the two masking filters. To fulfill the first role, the decoupling filter $M_c(z^{L_c})$ is employed to mask $B(z)$ so that the transition-band of $B(z)$ is preserved to form the sharp transition-band of the overall filter. As the passband of $B(z)$ is very narrow, it is necessary to interpolate $M_c(z)$ by a factor of L_C in order to reduce its complexity. Let the output of $M_c(z^{L_c})$ be $C(z)$ and its complement be $D(z)$. It is clear from Figs. 2.5(e-f) and 2.6(d-e) that $D(z)$ becomes a new bandedge shaping filter. Since $D(z)$ is the bandedge shaping filter, the masking

filters $G_C(z)$ and $G_D(z)$ will only depend on $D(z)$, i.e., the masking filters are decoupled from $A(z)$. To balance the complexity of the masking filters as the second role performed by the decoupling filter, the passband and stopband widths of $M_c(z^{L_c})$ should be chosen as close to each other as possible to produce an overall filter with the minimum complexity. Until now, a new FRM approach has been introduced that allows the designer to choose the interpolation factors freely and brings the complexity of two masking filters close to each other. To synthesize a filter using the proposed structure, the bandedges of each subfilter are required. This will be presented in the following section.

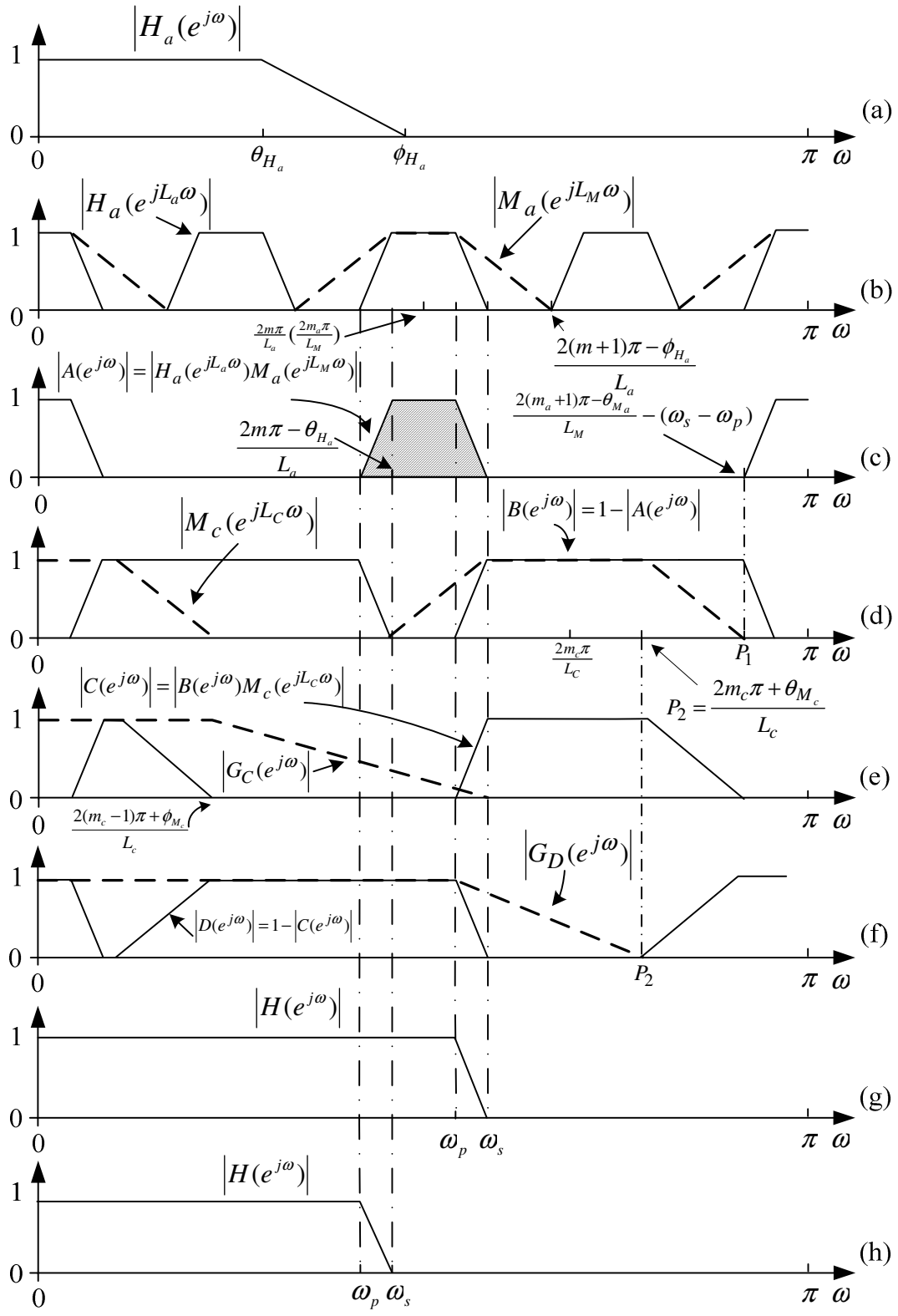

Figure 2.5 Frequency responses of the subfilters.

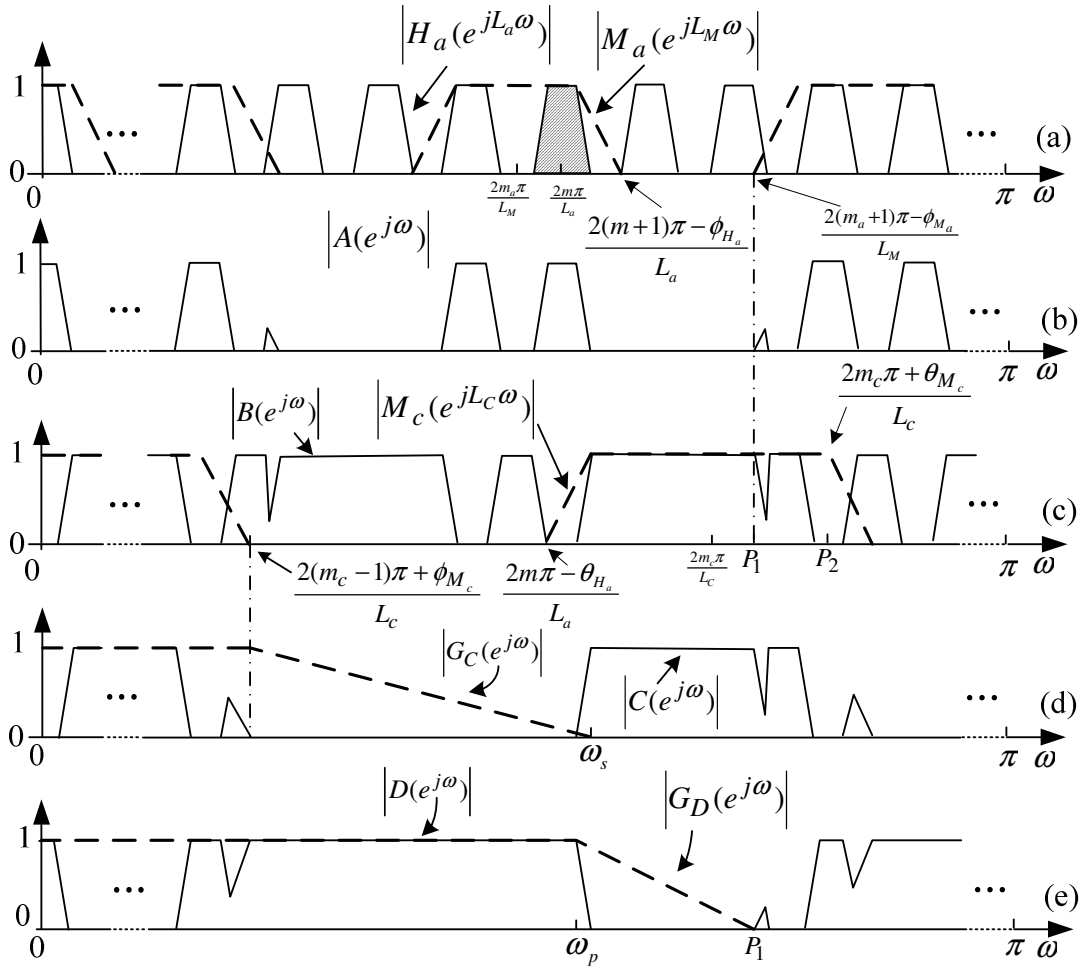

Figure 2.6 Frequency responses of the subfilters for a non-IFIR case.

2.4 Design Equations for Subfilters

In this section, design equations are derived for lowpass filters. The procedure can also be easily applied to the design of highpass filters as well. Let us consider a lowpass filter with passband and stopband edges at ω_p and ω_s, respectively. In the FRM approach, the transition-band of the overall filter can be determined by either $H_a(z^{L_a})$ or its complement. Let us denote the case of Fig. 2.5(g) by Case A, where the transition-band of the overall filter is determined by $H_a(z^{L_a})$, and the case of Fig. 2.5(h) by Case B, where the transition-band of the overall filter is determined by the

complement of $H_a(z^{L_a})$. Let us denote θ and ϕ as the passband and stopband edges for each subfilter, respectively, i.e., θ_{H_a} and ϕ_{H_a} will represent the passband and stopband edges of $H_a(z)$, respectively. Similar notations are applied to the subfilters $M_a(z)$, $M_c(z)$, $G_C(z)$, and $G_D(z)$.

For Case A, it can be shown [21] that

$$\omega_p = \frac{2m\pi + \theta_{H_a}}{L_a} \tag{2.9}$$

$$\omega_s = \frac{2m\pi + \phi_{H_a}}{L_a} \tag{2.10}$$

where L_a is the interpolation factor for $H_a(z)$ and m is an integer less than L_a, as shown in Figs. 2.5(b) and 2.6(a). To ensure that (2.9) and (2.10) yield a practical solution with $0 < \theta_{H_a} < \phi_{H_a} < \pi$, we have

$$m = \left\lfloor \frac{\omega_p L_a}{2\pi} \right\rfloor \tag{2.11}$$

$$\theta_{H_a} = \omega_p L_a - 2m\pi \tag{2.12}$$

$$\phi_{H_a} = \omega_s L_a - 2m\pi \tag{2.13}$$

where $\lfloor x \rfloor$ denotes the largest integer less than or equal to x.

For Case B, a similar set of equations can be found [21], that is,

$$m = \left\lceil \frac{\omega_s L_a}{2\pi} \right\rceil \tag{2.14}$$

$$\theta_{H_a} = 2m\pi - \omega_s L_a \tag{2.15}$$

$$\phi_{H_a} = 2m\pi - \omega_p L_a \tag{2.16}$$

where $\lceil x \rceil$ denotes the smallest integer larger than or equal to x. The same method can be applied to obtain the passband and stopband edges of $M_a(z)$ and $M_c(z)$ as shown in Fig 2.5.

For Case A, we have

$$m_a = \left\lfloor \frac{\omega_p L_M}{2\pi} \right\rfloor \tag{2.17}$$

$$\theta_{M_a} = \omega_p L_M - 2m_a\pi \tag{2.18}$$

$$\phi_{M_a} = \frac{\left[2(m+1)\pi - \phi_{H_a}\right] L_M}{L_a} - 2m_a\pi \tag{2.19}$$

$$m_c = \left\lceil \frac{\omega_s L_C}{2\pi} \right\rceil \tag{2.20}$$

$$\theta_{M_c} = 2m_c\pi - \omega_s L_C \tag{2.21}$$

$$\phi_{M_c} = 2m_c\pi - \frac{\left(2m\pi - \theta_{H_a}\right) L_C}{L_a} \tag{2.22}$$

where m_a and m_c are integers less than L_M and L_C, respectively, as shown on Figs. 2.5(b), 2.5(d), 2.6(a), and 2.6(c).

Using the same method for Case A, for Case B, we have

$$m_a = \left\lceil \frac{\omega_s L_M}{2\pi} \right\rceil \tag{2.23}$$

$$\theta_{M_a} = 2m_a\pi - \omega_s L_M \tag{2.24}$$

$$\phi_{M_a} = 2m_a\pi - \frac{\left[2(m-1)\pi + \phi_{H_a}\right] L_M}{L_a} \tag{2.25}$$

$$m_c = \left\lfloor \frac{\omega_p L_C}{2\pi} \right\rfloor \tag{2.26}$$

$$\theta_{M_c} = \omega_p L_C - 2m_c\pi \tag{2.27}$$

$$\phi_{M_c} = \frac{\left(2m\pi + \theta_{H_a}\right) L_M}{L_a} - 2m_c\pi \tag{2.28}$$

To find the passband and stopband edges of $G_C(z)$ and $G_D(z)$, two additional frequency points P_1 and P_2 are found on $\left|B(e^{j\omega})\right|$ and $\left|M_c(e^{j\omega L_C})\right|$, respectively, as shown in Figs. 2.5(d) and 2.6(c), respectively. For Case A, P_1 and P_2 are located at

$$P_1 = \begin{cases} \dfrac{2\left(m_a+1\right)\pi - \theta_{M_a}}{L_M} - \left(\omega_s - \omega_p\right) & \text{if } L_a \text{ is a multiple of } L_M \\ \dfrac{2\left(m_a+1\right)\pi - \phi_{M_a}}{L_M} & \text{if } L_a \text{ is not a multiple of } L_M \end{cases} \tag{2.29}$$

$$P_2 = \frac{2m_c\pi + \theta_{M_c}}{L_C} \tag{2.30}$$

With the help of P_1 and P_2, the passband and stopband edges of $G_C(z)$ and $G_D(z)$ are given by

$$\theta_{G_C} = \frac{2\left(m_c - 1\right)\pi + \phi_{M_c}}{L_C} \tag{2.31}$$

$$\phi_{G_C} = \omega_s \tag{2.32}$$

$$\theta_{G_D} = \omega_p \tag{2.33}$$

$$\phi_{G_D} = \begin{cases} P_2 & \text{if } P_2 \le P_1 \\ P_1 & \text{if } P_2 > P_1 \end{cases} \tag{2.34}$$

Similarly, for Case B, P_1 and P_2 are located at

$$P_1 = \begin{cases} \dfrac{2(m_a - 1)\pi + \theta_{M_a}}{L_M} + (\omega_s - \omega_p) & \text{if } L_a \text{ is a multiple of } L_M \\ \dfrac{2(m_a - 1)\pi + \phi_{M_a}}{L_M} & \text{if } L_a \text{ is not a multiple of } L_M \end{cases} \tag{2.35}$$

$$P_2 = \frac{2m_c\pi - \theta_{M_c}}{L_C} \tag{2.36}$$

With the help of P_1 and P_2, the passband and stopband edges of $G_C(z)$ and $G_D(z)$ are given by

$$\theta_{G_C} = \omega_p \tag{2.37}$$

$$\phi_{G_C} = \frac{2(m_c + 1)\pi - \phi_{M_c}}{L_C} \tag{2.38}$$

$$\theta_{G_D} = \begin{cases} P_1 & \text{if } P_2 \le P_1 \\ P_2 & \text{if } P_2 > P_1 \end{cases} \tag{2.39}$$

$$\phi_{G_D} = \omega_s \tag{2.40}$$

The above design equations provide detailed information on each subfilter. The designer has to decide the optimal interpolation factors L_a, L_M and L_C for given specifications before the filter can be synthesized. The discussion on how to find L_a, L_M and L_C that achieve the minimum overall complexity will be provided in next section, and the specifications of the ripples for each subfilter will be determined in Section 2.6.

2.5 Optimization of L_a, L_M and L_C

Before synthesizing each subfilter, L_a, L_M and L_C must be determined. Unfortunately, there are no known closed-form analytic expressions to find the values of L_a, L_M and

L_C that will guarantee the global optimum. However, a search for the best values for L_a, L_M and L_C can be done with the help of a simple program. It is well-known that the filter length is mainly determined by the transition-width of the filter when the passband and stopband ripples are fixed, and is inversely proportional to the transition-width. A cost function $C(\Delta)$ is defined to measure the overall complexity of the filter as follows:

$$C(\Delta) = \frac{1}{\Delta_{H_a}} + \frac{1}{\Delta_{M_a}} + \frac{1}{\Delta_{M_c}} + \frac{1}{\Delta_{G_C}} + \frac{1}{\Delta_{G_D}} \tag{2.41}$$

where $\Delta_{H_a} = \phi_{H_a} - \theta_{H_a}$ is the transition-width of $H_a(z)$. Similar definitions are applied to the transition-widths of other subfilters. The transition-widths subfilters can be easily calculated using the corresponding design equations in Section 2.4. A simple searching program can be written to find the values of L_a, L_M and L_C that minimize the cost function $C(\Delta)$. Fig. 2.7 shows the flowchart of such a search program, where $\Delta\omega$ denotes the transition-width of the filter under design. $C(best)$ is the minimum value calculated using (2.41) among all the values of L_a. From our experience, the maximum value of L_a will not go beyond 50 if the required normalized transition-width is greater than 0.001.

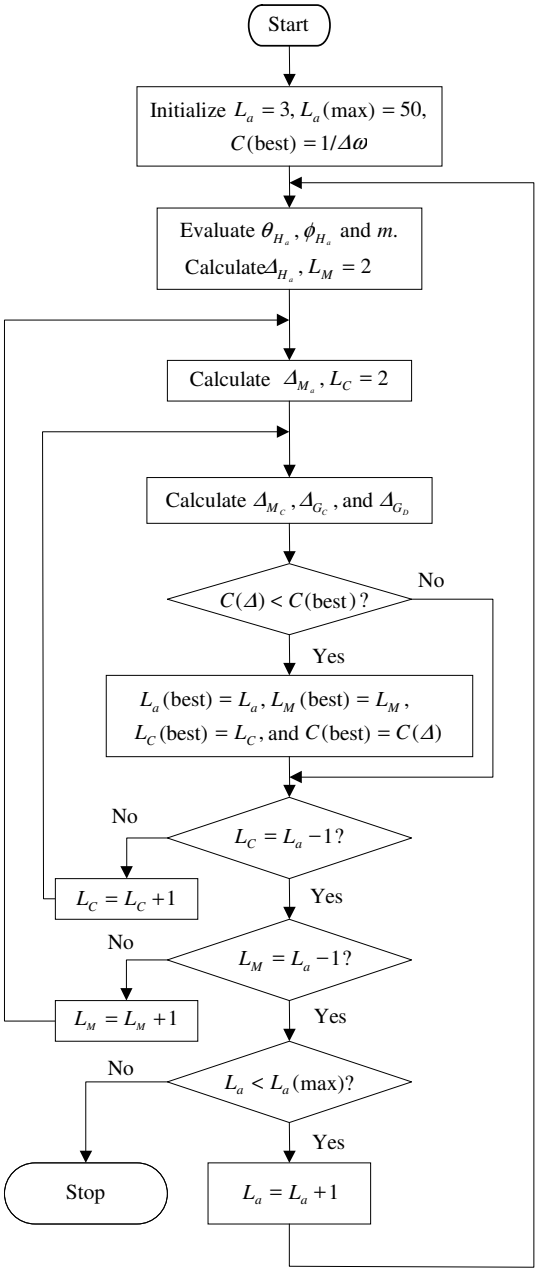

Figure 2.7 Flowchart for the searching program.

2.6 Design Procedure

To synthesize a filter using the proposed structure, five subfilters must be designed so that the overall filter $H(z)$ meets the design specifications. To achieve the global optimization, the five subfilters have to be designed simultaneously. Unfortunately,

this is a non-linear problem, and is difficult to solve. An iterated design approach is adopted that uses a sub-optimization technique to optimize one subfilter at a time such that the remaining subfilters are used as prefilters. To develop a useful design procedure, it is desirable to know how each subfilter affects the passband and stopband ripples of $H(z)$. To analyze the ripple effects of each subfilter, let $H(\omega)$ denote the zero-phase frequency response of the overall filter $H(z)$. Similar definitions are applied to other subfilters. According to Fig. 2.4 the zero-phase frequency response of $H(z)$ is given by

$$H(\omega) = G_D(\omega) + M_c(L_C\omega)\left[G_C(\omega) - G_D(\omega)\right]\left[1 - H_a(L_a\omega)M_a(L_M\omega)\right]. \quad (2.42)$$

Let $F(\omega)$ and $\delta(\omega)$ denote the gain and deviation of $H(z)$. Let $F_{H_a'}(\omega)$ and $\delta_{H_a'}(\omega)$ represent the gain and deviation of $H_a(L_a\omega)$. Similar representations are used for $M_a(L_M\omega)$, $M_c(L_C\omega)$, $G_C(\omega)$, and $G_D(\omega)$. Substituting the gain and deviation of each subfilter into (2.42), we have

$$\begin{aligned} F(\omega) + \delta(\omega) = {} & F_{G_D}(\omega) + \delta_{G_D}(\omega) + \left[F_{M_c'}(\omega) + \delta_{M_c'}(\omega)\right]\left[F_{G_C}(\omega) + \delta_{G_C}(\omega) - \right. \\ & \left. F_{G_D}(\omega) - \delta_{G_D}(\omega)\right]\left\{1 - \left[F_{H_a'}(\omega) + \delta_{H_a'}(\omega)\right]\left[F_{M_a'}(\omega) + \delta_{M_a'}(\omega)\right]\right\}. \end{aligned} \quad (2.43)$$

The case in Fig. 2.5 is used to examine the ripple effects of the subfilters on the frequency response of $H(z)$ in the following 4 frequency ranges. Similar results can be expected for other cases.

Frequency range 1: $0 \le \omega < \dfrac{2(m_c - 1)\pi + \phi_{M_c}}{L_C}$ for Case A and $0 \le \omega < \dfrac{2m_c\pi - \theta_{M_c}}{L_C}$ for Case B.

In this frequency range, $F(\omega) = F_{G_C}(\omega) = F_{G_D}(\omega) = 1$, thereby, (2.43) is simplified to the following form:

$$\begin{aligned}\delta(\omega) = \delta_{G_D}(\omega) + \left[F_{M'_c}(\omega) + \delta_{M'_c}(\omega)\right]\left[\delta_{G_C}(\omega) - \delta_{G_D}(\omega)\right]\times \\ \left\{1 - \left[F_{H'_a}(\omega) + \delta_{H'_a}(\omega)\right]\left[F_{M'_a}(\omega) + \delta_{M'_a}(\omega)\right]\right\}\end{aligned} \tag{2.44}$$

Ignoring the second order terms, the following relations are obtained:

When $F_{M'_c}(\omega) = 1$,

$$\delta(\omega) \approx \delta_{G_D}(\omega), \qquad \text{for } F_{H'_a}(\omega) = F_{M'_a}(\omega) = 1. \tag{2.45}$$

$$\delta(\omega) \approx \delta_{G_C}(\omega), \qquad \text{for } F_{H'_a}(\omega) \times F_{M'_a}(\omega) = 0. \tag{2.46}$$

When $F_{M'_c}(\omega) = 0$,

$$\delta(\omega) \approx \delta_{G_D}(\omega). \tag{2.47}$$

When $0 < F_{M'_c}(\omega) < 1$,

$$\delta(\omega) \approx \delta_{G_C}(\omega). \tag{2.48}$$

Frequency range 2: $\dfrac{2(m_c - 1)\pi + \phi_{M_c}}{L_C} \le \omega < \omega_p$ for Case A and $\dfrac{2m_c\pi - \theta_{M_c}}{L_C} \le \omega < \omega_p$ for Case B.

Under Case A, $F(\omega) = F_{G_D}(\omega) = 1$ and $F_{G_C}(\omega)$ decreases from unity to zero as ω increases. In this case, (2.43) is simplified to

$$\begin{aligned}\delta(\omega) = \delta_{G_D}(\omega) + \left[F_{M'_c}(\omega) + \delta_{M'_c}(\omega)\right]\left[\delta_{G_C}(\omega) - \delta_{G_D}(\omega) + F_{G_C}(\omega) - 1\right]\times \\ \left\{1 - \left[F_{H'_a}(\omega) + \delta_{H'_a}(\omega)\right]\left[F_{M'_a}(\omega) + \delta_{M'_a}(\omega)\right]\right\}.\end{aligned} \tag{2.49}$$

Ignoring the second order terms, the following relations are obtained:

When $F_{M'_c}(\omega)=0$,

$$\delta(\omega)\approx\delta_{G_D}(\omega),\qquad \text{for } F_{H'_a}(\omega)=F_{M'_a}(\omega)=1. \tag{2.50}$$

$$\left|\delta(\omega)\right|\le\left|\delta_{G_D}(\omega)\right|+\left|\delta_{M'_c}(\omega)\right|,\qquad \text{for } F_{H'_a}(\omega)\times F_{M'_a}(\omega)=0. \tag{2.51}$$

When $0<F_{M'_c}(\omega)\le 1$ and $F_{H'_a}(\omega)=F_{M'_a}(\omega)=1$,

$$\left|\delta(\omega)\right|\le\left|\delta_{G_D}(\omega)\right|+\left|\delta_{M'_a}(\omega)\right|+\left|\delta_{H'_a}(\omega)\right| \tag{2.52}$$

Under case B, we have $F(\omega)=F_{G_C}(\omega)=F_{M'_c}(\omega)=1$, and $F_{G_D}(\omega)$ decreases from unity to zero as ω increases. In this case, (2.43) is simplified to

$$\begin{aligned}1+\delta(\omega)=F_{G_D}(\omega)+\delta_{G_D}(\omega)+\Big[1-F_{G_D}(\omega)+\delta_{G_C}(\omega)-\delta_{G_D}(\omega)+\delta_{M'_c}(\omega)\times\\ (1-F_{G_D}(\omega)\Big]\Big\{1-\Big[F_{H'_a}(\omega)+\delta_{H'_a}(\omega)\Big]\Big[F_{M'_a}(\omega)+\delta_{M'_a}(\omega)\Big]\Big\}.\end{aligned} \tag{2.53}$$

Ignoring the second order terms, the following relations are obtained:

When $F_{M'_a}(\omega)=0$,

$$\left|\delta(\omega)\right|\le\left|\delta_{G_C}(\omega)\right|+\left|\delta_{M'_a}(\omega)\right|+\left|\delta_{M'_c}(\omega)\right|. \tag{2.54}$$

When $F_{H'_a}(\omega)=1$,

$$\left|\delta(\omega)\right|\le\left|\delta_{G_C}(\omega)\right|+\left|\delta_{H'_a}(\omega)\right|+\left|\delta_{M'_c}(\omega)\right|+\left|\delta_{M'_a}(\omega)\right|. \tag{2.55}$$

Frequency range 3: $\omega_s\le\omega<\dfrac{2m_c\pi+\theta_{M_c}}{L_C}$ for Case A and $\omega_s\le\omega<\dfrac{2(m_c+1)\pi-\phi_{M_c}}{L_C}$ for Case B.

In this frequency range, $F(\omega)=F_{G_C}(\omega)=0$, $0<F_{G_D}(\omega)<1$, $F_{M'_c}(\omega)=1$, and $F_{H'_a}(\omega)\times F_{M'_a}(\omega)=0$ for Case A. In this case, (2.43) is simplified to

$$\begin{aligned}\delta(\omega) = F_{G_D}(\omega) + \delta_{G_D}(\omega) + \left[\delta_{G_C}(\omega) - F_{G_D}(\omega) - \delta_{G_D}(\omega) - F_{G_D}(\omega)\delta_{M'_c}(\omega)\right] \times \\ \left\{1 - \left[F_{H'_a}(\omega) + \delta_{H'_a}(\omega)\right]\left[F_{M'_a}(\omega) + \delta_{M'_a}(\omega)\right]\right\}.\end{aligned} \tag{2.56}$$

Ignoring the second order terms, we have

$$\left|\delta(\omega)\right| \le \left|\delta_{G_C}(\omega)\right| + \left|\delta_{M'_a}(\omega)\right| + \left|\delta_{M'_c}(\omega)\right| + \left|\delta_{H'_a}(\omega)\right|. \tag{2.57}$$

Under case B, we have $F(\omega) = F_{G_D}(\omega) = 0$ and $0 < F_{G_C}(\omega) < 1$. In this case, (2.43) is simplified to

$$\begin{aligned}\delta(\omega) = \delta_{G_D}(\omega) + \left[F_{M'_c}(\omega) + \delta_{M'_c}(\omega)\right]\left[F_{G_C}(\omega) + \delta_{G_C}(\omega) - \delta_{G_D}(\omega)\right] \times \\ \left\{1 - \left[F_{H'_a}(\omega) + \delta_{H'_a}(\omega)\right]\left[F_{M'_a}(\omega) + \delta_{M'_a}(\omega)\right]\right\}.\end{aligned} \tag{2.58}$$

Ignoring the second order terms, the following relations are obtained:

When $F_{M'_c}(\omega) = 0$ and $F_{H'_a}(\omega) \times F_{M'_a}(\omega) = 0$,

$$\left|\delta(\omega)\right| \le \left|\delta_{G_D}(\omega)\right| + \left|\delta_{M'_c}(\omega)\right|. \tag{2.59}$$

When $0 < F_{M'_c}(\omega) < 1$ and $F_{H'_a}(\omega) = F_{M'_a}(\omega) = 1$,

$$\left|\delta(\omega)\right| \le \left|\delta_{G_D}(\omega)\right| + \left|\delta_{M'_c}(\omega)\right| + \left|\delta_{H'_a}(\omega)\right| + \left|\delta_{M'_a}(\omega)\right|. \tag{2.60}$$

Frequency range 4: $\dfrac{2m_c\pi + \theta_{M_c}}{L_C} \le \omega \le \pi$ for Case A and $\dfrac{2(m_c+1)\pi - \phi_{M_c}}{L_C} \le \omega \le \pi$ for Case B.

In this frequency range, $F(\omega) = F_{G_D}(\omega) = F_{G_C}(\omega) = 0$. Hence, (2.43) is simplified to

$$\begin{aligned}\delta(\omega) = \delta_{G_D}(\omega) + \left[F_{M'_c}(\omega) + \delta_{M'_c}(\omega)\right]\left[\delta_{G_C}(\omega) - \delta_{G_D}(\omega)\right] \times \\ \left\{1 - \left[F_{H'_a}(\omega) + \delta_{H'_a}(\omega)\right]\left[F_{M'_a}(\omega) + \delta_{M'_a}(\omega)\right]\right\}.\end{aligned} \tag{2.61}$$

Ignoring the second order terms, the following relations are obtained:

When $F_{M'_c}(\omega)=1$,

$$\delta(\omega)\approx\delta_{G_D}(\omega), \qquad \text{for } F_{H'_a}(\omega)=F_{M'_a}(\omega)=1. \tag{2.62}$$

$$\delta(\omega)\approx\delta_{G_C}(\omega), \qquad \text{for } F_{H'_a}(\omega)\times F_{M'_a}(\omega)=0. \tag{2.63}$$

When $F_{M'_c}(\omega)=0$,

$$\delta(\omega)\approx\delta_{G_D}(\omega). \tag{2.64}$$

The above analysis provides a very useful insight for designing the overall filter. It can be seen from (2.45)–(2.48) and (2.62)–(2.64) that in the frequency ranges 1 and 4 the deviation of the overall filter is determined mainly by the two masking filters, i.e., the two additional filters $M_a(z)$ and $M_c(z)$ do not contribute to these two ranges significantly. This is the same as the original FRM approach. In frequency range 2 for Case A, the subfilters $G_D(z)$, $M_a(z)$, $M_c(z)$, and $H_a(z)$ determine the passband ripple according to (2.50)–(2.52). Similarly, the subfilters $G_C(z)$, $M_a(z)$, $M_c(z)$, and $H_a(z)$ determine the stopband attenuation in frequency range 3 for Case A according to (2.57). Similar conclusions can be drawn for Case B based on (2.54), (2.55), (2.59) and (2.60). Since the ripples of these subfilters compensate for each other in the frequency range 2 and 3, the following iterated design procedure is employed:

Step 1. Find a set of values for L_a, L_M and L_C using the search program discussed in Section 2.5.

Step 2. Design $G_C(z)$ and $G_D(z)$ according to design equations discussed in Section 2.4 for Case A or Case B, respectively. Set the ripple of each subfilter to 85% of $H(z)$ [21].

Step 3. Design $M_a(z)$ and $M_c(z)$ according to (2.17)–(2.22) for Case A and (2.23)–(2.28) for Case B. Set the ripple of each filter to 90% of $H(z)$.

Step 4. Design $H_a(z)$ in the frequency ranges 2 and 3 by taking $M_a(z)$, $M_c(z)$, $G_C(z)$ and $G_D(z)$ as prefilters. The zero-phase frequency response of $H_a(z^{L_a})$ can be written as

$$H\left(L_a\omega\right)=\sum_i h_a\left(n\right)\mathrm{trig}\left(L_a\omega,i\right) \tag{2.65}$$

where trig$(L_a\omega,i)$ is a proper trigonometric function depending on the type of filter under consideration, $h_a(n)$ is the impulse response of $H_a(z)$. Similar definitions are applied to other subfilters. Substituting (2.65) into (2.42) , we have

$$\begin{aligned} H\left(\omega\right)=G_D\left(\omega\right)+M_c\left(L_C\omega\right)\left[G_C\left(\omega\right)-G_D\left(\omega\right)\right]\times \\ \left\{1-M_a\left(L_M\omega\right)\left[\sum_i h_a\left(n\right)\mathrm{trig}\left(L_a\omega,i\right)\right]\right\}. \end{aligned} \tag{2.66}$$

By evaluating (2.66) on a dense grid of frequencies, a set of inequalities are produced as shown in (2.67) and (2.68). In the frequency range 2, $H_a(z)$ has to satisfy

$$\delta_p^-\left(\omega\right)\le\left[G_D\left(\omega\right)-G_C\left(\omega\right)\right]M_c\left(L_C\omega\right)M_a\left(L_M\omega\right)[\sum_i h_a\left(n\right)\mathrm{trig}\left(L_a\omega,i\right)]\le\delta_p^+\left(\omega\right) \tag{2.67}$$

where

$$\delta_p^-\left(\omega\right)=1-\delta_p\left(\omega\right)-G_D\left(\omega\right)\left[1-M_c\left(L_C\omega\right)\right]-G_C\left(\omega\right)M_c\left(L_C\omega\right)$$

and

$$\delta_p^+\left(\omega\right)=1+\delta_p\left(\omega\right)-G_D\left(\omega\right)\left[1-M_c\left(L_C\omega\right)\right]-G_C\left(\omega\right)M_c\left(L_C\omega\right).$$

Here, $\delta_p(\omega)$ is the required passband ripple. In the frequency range 3, we have

$$\delta_s^-\left(\omega\right)\le\left[G_D\left(\omega\right)-G_C\left(\omega\right)\right]M_c\left(L_C\omega\right)M_a\left(L_M\omega\right)\left[\sum_i h_a\left(n\right)\mathrm{trig}\left(L_a\omega,i\right)\right]\le\delta_s^+\left(\omega\right) \tag{2.68}$$

where

$$\delta_s^-\left(\omega\right)=-\delta_s\left(\omega\right)-G_D\left(\omega\right)\left[1-M_c\left(L_C\omega\right)\right]-G_C\left(\omega\right)M_c\left(L_C\omega\right)$$

and

$$\delta_s^+(\omega) = \delta_s(\omega) - G_D(\omega)\left[1 - M_c(L_C\omega)\right] - G_C(\omega)M_c(L_C\omega).$$

Here, $\delta_s(\omega)$ is the required stopband ripple. Linear programming [78] or any other suitable techniques may be used to optimize (2.67) and (2.68).

Step 5. Design $M_a(z)$ again in the frequency ranges 2 and 3 by using $H_a(z)$, $M_c(z)$, $G_c(z)$, and $G_D(z)$ as prefilters.

Step 6. Repeat Step 5 by picking one of subfilters from: $M_c(z)$, $G_c(z)$, $G_D(z)$, or $H_a(z)$, swapping it with $M_a(z)$ in step 5, and using the remaining subfilters as prefilters until no further improvement is achieved.

2.7 Examples and Comparisons

Example 1

To illustrate the new approach, an example is taken from [28]. The passband edge is at $\omega_p = 0.3\times 2\pi$ and stopband edge is at $\omega_s = 0.301\times 2\pi$. The maximum allowable passband ripple and the minimum stopband attenuation are 0.1 dB and 80 dB, respectively. To design such a filter by a conventional method, the estimated filter length is 3177. If designed by the original single-stage FRM technique with $M = 14$, the minimal lengths for $H_a(z)$, $G_1(z)$, and $G_2(z)$ are 235, 80, and 112, respectively. For this design, 214 multipliers are needed. If designed using the synthesis scheme described in [28], the optimal lengths for $H_a(z)$, $H_g(z)$, $G_1(z)$, and $G_2(z)$ are 157, 29, 31, and 117, respectively. The interpolation factors for $H_a(z)$ and $H_g(z)$ are 21 and 7, respectively. In this case, 169 multipliers are required. Using the proposed

method, the interpolation factors are $L_a = 39$, $L_M = 13$, and $L_C = 4$. The lengths for $H_a(z)$, $M_a(z)$, $M_c(z)$, $G_c(z)$, and $G_D(z)$ are 83, 21, 57, 56, and 24, respectively. This filter requires 122 multipliers which yields 43% savings in the number of multipliers compared to the original FRM approach [21] and 27.8% savings compared to the IFIR-FRM approach [28]. If the filter is synthesized by the two-stage FRM approach, the optimal interpolation factors are $M_1 = M_2 = 6$ and the total number of multipliers is 131. A three-stage FRM approach with $M_1 = M_2 = M_3 = 4$ will require 126 multipliers [28]. Figs. 2.8–2.13 show the magnitude responses of the subfilters and the overall filter designed using the proposed approach.

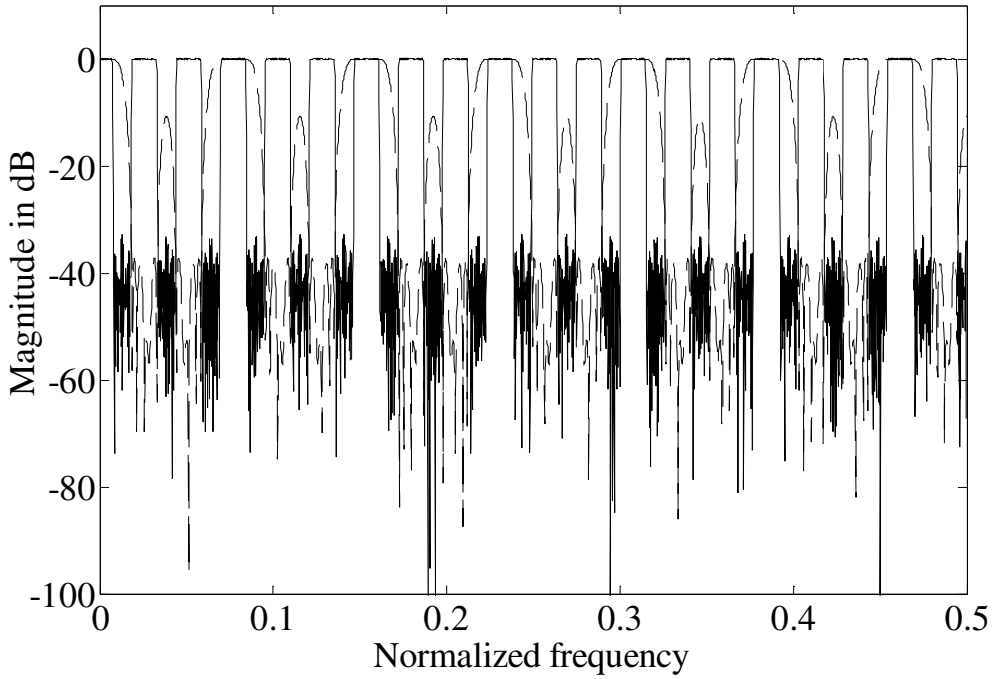

Figure 2.8 Magnitude responses of $H_a(z^{L_a})$ (solid line) and $M_a(z^{L_M})$ (dashed line) in example 1.

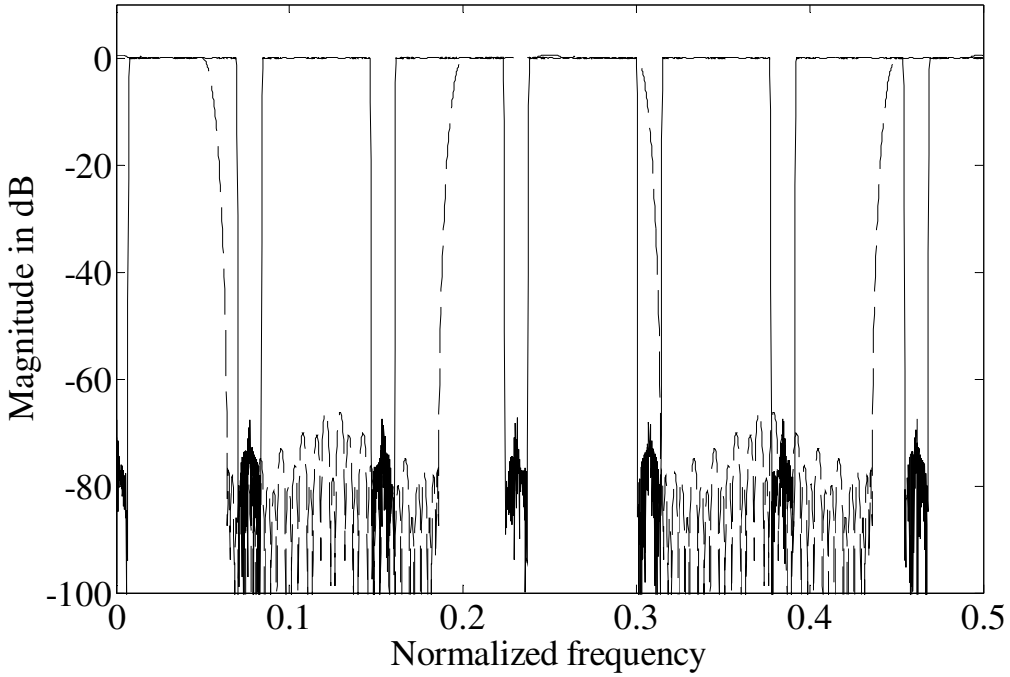

Figure 2.9 Magnitude responses of $B(z)$ (solid line) and $M_c(z^{L_c})$ (dashed line) in example 1.

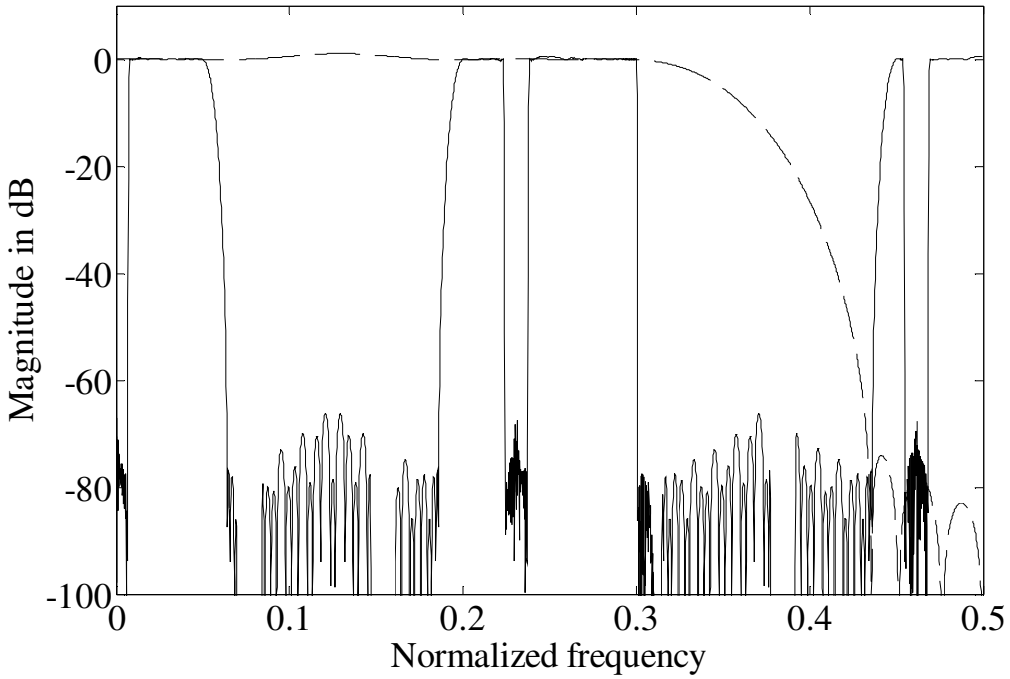

Figure 2.10 Magnitude responses of $C(z)$ (solid line) and $G_C(z)$ (dashed line) in example 1.

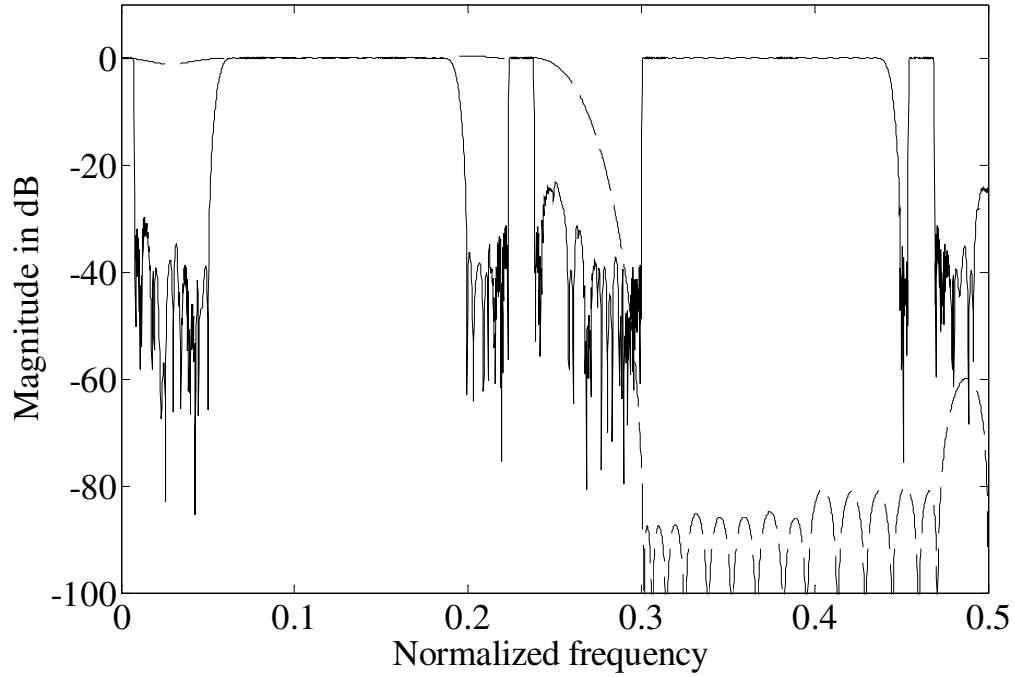

Figure 2.11 Magnitude responses of $D(z)$ (solid line) and $G_D(z)$ (dashed line) in example 1.

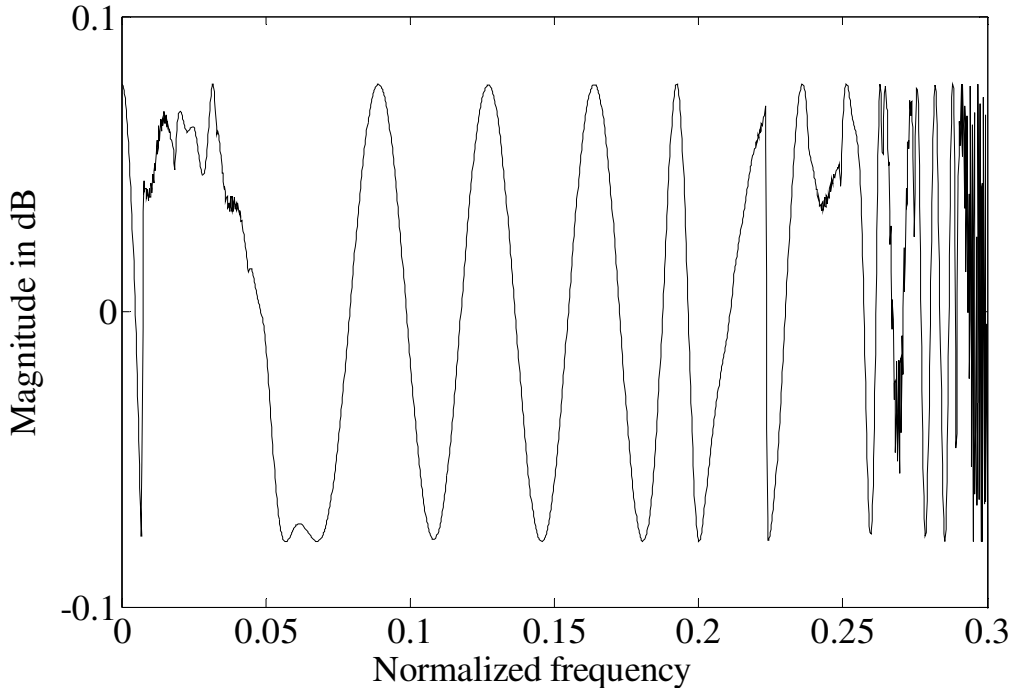

Figure 2.12 Magnitude response of the passband of the overall filter in example 1.

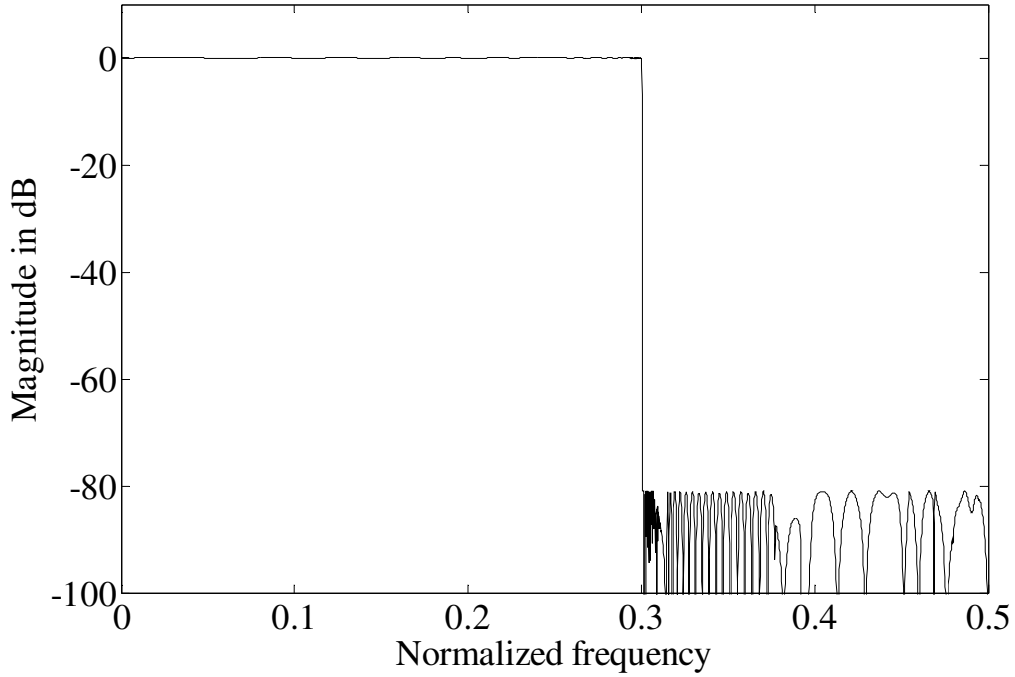

Figure 2.13 Magnitude response of the overall filter in example 1.

Example 2

In this example a sharp FIR filter is designed such that L_a is not a multiple of L_M. The passband edge is at $\omega_p = 0.27\times 2\pi$ and the stopband edge is at $\omega_s = 0.271\times 2\pi$. The passband deviation is at most 0.01 and the stopband attenuation is at least 60 dB. The set of interpolation factors for $H_a(z)$, $M_a(z)$ and $M_c(z)$ are $L_a = 42$, $L_M = 8$, and $L_C = 3$, respectively. The lengths for $H_a(z)$, $M_a(z)$, $M_c(z)$, $G_C(z)$ and $G_D(z)$ are 63, 51, 53, 37, and 19, respectively. The resulting overall filter requires 114 multipliers. If this filter is designed by the original single-stage FRM with $M = 14$, the lengths for $H_a(z)$, $G_1(z)$, and $G_2(z)$ are 183, 85, and 65, respectively. The two-stage FRM approach will lead to a design with $M_1 = 10$ and $M_2 = 6$, the lengths of $H_a(z)$, $G_1^{(1)}(z)$, $G_2^{(1)}(z)$, $G_1^{(2)}(z)$ and $G_2^{(2)}(z)$ (where the superscript "(1)" or "(2)" denotes the first or second masking stage, respectively) are 47, 35, 35, 69, and 59, respectively. In

this case, 125 multipliers are required. Figs. 2.14–2.19 show the magnitude responses of the subfilters and the overall filter designed by the proposed method.

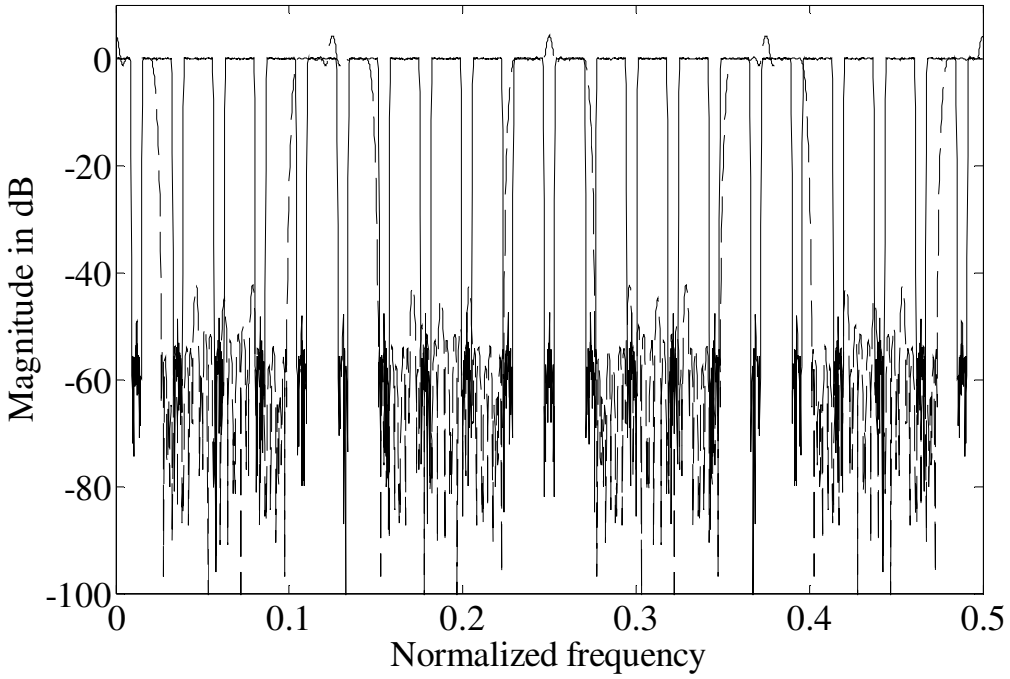

Figure 2.14 Magnitude responses of $H_a(z^{L_a})$ (solid line) and $M_a(z^{L_M})$ (dashed line) in example 2.

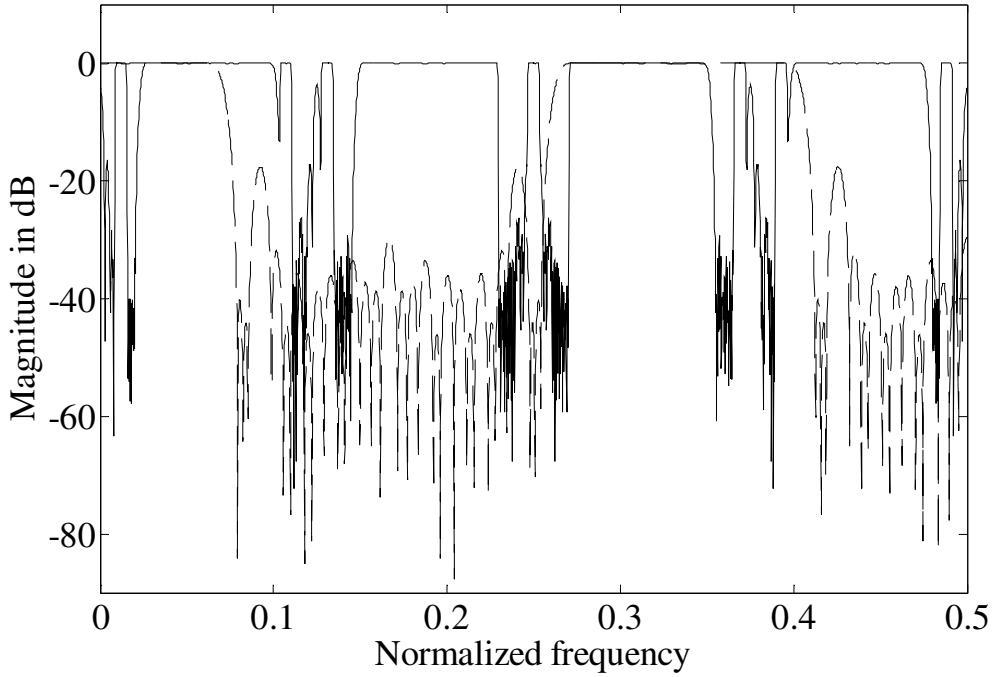

Figure 2.15 Magnitude responses of $B(z)$ (solid line) and $M_c(z^{L_c})$ (dashed line) in example 2.

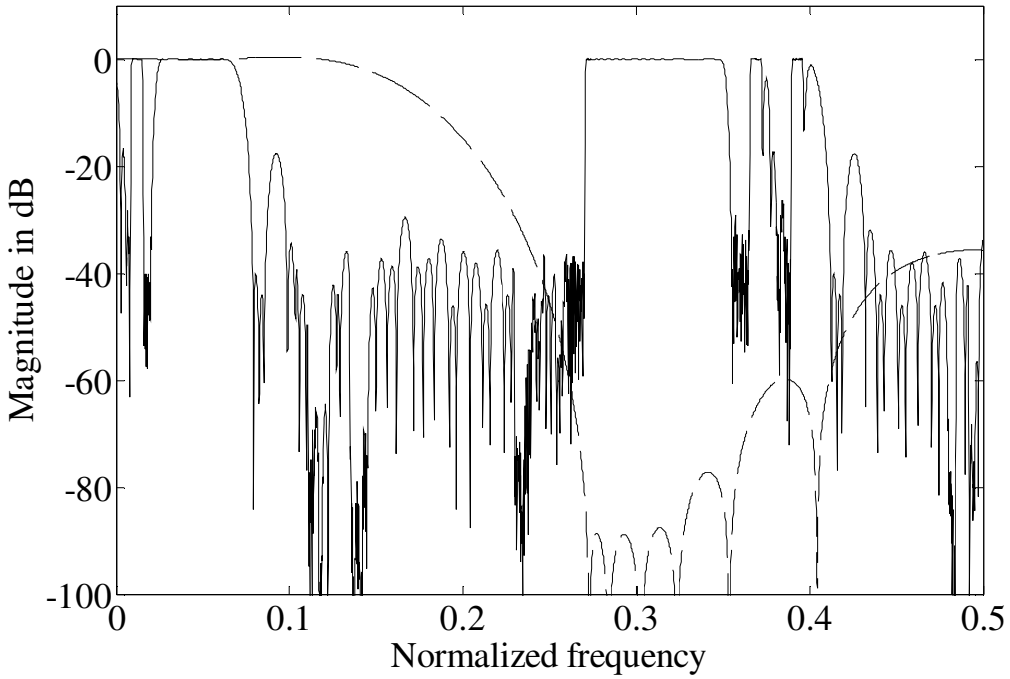

Figure 2.16 Magnitude responses of $C(z)$ (solid line) and $G_C(z)$ (dashed line) in example 2.

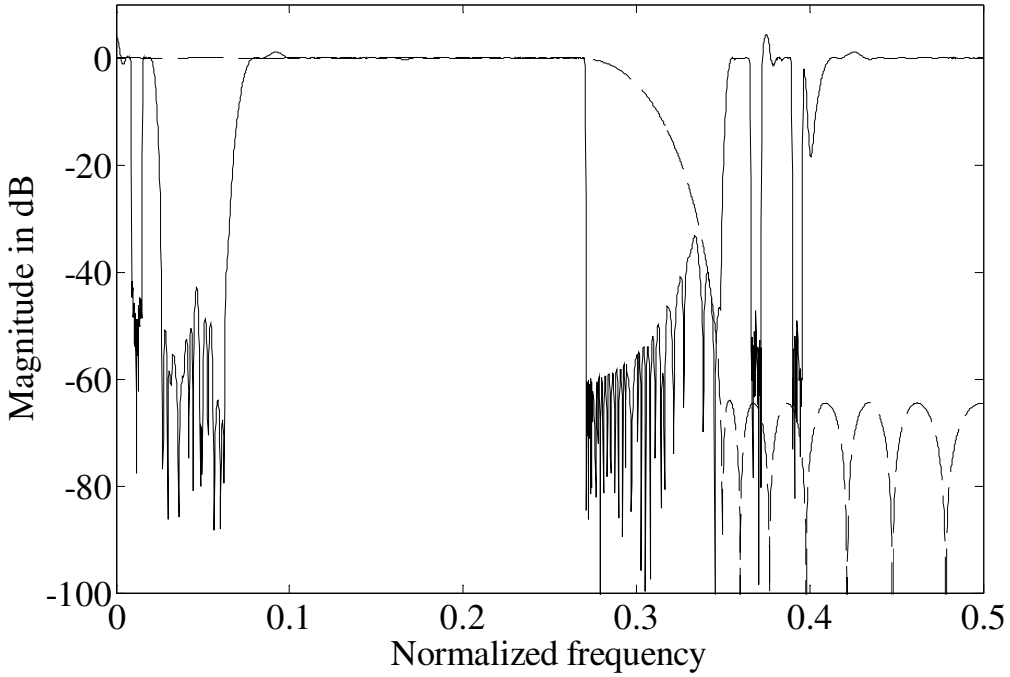

Figure 2.17 Magnitude responses of $D(z)$ (solid line) and $G_D(z)$ (dashed line) in example 2.

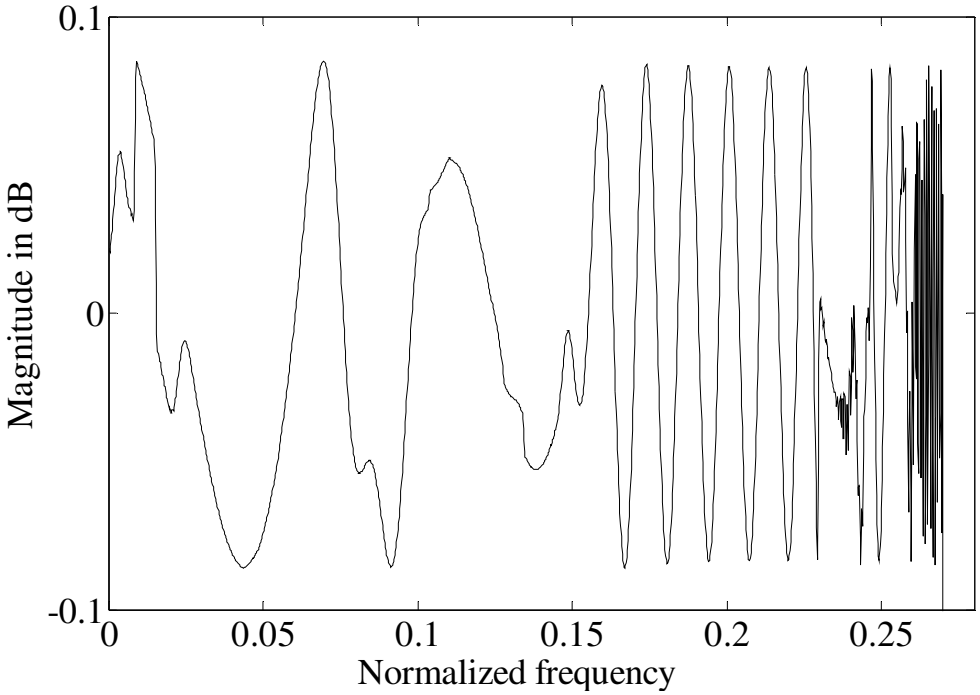

Figure 2.18 Magnitude response of the passband of the overall filter in example 2.

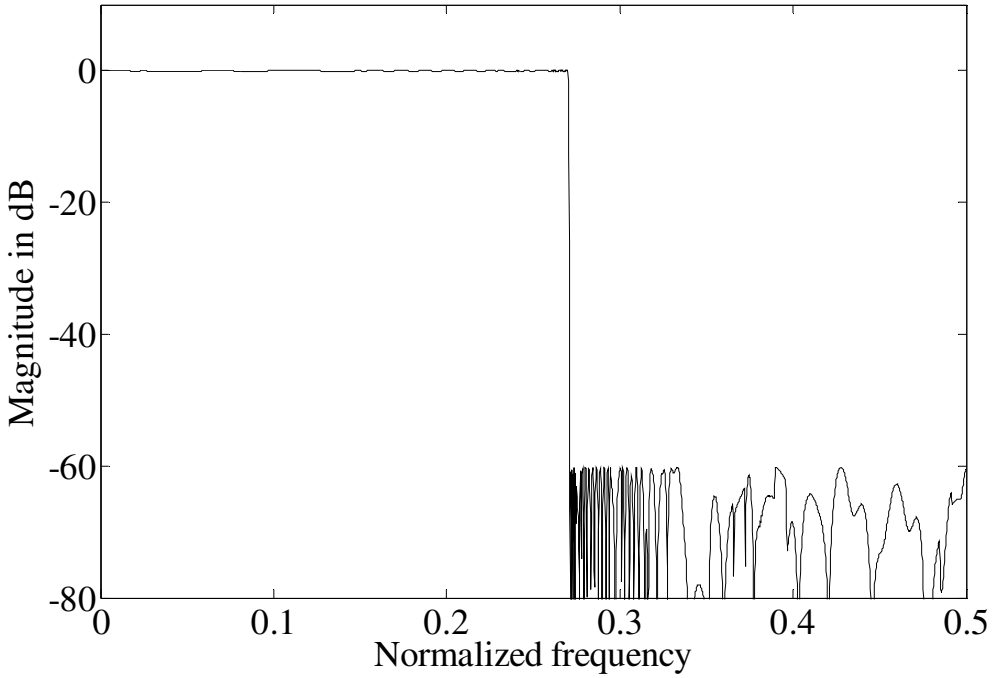

Figure 2.19 Magnitude response of the overall filter in example 2.

Comparisons with other FRM approaches

The comparisons with other FRM approaches for both examples are listed in Tables 2.1 and 2.2. It is interesting to compare the proposed structure with the original two-stage FRM approach as both approaches employ 5 subfilters. It is found that the proposed structure yields more savings in both addition and multiplication at the cost of slightly longer group delays. In example 1, the proposed filter not only outperforms the original two-stage FRM design but also the three-stage FRM with less group delay as well. Moreover, it is noticed in example 2 that the proposed structure produces about 9% more savings in both multipliers and adders with less than 1% increase in group delay compared with the two-stage FRM approach. In conclusion, the proposed filter will yield more savings in terms of arithmetic operations than the ones designed by the two-stage FRM or the IFIR-FRM approach.

Table 2.1 Comparison of different design methods for example 1.

Design	Multipliers	Adders	Group Delay
Minimax	1589	3176	1588
1-stage FRM	214	426	1693.5
2-stage FRM	131	256	1771
3-stage FRM	126	246	2134.5
IFIR-FRM [28]	169	332	1794
Proposed	122	239	1868.5

Table 2.2 Comparison of different design methods for example 2.

Design	Multipliers	Adders	Group Delay
Minimax	1268	2534	1267.5
1-stage FRM	168	332	1316
2-stage FRM	125	244	1584
Proposed	114	221	1598

2.8 Summary

In this chapter, a new structure that reduces the complexity for the design of sharp FIR filters using frequency-response masking technique has been introduced. The success of the proposed method is based on a newly introduced decoupling stage between the bandedge shaping and the masking filters in the FRM approach. This method can achieve considerable savings in terms of arithmetic operations compared with the original FRM and the IFIR-FRM approach.

Chapter 3

Modified FRM Filters Using New Prefilter-Equalizer Structures

3.1 Introduction

In order to improve the design of FRM filters, let us examine the role of each subfilter in the FRM technique. The bandedge shaping filter and its complement are used to form the arbitrary bandwidth and the transition-band for the overall filter. The two masking filters remove the passband replicas of both the bandedge shaping filter and its complement such that the overall stopband attenuation is satisfied. The interpolation factor determines the complexity of the two masking filters, i.e., a large interpolation factor leads to high complexity of masking filters. According to the ripple compensation effect [21] in the FRM approach, it is possible to use an additional filter/filters to remove the passband replicas in the vicinity of the transition-band of the overall filter to reduce the complexity of the masking filters, as demonstrated in the IFIR-FRM method [27, 28] and the interpolated masking-filters approach [22]. The methods proposed by [22], [27] and [28] share a common feature that additional

interpolated masking filter/filters are introduced to relieve the tasks of the original masking filters. The problem is whether other simple multiplication-free prefilters can be employed to replace the additional interpolated masking filter. In this chapter, new structures using multiplication-free prefilters will be developed to reduce the workload of the masking filters.

The rest of the chapter is organized as follows. In Section 3.2, two modified FRM structures are presented. New prefilter structures for the design of the modified FRM filters are proposed in Section 3.3. Design equations and procedures are introduced in Section 3.4. In Section 3.5 some examples and comparisons of different design methods are given to illustrate the proposed method. A summary is presented in Section 3.6.

3.2 Modified FRM Structures

A modified FRM structure is shown in Fig. 3.1, where $F_s\left(z^M\right)$ is the bandedge shaping filter, $H_r\left(z\right)F_1\left(z\right)$ forms a prefilter-equalizer filter $H_p\left(z\right)$, and $F_2\left(z\right)$ is a masking filter. Two modifications have been made to the original FRM structure. First, the upper masking branch was removed by pushing one of the masking filter $F_1\left(z\right)$ to the bandedge shaping branch. By moving $F_1\left(z\right)$ to bandedge shaping branch, $F_1\left(z\right)$ and $H_r\left(z\right)$ can form a prefilter-equalizer pair to reduce the overall filter complexity; Second, the masking filter $F_2\left(z\right)$ may be designed using the FRM technique as shown in Fig. 3.2 if the transition-width of $F_2\left(z\right)$ is narrow. The z-transform transfer function of the proposed filter is given by

$$H(z)=\left[z^{-GD}-F_s\left(z^M\right)H_r(z)F_1(z)\right]F_2(z) \tag{3.1}$$

where *GD* is the total number of group delay of $F_s\left(z^M\right)H_r(z)F_1(z)$. If the structure of Fig. 3.2 is used, $F_2(z)$ is expressed as

$$F_2(z)=D\left(N_{G_2},N_{G_1}\right)G_s\left(z^{M_1}\right)G_1(z)+D\left(N_{G_1},N_{G_2}\right)\left[z^{-GD_1}-G_s\left(z^{M_1}\right)\right]G_2(z), \tag{3.2}$$

assuming GD_1 is the group delay of $G_s\left(z^{M_1}\right)$, N_{G_1} and N_{G_2} are the filter lengths of $G_1(z)$ and $G_2(z)$, respectively, $D\left(N_{G_1},N_{G_2}\right)$ is defined by (2.3). The frequency responses of subfilters in Fig. 3.1 are shown in Fig. 3.3.

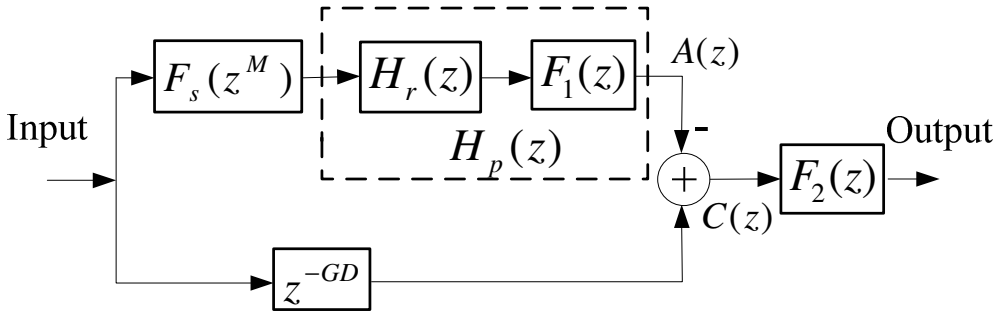

Figure 3.1 A modified FRM structure.

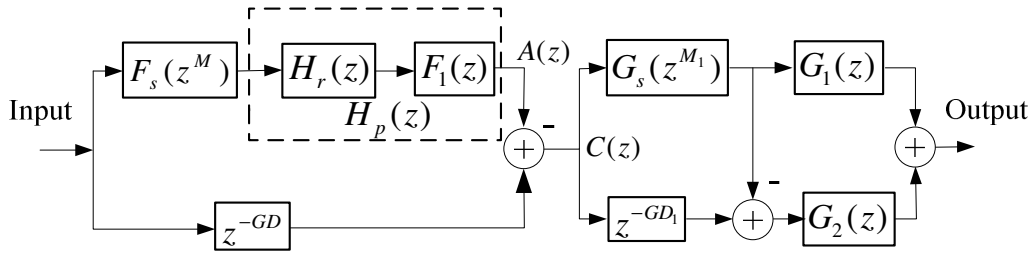

Figure 3.2 A modified FRM structure with $F_2(z)$ replaced by an FRM filter.

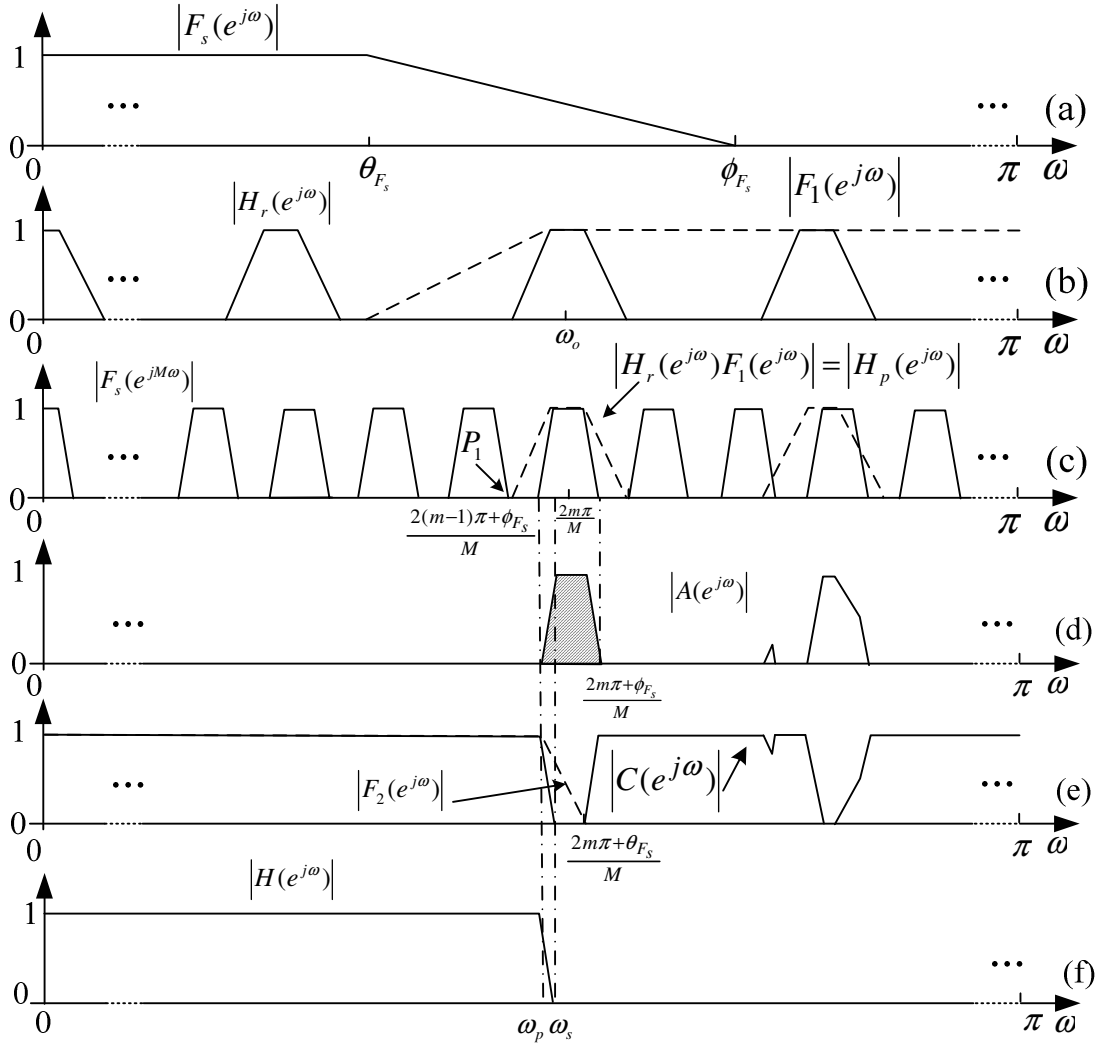

Figure 3.3 Magnitude responses of subfilters in Fig. 3.1.

The design starts with a prototype model filter $F_s(z)$ with passband and stopband edges located at θ_{F_s} and ϕ_{F_s}, respectively, as shown in Fig. 3.3(a). The frequency responses of $F_1(z)$ and $H_r(z)$ are sketched in Fig. 3.3(b). $F_1(z)$ and $H_r(z)$ forms a prefilter-equalizer $H_p(z)$, as shown in Fig. 3.3(c). Substituting each delay element of $F_s(z)$ by M delay elements, the frequency response of $F_s(z)$ is compressed by a factor of M and sharp transition-bands are formed, as shown in Fig. 3.3(c). Cascading $F_s(z^M)$ with $H_p(z)$, a pair of new complementary bandedge shaping filters $A(z)$

and $C(z)$ are formed, as shown in Figs. 3.3(d) and (e), where $A(z)$ has much wider stopband width than that of $F_s(z^M)$. In Fig. 3.3(d), the shaded area is called the bandedge shaping (BS) tooth which is essential to form the transition band of the overall filter. The corresponding frequency responses of $F_2(z)$ and the overall filter $H(z)$ are shown in Figs. 3.3(e) and 3.3(f). In Fig. 3.3, the transition-band of $H(z)$ is determined by $C(z)$. The structure for the case where the final transition-band is determined by $A(z)$ is shown in Fig. 3.4 where GD_{F_2} is the number of group delay of $F_2(z)$. It should be noted that $F_2(z)$ in Fig. 3.4 can be replaced by an FRM filter to reduce the complexity further. The z-transform transfer function for this case is given by:

$$H(z) = z^{-GD_{F_2}} F_s(z^M) H_r(z) F_1(z) + \left[z^{-GD} - F_s(z^M) H_r(z) F_1(z) \right] F_2(z), \qquad (3.3)$$

where GD_{F_2} is the group delay of $F_2(z)$. The frequency responses of subfilters in Fig. 3.4 are sketched in Fig. 3.5.

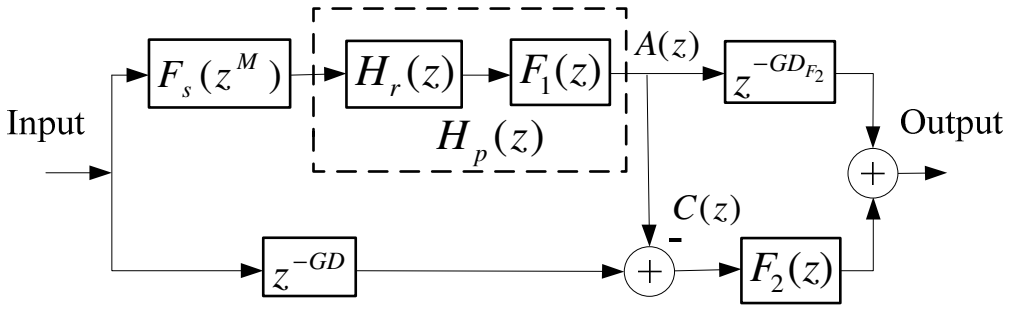

Figure 3.4 A modified FRM structure for a different case.

Before embarking on the design procedure, new prefilter structures for $H_p(z)$ are proposed in the following section.

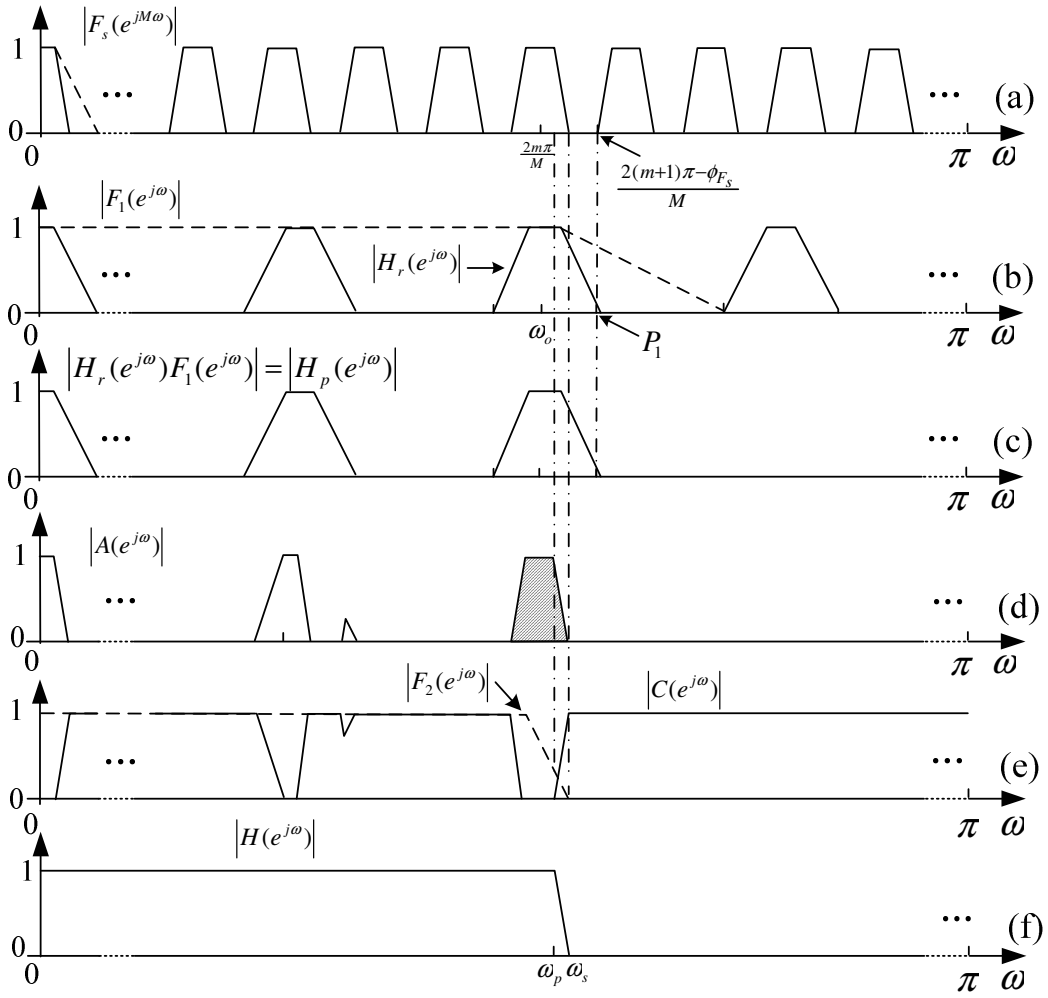

Figure 3.5 Frequency responses of subfilters in Fig. 3.4.

3.3 New Prefilter Structures

There are many multiplication-free prefilters reported in [3, 5–9, 14]. In [9], a 4th-order multiplication-free FIR filter was proposed which is attractive for the design of $H_p(z)$. The transfer function and the magnitude response of the prefilter are given by

$$P_{L4}(z) = \frac{1}{8}\left(1+z^{-1}\right)^2\left(1+z^{-2}\right) \tag{3.4}$$

and

$$\left|P_{L4}\left(e^{j\omega}\right)\right| = \frac{1}{2}\left|\left(\cos^2\omega + \cos\omega\right)\right|. \tag{3.5}$$

$P_{L4}(z)$ provides about 18 dB stopband attenuation, which is not enough for most of FRM filter designs. There are two ways to increase the stopband attenuation. The first way is to cascade L numbers of $P_{L4}\left(z^N\right)$ with different interpolation factor N as in [9] which is suitable for the design of narrowband FIR filters. The second is to utilize the "sharpening technique" [80] by cascading L sections of identical $P_{L4}\left(z^N\right)$. In this chapter, the second way is chosen as it provides more flexibility to meet the design requirement. Therefore, the z-transform transfer function and the magnitude response of a new prefilter $P_{4r}(N, L, z)$ are given by

$$P_{4r}(N, L, z) = \left[\frac{1}{8}\left(1 + z^{-2N}\right)\left(1 + z^{-N}\right)^2\right]^L \tag{3.6}$$

and

$$\left|P_{4r}\left(e^{j\omega}\right)\right| = \frac{1}{2^L}\left[\cos\left(N\omega\right) + \cos^2\left(N\omega\right)\right]^L \tag{3.7}$$

where N is an interpolation factor and L is the number of $P_{L4}(z)$ used. As the coefficients of $P_{4r}(N, L, z)$ do not involve any multiplication, $P_{4r}(N, L, z)$ is a multiplication-free filter except for the scaling factor. Fig. 3.6 shows the frequency response of $P_{4r}(8, 4, z)$. $P_{4r}(N, L, z)$ has periodic frequency response with main lobes centered at $\frac{2n\pi}{N}$, where $n = 0,\ 1,\ ...,\ N-1$, and it produces about $18L$ dB stopband attenuation.

As discussed in [2], the role of prefilter in a prefilter-equalizer approach is to provide sufficient stopband attenuation. It is desirable to increase the stopband attenuation further for the proposed prefilter. Let us consider a second order multiplication-free FIR filter with the transfer function and the magnitude response given by

$$P_{L2}(z) = \frac{1}{3}\left(1 + z^{-1} + z^{-2}\right) \tag{3.8}$$

and

$$\left|P_{L2}\left(e^{j\omega}\right)\right| = \frac{1}{3}\left|(1 + 2\cos\omega)\right|. \tag{3.9}$$

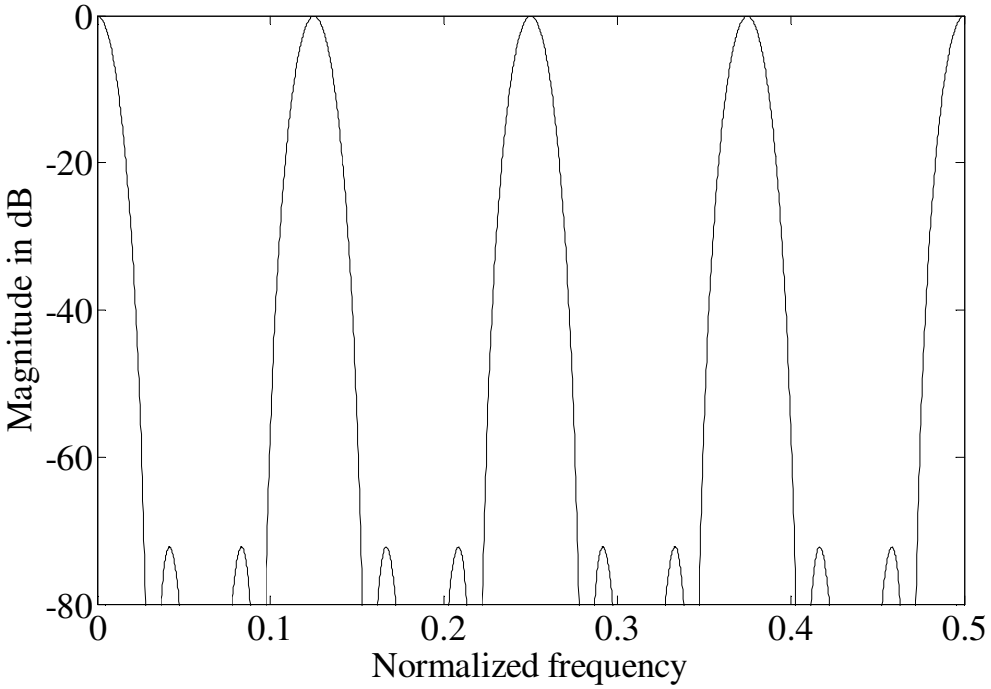

Figure 3.6 Magnitude response of $P_{4r}(8, 4, z)$.

It is easy to show from (3.5) and (3.9) that $P_{L2}(z)$ has a null occurring at $\frac{2\pi}{3}$ which coincides with the peak of the side lobe of $P_{L4}(z)$. The cascade of $P_{L2}(z)$ and $P_{L4}(z)$

creates a prefilter that provides about 36 dB stopband attenuation, as shown in Fig. 3.7. The interpolated version of $P_{L4}(z)P_{L2}(z)$ is expressed as

$$H_{r1}(L_1,K,z)=\left[\frac{1}{8}\left(1+z^{-N}\right)^2\left(1+z^{-2N}\right)\right]^{L_1}\left[\frac{1}{3}\left(1+z^{-N}+z^{-2N}\right)\right]^{K} \tag{3.10}$$

and its magnitude response is written as

$$\left|H_{r1}\left(e^{j\omega}\right)\right|=\left|\frac{1}{2^{L_1}}\left[\cos^2(N\omega)+\cos(N\omega)\right]^{L_1}\frac{1}{3^K}\left[2\cos(N\omega)+1\right]^{K}\right| \tag{3.11}$$

where L_1 and K are called sharpening factors for the purpose of providing enough stopband attenuation. The magnitude response of $H_{r1}(z)$, for $L_1=1$, $K=1$, and $N=6$, is plotted in Fig. 3.8. By selecting different values of L_1 and K, desired stopband attenuations are obtained.

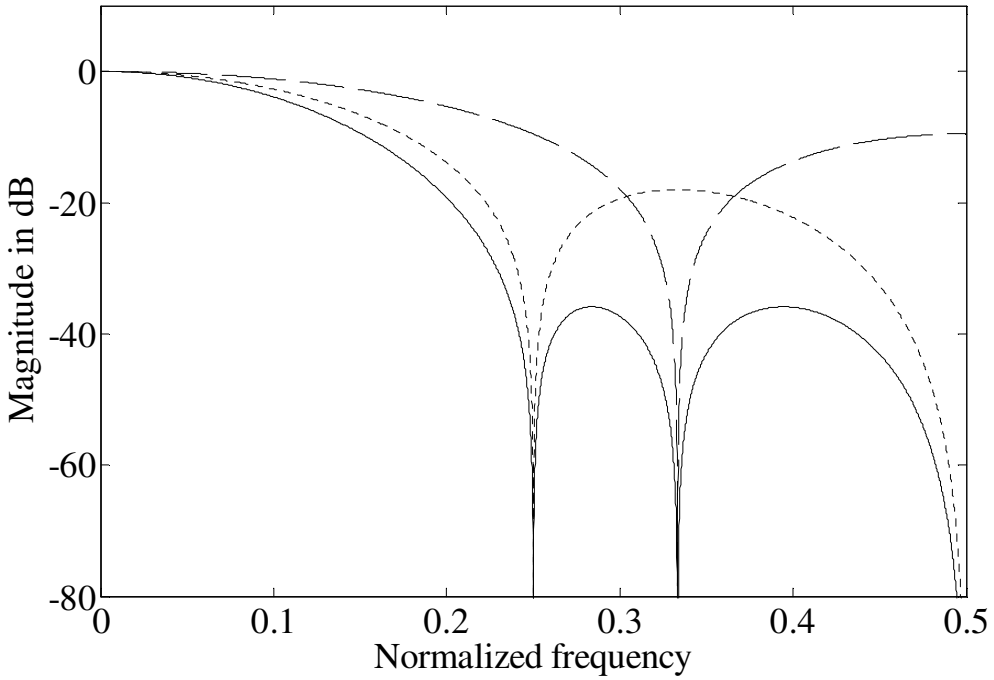

Figure 3.7 Magnitude responses of $P_{L4}(z)$ (dotted line), $P_{L2}(z)$ (dashed line) and $P_{L4}(z)P_{L2}(z)$ (solid line).

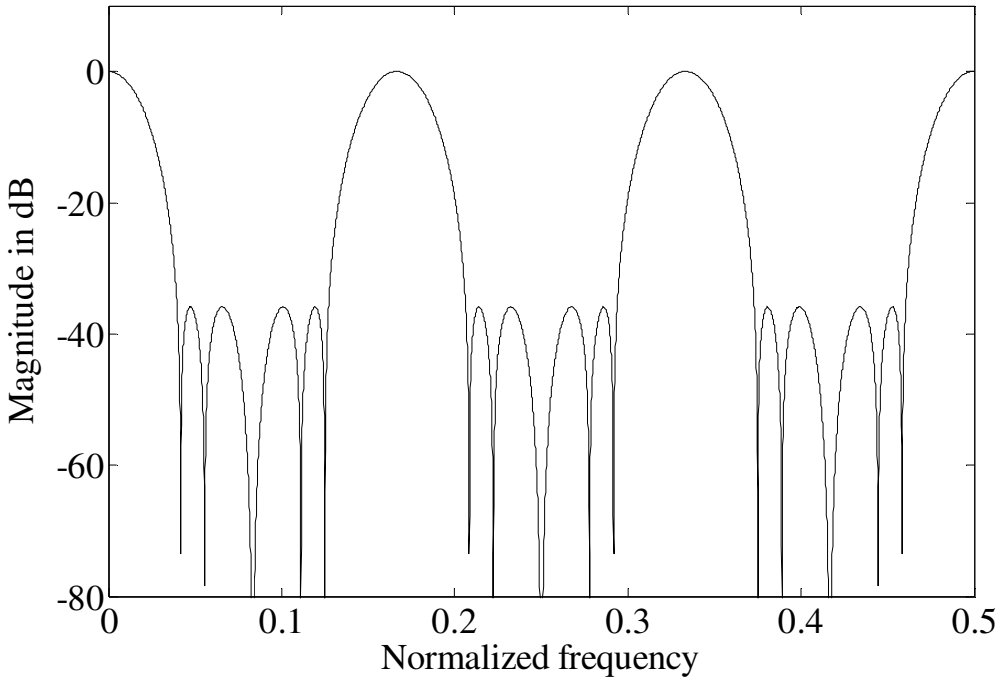

Figure 3.8 Magnitude response of $H_{r1}(z)$ for $N=6$, $K=1$, and $L_1=1$.

$H_{r1}(z)$ has periodic frequency response with main lobes centered at $\frac{2\pi n}{N}$ ($n=0,\ 1,\ ...,\ N-1$). Fig. 3.9 shows the magnitude response of $H_{r1}(z)$ (solid line) for $N=7$, $L_1=2$ and $K=1$. The dashed line in Fig. 3.9 is the magnitude response of $P_{4r}(7,3,z)$. It is interested to note that $H_{r1}(z)$ and $P_{4r}(N,L,z)$ have almost the same magnitude response except that $H_{r1}(z)$ has additional nulls generated by the interpolated version of $P_{L2}(z)$. However, the complexity of $H_{r1}(z)$ is lower than that of $P_{4r}(N,L,z)$ if they have the same stopband attenuations. Furthermore, the group delay of $H_{r1}(z)$ is shorter than that of $P_{4r}(N,L,z)$. Table 3.1 summarizes the implementation costs and group delays of $H_{r1}(z)$ and $P_{4r}(N,L,z)$ for different L, L_1 and K. It is reasonable to believe that replacing $H_r(z)$ by $H_{r1}(z)$, in Fig. 3.1 or Fig. 3.4, additional arithmetic savings can be achieved when designing the overall filter.

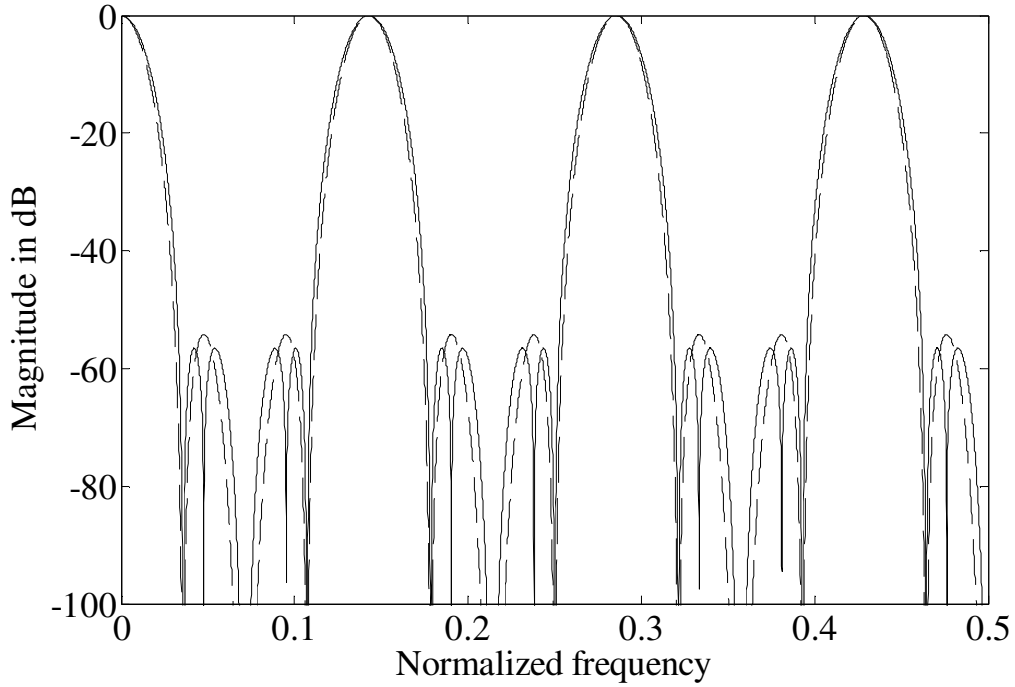

Figure 3.9 Magnitude responses of $H_{r1}(z)$ (solid line) ($N=7$, $L=2$ and $K=1$) and $P_{4r}(7,3,z)$ (dashed line).

Table 3.1 Comparison of $H_{r1}(z)$ and $P_{4r}(N,L,z)$.

$H_{r1}(z)$				$P_{4r}(N,L,z)$			
	Attenuation (dB)	adders	Group delay		Attenuation (dB)	adders	Group delay
$L_1=1$ $K=1$	35.89	5	$3N$	$L=2$	36.12	6	$4N$
$L_1=2$ $K=1$	56.53	8	$5N$	$L=3$	54.18	9	$6N$
$L_1=2$ $K=2$	71.79	10	$6N$	$L=4$	72.24	12	$8N$
$L_1=3$ $K=1$	76.19	11	$7N$	$L=5$	90.31	15	$10N$
$L_1=3$ $K=2$	92.80	13	$8N$	$L=6$	108.37	18	$12N$

Let ω_o be the center frequency of one of the main lobes of $H_{r1}(z)$. If ω_o is near the center of the BS tooth, the main lobe corresponding to ω_o can be used to "mask" the BS tooth as shown in Figs. 3.3(b)–(d). For a given *N*, $H_{r1}(z)$ has main lobes centered at $\frac{2\pi n}{N}$ ($n = 0,\ 1,\ ...,\ N-1$), from which one main lobe is selected to "mask" the BS tooth. To provide more choices, a highpass version of the prefilter structure is given by

$$H_{r2}(z) = \frac{1}{8^{L_1}}\left[\left(1+z^{-2N}\right)\left(1-z^{-N}\right)^2\right]^{L_1} \frac{1}{3^K}\left[\left(1-z^{-1}+z^{-2}\right)\right]^K. \tag{3.12}$$

The magnitude response of $H_{r2}(z)$ is given by

$$\left|H_{r2}\left(e^{j\omega}\right)\right| = \left|\frac{1}{2^{L_1}}\left[\cos^2(N\omega)-\cos(N\omega)\right]^{L_1} \frac{1}{3^K}\left[1-2\cos(N\omega)\right]^K\right|. \tag{3.13}$$

The magnitude response of $H_{r2}(z)$ for $N = 7$, $L_1 = 2$ and $K = 1$ is shown in Fig. 3.10. $H_{r2}(z)$ has periodic frequency response with main lobes centered at $\frac{2\pi(0.5+n)}{N}$, where $n = 0,\ 1,\ ...,\ N-1$. Comparing Fig. 3.9 with Fig. 3.10, $H_{r2}(z)$ may be considered as a "complementary part" of $H_{r1}(z)$ in terms of the location of main lobes. Hence, $H_{r2}(z)$ is another good candidate for the replacement of $H_r(z)$. To employ the new prefilters in the proposed structure, a set of *N*, L_1 and *K* must be determined. This will be discussed in the following sections.

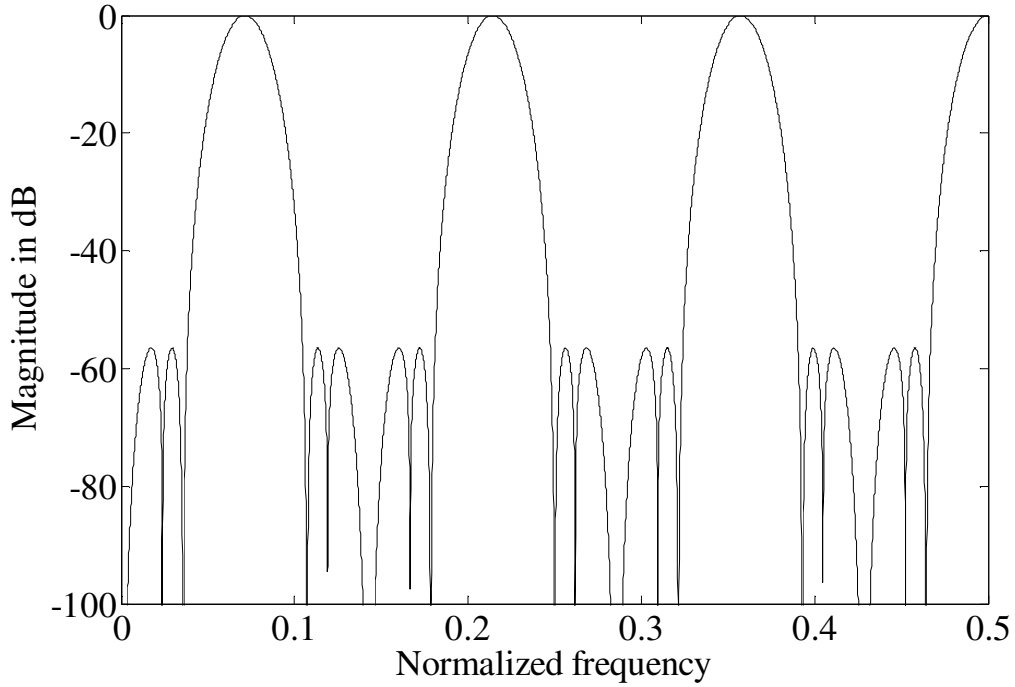

Figure 3.10 Magnitude response of $H_{r2}(z)$ for $N = 7$, $L_1 = 2$ and $K = 1$.

3.4 Filter Design

3.4.1 Design Equations

In this section, design equations are derived for lowpass filters using prefilter $H_{r1}(z)$. Similar equations can be obtained if $H_{r2}(z)$ is employed as prefilter. Meanwhile, the similar procedure can be applied to derive design equations for highpass filters. Let us denote the structure of Fig. 3.1 as Case A and the structure of Fig. 3.4 as Case B. Let the passband and stopband edges of the desired lowpass filter be ω_p and ω_s, respectively. Assume that θ and ϕ are used to denote the passband and stopband edges of a subfilter such that the passband and stopband edges of $F_s(z)$ are θ_{F_s} and ϕ_{F_s}, respectively. Similar definitions are applied to other subfilters. To determine the bandedges of $F_s(z)$, it can be shown that [21]

$$\omega_p = \begin{cases} \dfrac{2m\pi - \phi_{F_s}}{M} & \text{(for Case A)} \\ \dfrac{2m\pi + \theta_{F_s}}{M} & \text{(for Case B)} \end{cases} \tag{3.14}$$

and

$$\omega_s = \begin{cases} \dfrac{2m\pi - \theta_{F_s}}{M} & \text{(for Case A)} \\ \dfrac{2m\pi + \phi_{F_s}}{M} & \text{(for Case B)} \end{cases} \tag{3.15}$$

where m is an integer. To ensure that (3.14) and (3.15) yield a solution with $0 < \theta_{F_s} < \phi_{F_s} < \pi$, two sets of equations are derived for Case A and B, respectively.

For Case A, we have

$$m = \left\lceil \frac{\omega_s M}{2\pi} \right\rceil \tag{3.16}$$

$$\theta_{F_s} = 2m\pi - \omega_s M \tag{3.17}$$

$$\phi_{F_s} = 2m\pi - \omega_p M \tag{3.18}$$

where $\lceil x \rceil$ denotes the smallest integer larger than or equal to x. For Case B, we have

$$m = \left\lfloor \frac{\omega_p M}{2\pi} \right\rfloor \tag{3.19}$$

$$\theta_{F_s} = \omega_p M - 2m\pi \tag{3.20}$$

$$\phi_{F_s} = \omega_s M - 2m\pi \tag{3.21}$$

where $\lfloor x \rfloor$ denotes the largest integer less than or equal to x. To determine the bandedges of $F_2(z)$, let us examine Figs. 3.3(e) and 3.5(e). It is clear that the bandedges of $F_2(z)$ are not affected by $H_r(z)$. For Case A, we have

$$\theta_{F_2} = \omega_p \tag{3.22}$$

$$\phi_{F_2} = \frac{2m\pi + \theta_{F_s}}{M} \tag{3.23}$$

For Case B, we have

$$\theta_{F_2} = \frac{2m\pi - \theta_{F_s}}{M} \tag{3.24}$$

$$\phi_{F_2} = \omega_s \tag{3.25}$$

As shown in Figs. 3.3(c), 3.3(d), 3.5(c) and 3.5(d), the role of $H_p(z)$ is to create $A(z)$ from $F_s(z^M)$ in two ways that

a) $H_p(z)$ should introduce the least deviation to the frequency-response of the BS tooth,

b) and $H_p(z)$ removes the unwanted passbands of $F_s(z^M)$.

For this reason, $H_p(z)$ is in fact a bandpass alike filter with the bandedges given by the following equations. For Case A, we have

$$\begin{cases} \theta_{H_{p1}} = \omega_s \\ \theta_{H_{p2}} = \dfrac{2m\pi + \theta_{F_s}}{M} \end{cases} \tag{3.26}$$

where $\theta_{H_{p1}}$ and $\theta_{H_{p2}}$ are the passband edges of $H_p(z)$, and

$$\phi_{H_p} = \frac{2(m-1)\pi + \phi_{F_s}}{M} \tag{3.27}$$

where ϕ_{H_p} are the stopband edge of $H_p(z)$. Another stopband edge of $H_p(z)$ is not cared because only the passbands to the left of the BS tooth need to be removed, as shown in Fig. 3.3(c). Similarly, for Case B, we have

$$\begin{cases} \theta_{H_{p1}} = \dfrac{2m\pi - \theta_{F_s}}{M} \\ \theta_{H_{p2}} = \omega_p \end{cases} \tag{3.28}$$

$$\phi_{H_p} = \frac{2(m+1)\pi - \phi_{F_s}}{M} \tag{3.29}$$

3.4.2 Determination of M, N, L_1 and K

Before the overall filter $H(z)$ is synthesized, the values of M , N , L_1 , and K for $H_{r1}(z)$ must be determined. Unfortunately, there are no known closed-form expressions for M , N , L_1 , and K. Nevertheless, there are conditions that N, L_1 and K should meet for a set of given specifications. These conditions are helpful to find the values of N, L_1 and K.

As shown in Figs. 3.3 and 3.5, one main lobe of the prefilter is used to mask the BS tooth for generating the overall transition-band. Let us denote such a main lobe as the bandedge shaping (BS) lobe. The center frequency ω_o of the BS lobe should be located inside the BS tooth, and the width of the BS lobe should be wider than that of the BS tooth, as shown in Figs. 3.3(b) and 3.5(b). This constraint leads to

$$\begin{cases} \dfrac{2m\pi - \theta_{F_s}}{M} < \omega_o = \dfrac{2k\pi}{N} < \dfrac{2m\pi + \theta_{F_s}}{M} \\ N < M \end{cases} \tag{3.30}$$

where k is an integer less than N. From (3.11), the peak of the first side-lobe of $H_{r1}(z)$ occurs at

$$\omega_{br} \approx 0.284 \times \frac{2\pi}{N}. \tag{3.31}$$

To remove the unwanted passbands to the left of the BS tooth, substituting ω_{br} into (3.11), for Case A, we get

$$\left| \frac{1}{2^{L_1} \cdot 3^K} \left[\cos^2(\omega_{br}) + \cos(\omega_{br}) \right]^{L_1} \left[2\cos(\omega_{br}) + 1 \right]^K \right| < \delta_p. \tag{3.32}$$

For Case B, we have

$$\left| \frac{1}{2^{L_1} \cdot 3^K} \left[\cos^2(\omega_{br}) + \cos(\omega_{br}) \right]^{L_1} \left[2\cos(\omega_{br}) + 1 \right]^K \right| < \delta_s \tag{3.33}$$

where δ_p and δ_s are the required passband and stopband ripples, respectively.

For a given M, a set of N, L_1 and K can be found that satisfy (3.30)–(3.33). It should be noted that smaller values of N, L_1 and K will lead to shorter group delays and less adders. To further narrow the selection of N, L_1 and K, two more facts should be considered:

(a) Let P_1 denote the stopband edge next to the BS tooth as shown in Figs. 3.3(c), and 3.5(b), respectively. The null near the BS lobe of $H_{r1}(z)$ should be located as close to P_1 as possible.

(b) The passband degradation of $H_{r1}(z)$ can be compensated by $F_s(z^M)$ and $F_1(z)$. However, the total compensation is limited within a few dB. Therefore, a good choice of N, L_1 and K should lead to a $H_{r1}(z)$ with less passband degradation.

So far several guidelines are presented for the selection of N, L_1 and K. An exhaustive search can be adopted to find a set of optimal values for M, N, L_1 and K. A cost function $C(\Delta)$ is defined to measure the overall complexity of the filter as

$$C(\Delta) = \frac{1}{\Delta_{F_s}} + \frac{1}{\Delta_{F_2}} \tag{3.34}$$

where $\Delta_{F_s} = \phi_{F_s} - \theta_{F_s}$ is the transition-width of $F_s(z)$. Similar definition is applied to $F_2(z)$. In (3.34), the complexity of $F_1(z)$ is not considered, because its length is much shorter than those of $F_s(z)$ and $F_2(z)$. For a given M, $C(\Delta)$ can be easily calculated using the above design equations. The exhaustive search program is to find the values of M, N, L_1, and K that satisfy (3.30)–(3.33) and minimize (3.34).

3.4.3 Ripple Analysis of Subfilters

It is useful to analyze the ripple effect of each subfilter on the overall filter. The ripple analysis is performed for Case A. Similar results can be obtained from Case B. Let $G(\omega)$ and $\delta(\omega)$ denote the gain and deviation of $H(e^{j\omega})$. Let $G_{F_s'}(\omega)$ and $\delta_{F_s'}(\omega)$ represent the gain and deviation of $F_s(e^{jM\omega})$. Similar expressions are used for $F_2(e^{j\omega})$ and $H_p(e^{j\omega})$, where

$$H_p(e^{j\omega}) = H_r(e^{j\omega}) F_1(e^{j\omega}). \tag{3.35}$$

We have

$$G(\omega) + \delta(\omega) = \left\{1 - \left[G_{F_s'}(\omega) + \delta_{F_s'}(\omega)\right]\left[G_{H_p}(\omega) + \delta_{H_p}(\omega)\right]\right\}\left[G_{F_2}(\omega) + \delta_{F_2}(\omega)\right]. \tag{3.36}$$

The ripple effects of the subfilters on the overall filter are examined in the following 4 frequency ranges.

Frequency range 1: $0 \le \omega < \dfrac{2(m-1)\pi + \phi_{F_s}}{M}$.

In this frequency range, $G_{H_p}(\omega) = 0$ and $G(\omega) = G_{F_2}(\omega) = 1$. Thereby, (3.36) is simplified to the following form:

$$\delta(\omega) = \delta_{F_2}(\omega) - \left[G_{F_s'}(\omega) + \delta_{F_s'}(\omega)\right]\delta_{H_p}(\omega)\left[1 + \delta_{F_2}(\omega)\right]. \tag{3.37}$$

Ignoring the second order terms, the following relations are obtained.

When $G_{F_s'}(\omega) = 1$,

$$\delta(\omega) \approx \delta_{F_2}(\omega) - \delta_{H_p}(\omega). \tag{3.38}$$

When $G_{F_s'}(\omega) = 0$,

$$\delta(\omega) \approx \delta_{F_2}(\omega). \tag{3.39}$$

When $0 < G_{F_s'}(\omega) < 1$,

$$\left|\delta(\omega)\right| \le \left|\delta_{F_2}(\omega)\right| + \left|\delta_{H_p}(\omega)\right|. \tag{3.40}$$

Frequency range 2: $\dfrac{2(m-1)\pi + \phi_{F_s}}{M} \le \omega \le \omega_p$.

In this frequency range, $G(\omega) = G_{F_2}(\omega) = 1$, $G_{F_s'}(\omega) = 0$ and $G_{H_p}(\omega)$ increases from zero to unity as ω increases. In this case, (3.36) is simplified to

$$\delta(\omega) = \delta_{F_2}(\omega) - \delta_{F_s'}(\omega)\left[G_{H_p}(\omega) + \delta_{H_p}(\omega)\right]\left[1 + \delta_{F_2}(\omega)\right]. \tag{3.41}$$

Ignoring the second order terms, the following relations are obtained:

$$\left|\delta(\omega)\right| \le \left|\delta_{F_2}(\omega)\right| + \left|\delta_{F_s'}(\omega)\right|. \tag{3.42}$$

Frequency range 3: $\omega_s \le \omega < \dfrac{2m\pi + \theta_{F_s}}{M}$.

In this frequency range, $G(\omega)=0$, $G_{H_p}(\omega)=G_{F_s'}(\omega)=1$ and $G_{F_2}(\omega)$ decreases from unity to zero as ω increases. In this case, (3.36) becomes

$$\delta(\omega)=G_{F_2}(\omega)+\delta_{F_2}(\omega)-\left[1+\delta_{F_s'}(\omega)\right]\left[1+\delta_{H_p}(\omega)\right]\left[G_{F_2}(\omega)+\delta_{F_2}(\omega)\right]. \quad (3.43)$$

Ignoring the second order terms, we have

$$\left|\delta(\omega)\right|\le\left|\delta_{F_s'}(\omega)\right|+\left|\delta_{H_p}(\omega)\right|. \quad (3.44)$$

Frequency range 4: $\dfrac{2m\pi+\theta_{F_s}}{M}\le\omega\le\pi$.

In this frequency range, $G(\omega)=G_{F_2}(\omega)=G_{H_p}(\omega)=0$. Hence, (3.36) is simplified to

$$\delta(\omega)=\delta_{F_2}(\omega)-\left[G_{F_s'}(\omega)+\delta_{F_s'}(\omega)\right]\delta_{H_p}(\omega)\delta_{F_2}(\omega). \quad (3.45)$$

Ignoring the second order terms, the following relation is obtained.

$$\delta(\omega)\approx\delta_{F_2}(\omega). \quad (3.46)$$

It can be seen from (3.38)–(3.40) and (3.46) that in the frequency ranges 1 and 4 the deviation of the overall filter is determined mainly by $H_p(z)$ and $F_2(z)$. In frequency range 2, $F_s(z^M)$ and $F_2(z)$ determine the passband ripple according to (3.42). Similarly, the subfilters $F_s(z^M)$ and $H_p(z)$ determine the stopband attenuation in frequency 3 according to (3.44). Similar conclusions can be drawn for Case B.

3.4.4 Design Procedures

Since the ripples of these subfilters compensate for each other in different frequency ranges, an iterated design procedure is employed to optimize one subfilter at a time

while using the other subfilters as prefilters. The following steps for Case A are proposed, which is applicable to Case B except for some minor modifications.

Step 1. Find a set of appropriate values of M, N, L_1, and K for $H_{r1}(z)$.

Step 2. Determine $H_p(z) = H_{r1}(z)F_1(z)$. The bandedges of $H_p(z)$ are given by (3.26) and (3.27). Set the stopband ripple of $H_p(z)$ to 85% of the passband ripple of $H(z)$ [21]. From our experience, the passband ripple is set to less than 10 dB. Using $H_{r1}(z)$ as a prefilter, $F_1(z)$ can be designed using any standard design technique for prefilter-equalizer based filters.

Step 3. Design $F_2(z)$ using the bandedges given by (3.22) and (3.23). Set the ripples of $F_2(z)$ to 85% of $H(z)$.

Step 4. Design $F_s(z)$ in the frequency range 2 and 3. Let the zero-phase frequency response of $F_s(z)$ be written as [88]

$$F_s(\omega) = \sum_i f_s(n)\,\mathrm{trig}(\omega, i) \tag{3.47}$$

where $\mathrm{trig}(\omega, i)$ is a proper trigonometric function depending on the type of the filter under design and $f_s(n)$ is the impulse response of $F_s(z)$. Similar notations are applied to the other subfilters. In frequency range 2, $F_s(z)$ needs to satisfy the following,

$$1-\delta_p - F_2(\omega) \le -F_2(\omega)H_p(\omega)\left[\sum_i f_s(n)\,\mathrm{trig}(M\omega, i)\right] \le 1+\delta_p - F_2(\omega). \tag{3.48}$$

In frequency range 3, we have

$$-\delta_s - F_2(\omega) \le -F_2(\omega)H_p(\omega)\left[\sum_i f_s(n)\,\mathrm{trig}(M\omega, i)\right] \le \delta_s - F_2(\omega). \tag{3.49}$$

Linear programming or any other optimization techniques may be used to optimize (3.48) and (3.49).

Step 5. Design $F_2(z)$ again by using the rest of subfilters, i.e., $F_s(z)$ and $H_p(z)$ as prefilters. The design equations can be derived similar to those in Step 4.

Repeat Step 4 by replacing $F_s(z)$ with $F_1(z)$ or $F_2(z)$ and using the other subfilters as prefilters, till there is no further improvement observed.

3.5 Examples and Comparisons

In this section, two examples are presented to demonstrate the advantages of the proposed structures for the design of lowpass FIR filters with narrow transition-width.

***Example* 1**

A lowpass filter is designed with passband edge at $\omega_p = 0.346\times 2\pi$ and stopband edge at $\omega_s = 0.347\times 2\pi$. The passband ripple is at most 0.01 and the stopband attenuation is at least 40 dB. Using the proposed method, the values of M, N, L_1 and K are found as follows, $M = 28$, $N = 7$, $L_1 = 2$ and $K = 1$. For $M = 28$, the prefilter $H_{r2}(z)$ is selected. To meet the overall specifications, the lengths for $F_s(z)$, $F_1(z)$ and $F_2(z)$ are 69, 23 and 71, respectively, where $F_2(z)$ is designed by the FRM approach with the interpolation factor to be 5. The magnitude responses of the subfilters and the overall filter using the proposed method are shown in Figs. 3.11–3.14.

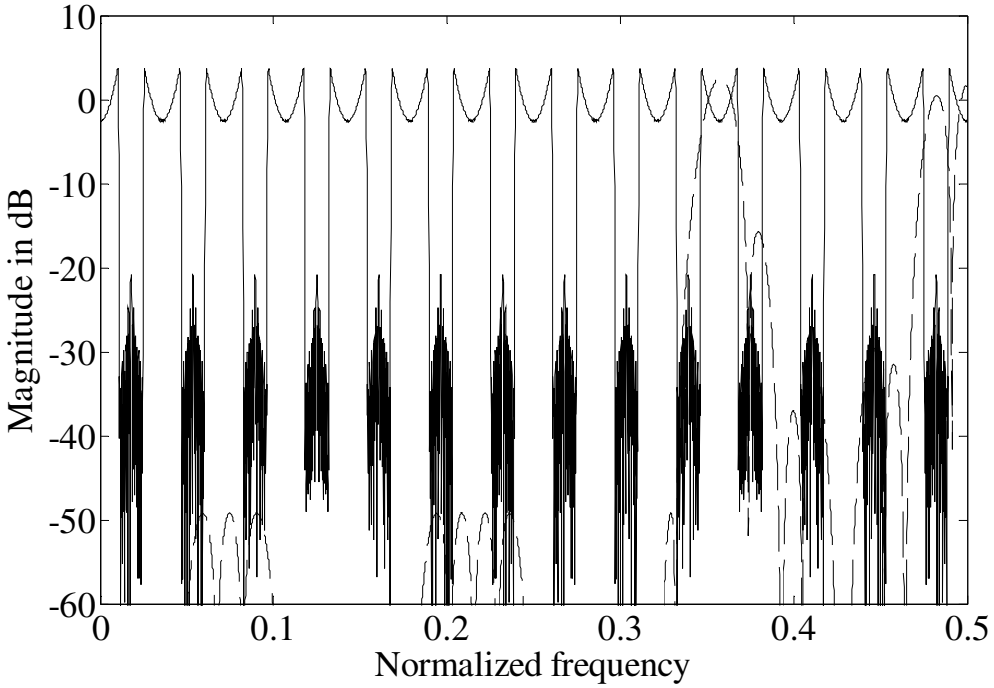

Figure 3.11 Magnitude responses of $F_s\left(z^M\right)$ (solid line) and $H_p\left(z\right)$ (dashed line) in example 1.

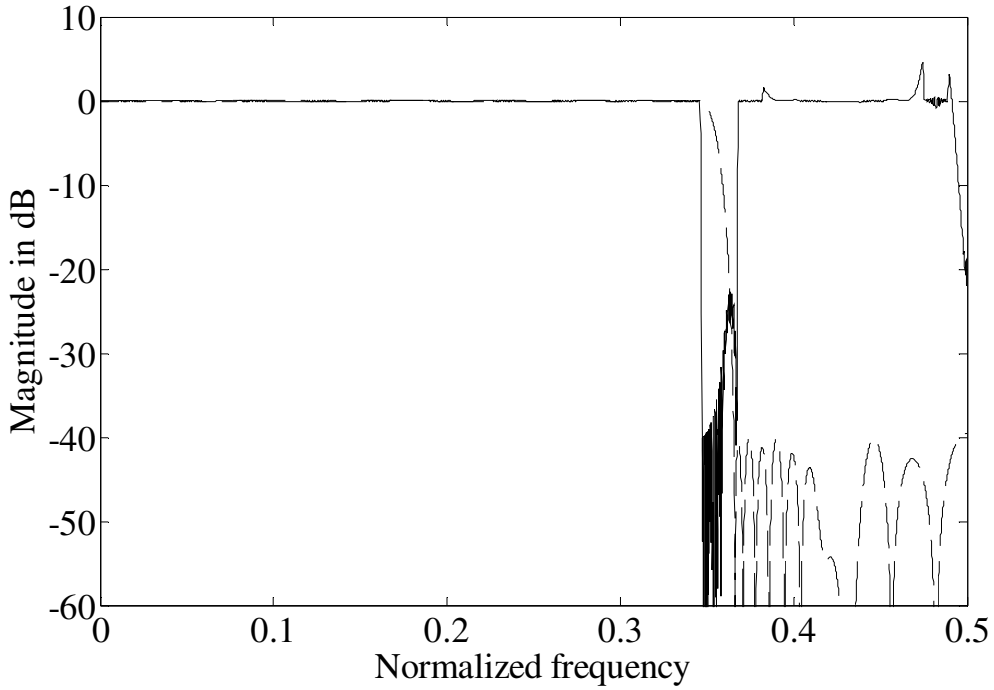

Figure 3.12 Magnitude responses of $C\left(z\right)$ (solid line) and $F_2\left(z\right)$ (dashed line) in example 1.

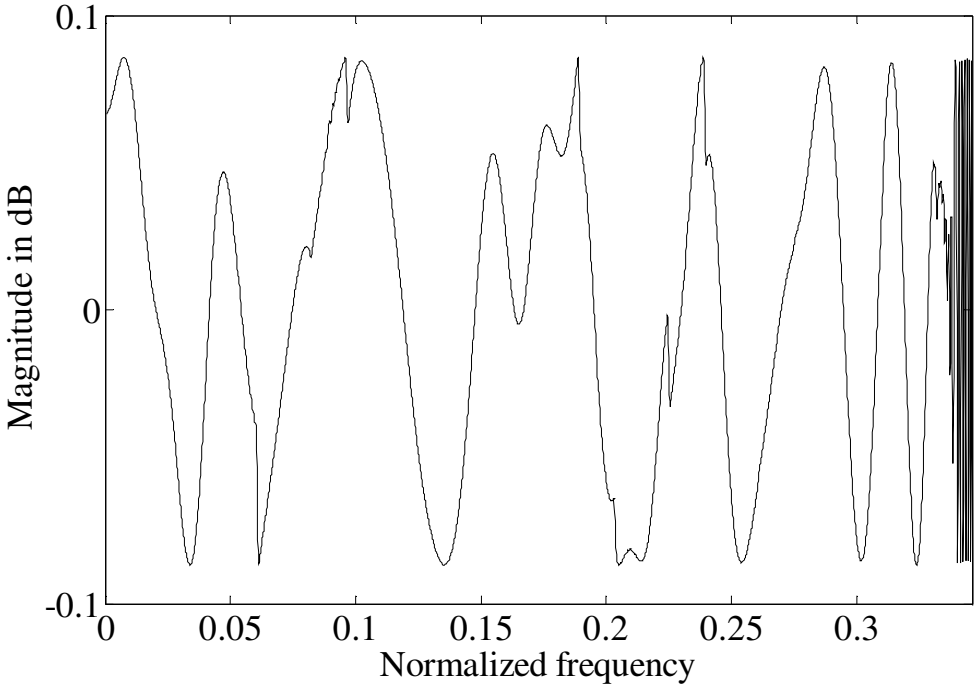

Figure 3.13 Magnitude response of the passband of the overall filter in example 1.

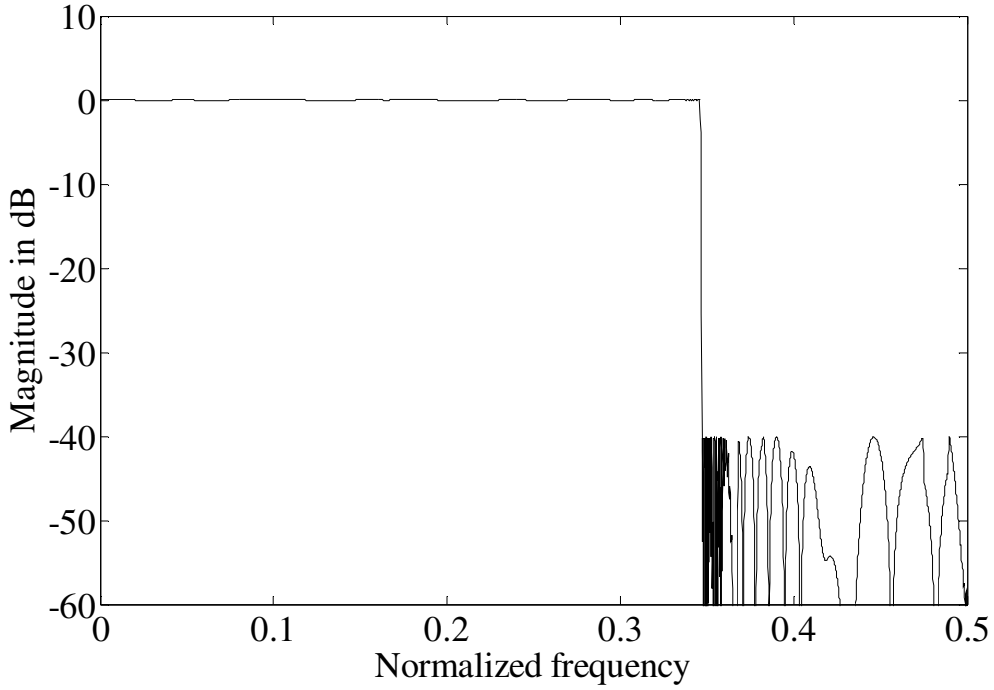

Figure 3.14 Magnitude response of the overall filter in example 1.

For comparison, the filter is also designed using other computationally efficient approaches. Using the single-stage FRM technique, the optimal interpolation factor M is 18, and the lengths for $F_s(z)$, $F_1(z)$ and $F_2(z)$ are 109, 69 and 75, respectively. To design such a filter with the IFIR-FRM approach, the total lengths for all subfilters are 202, and the two interpolation factors for the IFIR pair are 9 and 3, respectively. The two-stage FRM approach achieves a more efficient design with a total length of 179 for all subfilters. The two interpolation factors are 8 and 5 for the first and second stage, respectively. Using conventional design method, the estimated filter length is 1851. For clarity, the required number of multipliers, adders, and group delay of the overall filter using different design methods is summarized in Table 3.2. As indicated in Table 3.2, to implement the filter, 128 multipliers and 252 adders are required using the single-stage FRM approach, while using the proposed method only 84 multipliers and 169 adders are required which achieves more than 34% and 32% savings compared with the single-stage FRM technique. It is also clear that the proposed approach achieves more savings in the number of arithmetic operations than the IFIR-FRM approach which requires 103 multipliers and 200 adders, respectively, while the proposed filter has shorter group delay. The proposed method even outperforms the two-stage FRM approach in terms of hardware cost.

Table 3.2 Comparison of different design methods of example 1.

Design	Multipliers	Adders	Group delay
Conventional	925	1850	925
1-stage FRM	128	252	1009
2-stage FRM	92	178	1149
IFIR-FRM	103	200	1120
Proposed	84	169	1065

***Example* 2**

In this example, $H_{r1}(z)$ is used to design a sharp lowpass filter with the specification given by

$\omega_p = 0.3\times 2\pi$, $\omega_s = 0.301\times 2\pi$ (passband and stopband edges)

Maximum passband ripple: 0.01.

Minimum stopband attenuation: 40 dB.

Using the proposed method, the optimum values for M, N, L_1 and K are found to be 21, 7, 2 and 1, respectively. For $M = 21$, the structure of Case B is adopted. The lengths for $F_s(z)$, $F_1(z)$ and $F_2(z)$ are 93, 15 and 71, respectively. Figs. 3.15–3.18 show the magnitude responses of the subfilters and the overall filter using the proposed method.

The computational cost of different design methods for this example is summarized in Table 3.3. If the single-stage FRM technique is used, the optimum lengths for $F_s(z)$, $F_1(z)$ and $F_2(z)$ are 139, 49 and 69, respectively, with $M = 14$. The filter requires 130 multipliers. If the IFIR-FRM method is adopted, 104 multipliers are required with two interpolation factors of 7 and 3 for the IFIR pair. The two-stage FRM approach

produces a more efficient design which needs 92 multipliers with interpolation factor of 6 for both stages. Clearly, the proposed method achieves considerable reduction in the number of arithmetic operations compared with the original FRM and IFIR-FRM approach. Moreover, the proposed method even outperforms the two-stage FRM technique in terms of design complexity and group delay. If $F_2(z)$ is replaced by an FRM filter, the required number of arithmetic operations will be decreased further. It is interesting to compare the proposed method with the decoupling method in chapter 2. As shown in Table 3.3, the decoupling technique can achieve more arithmetic savings than the proposed method. However, the required delay elements are increased and the design complexity is also increased since 5 subfilters need to be designed in the decoupling technique.

Table 3.3 Comparison of different design methods of example 2.

Design	Multipliers	Adders	Group delay
Conventional	925	1850	925
1-stage FRM	130	256	1000
2-stage FRM	92	177	1105
IFIR-FRM	104	202	1084
Decoupling technique in chapter 2	88	169	1144
Proposed	91	186	1043

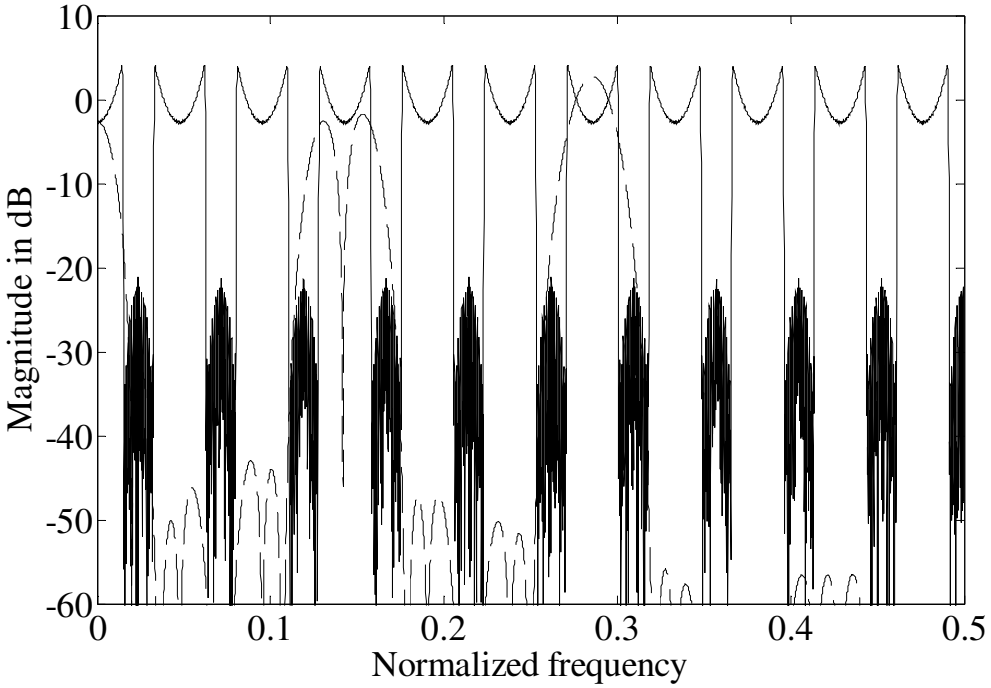

Figure 3.15 Magnitude responses of $F_s\left(z^M\right)$ (solid line) and $H_p\left(z\right)$ (dashed line) in the example 2.

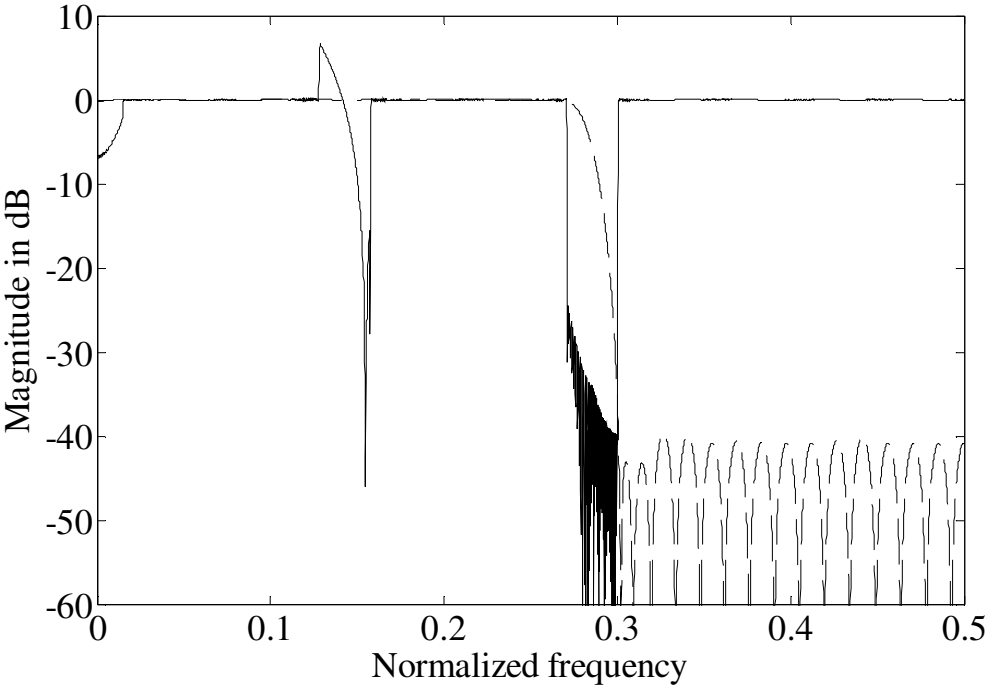

Figure 3.16 Magnitude responses of $C\left(z\right)$ (solid line) and $F_2\left(z\right)$ (dashed line) in example 2.

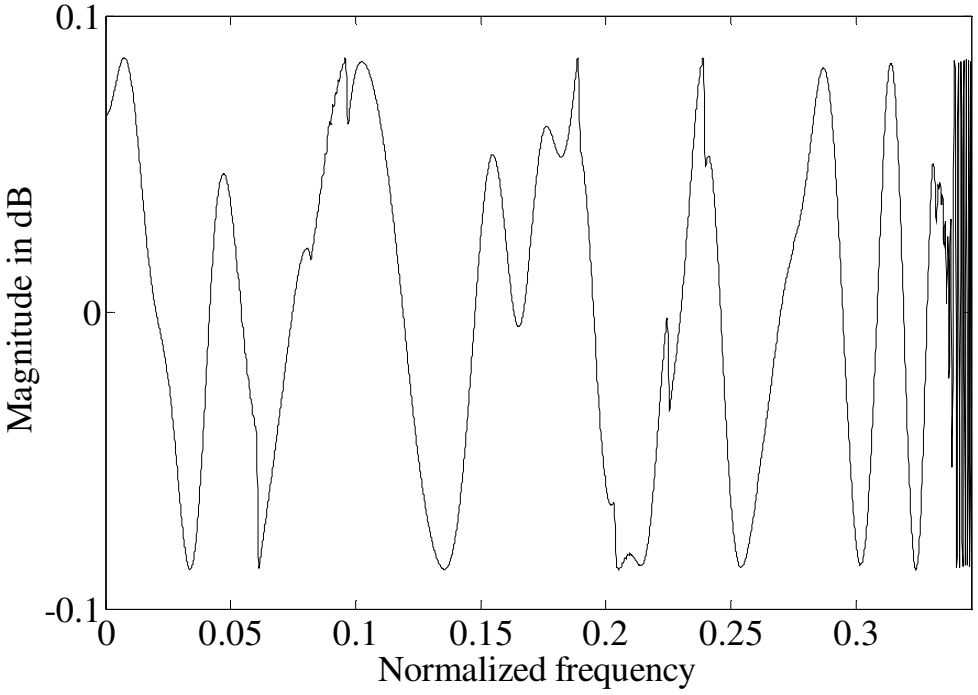

Figure 3.17 Magnitude response of the passband of the overall filter in example 2.

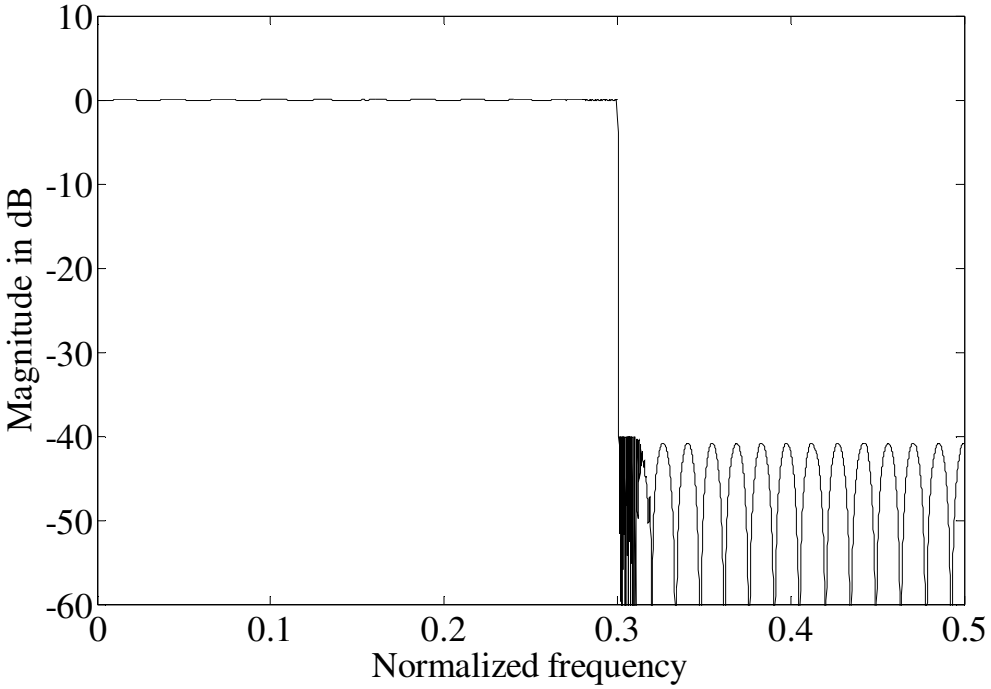

Figure 3.18 Magnitude response of the overall filter in example 2.

3.6 Summary

In this chapter, two modified FRM structures were introduced to reduce the computational complexity of FRM filters. The proposed structures utilize a prefilter-equalizer cascaded with the bandedge shaping filter. The cascade of the bandedge shaping filter and the prefilter-equalizer performs both the bandedge shaping and the masking tasks. New multiplication-free prefilters were developed for the design of the prefilter-equalizer. Results show that the proposed method achieves considerable savings in terms of arithmetic operations compared with the single-stage FRM, two-stage FRM and IFIR-FRM techniques. Furthermore, the group delays of the overall filters are shorter than those of the IFIR-FRM and two-stage FRM filters.

Chapter 4

FRM Filters Using Single Filter Frequency Masking Approach

4.1 Introduction

The FRM technique provides one of the most computationally efficient realizations for arbitrary bandwidth sharp FIR filters. The computational complexity of an FRM filter is determined by the model filter and the masking filters. Further improvements [22, 27, 28, 30–32] have been made to reduce the arithmetic complexity of FRM filters by realizing the bandedge shaping filter or masking filters using efficient FIR filter design methods. In this chapter, new structures to reduce the arithmetic complexity of FRM filters are proposed which employ a technique called single filter frequency masking (SFFM) filter [17–19]. The basic idea behind SFFM filters is to design IFIR filters using an identical model filter (with different periods) repeatedly to perform both the bandedge shaping and the masking tasks. The resulting filter has the form of

$$H(z) = \prod_{r=1}^{k} F\left(z^{M_r}\right) \tag{4.1}$$

where $M_1 > M_2 > ... > M_k$. By cascading interpolated subfilters $F\left(z^{M_r}\right)$ ($r \geq 2$) with $F\left(z^{M_1}\right)$, the unwanted passbands generated by $F\left(z^{M_1}\right)$ can be removed completely. A realization structure of lowpass SFFM filters is shown in Fig. 4.1. By mapping identical subfilters into a single hardware structure using folding transformation [81], the SFFM approach can achieve considerable savings in the number of multipliers and adders at the cost of increasing the number of delay elements.

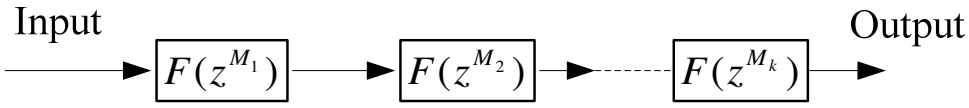

Figure 4.1 A realization of lowpass SFFM filters.

The SFFM technique is suitable for the design of FIR filters with narrow or wide passband. In this chapter, the SFFM and the FRM concepts are combined together to form new single frequency-response masking filter structures for the design of arbitrary bandwidth FIR filters. The proposed structures are extended to implement filters with varying specifications. Design examples show that the proposed approach achieves significant savings in terms of arithmetic operations at the price of increasing the delay elements.

The organization of this chapter is as follows. In Section 4.2, new structures are introduced for the design of lowpass filters. Design equations and procedures are discussed in Section 4.3. In Section 4.4, the structures are extended to design filters

with different specifications. Section 4.5 is dedicated to design examples. Conclusions are given in Section 4.6.

4.2 New Structures

Let a lowpass filter $H(z)$ be designed using the FRM approach. The passband and stopband edges of $H(z)$ are ω_p and ω_s, respectively. As discussed in Chapter 3, the transition-band of $H(z)$ is formed by one of the "teeth" of the bandedge shaping filter, as shown by the shaded areas in Figs. 3.3 and 3.5. If the same model filter with a reduced interpolation factor is cascaded to the bandedge shaping filter, those undesired frequency bands beyond ω_s may be removed while keeping the bandedge shaping (BS) tooth undistorted. For this reason, a modified FRM structure incorporating the SFFM technique is obtained as shown in Fig. 4.2 where *GD* is the total number of group delay of $\prod_{i=1}^{k} H_a\left(z^{M_r}\right)$ and GD_{G_c} is the number of group delay of $G_c(z)$.

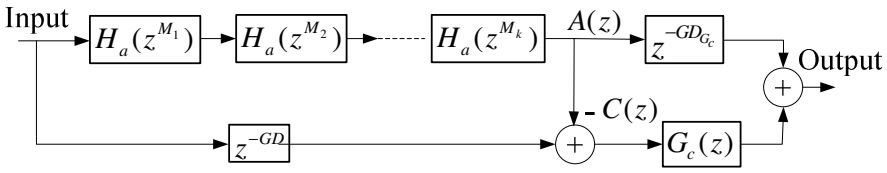

Figure 4.2 A realization structure for the proposed filter.

Fig. 4.3 illustrates the frequency responses of subfilters in Fig. 4.2. The design starts with a model filter $H_a\left(z\right)$ as shown in Fig. 4.3(a), $H_a^c\left(z\right)$ is the complement of $H_a\left(z\right)$. A new bandedge shaping filter $A\left(z\right)$ is formed by cascading the same model filter (with different interpolation factors) repeatedly, with $H_a\left(z^{M_1}\right)$, as shown in Fig. 4.3(b)–(d). $C\left(z\right)$ is the complement of $A\left(z\right)$. If $C\left(z\right)$ is cascaded with another

masking filter $G_c(z)$, and the outputs of $A(z)$ and $G_c(z)$ are added, we get the overall filter $H(z)$, as shown in Figs. 4.3(e) and 4.3(f). By mapping all the identical subfilters into a single hardware structure, the required number of multipliers and adders for implementation of $H(z)$ can be greatly decreased. In some cases, the complementary filter of $H_a\left(z^{M_r}\right)$ ($r \geq 2$), denoted as $H_a^c\left(z^{M_r}\right)$, instead of $H_a\left(z^{M_r}\right)$ itself, may be used to cascade with $H_a\left(z^{M_1}\right)$ to remove the undesired passbands. $H_a^c\left(z^{M_r}\right)$ can be easily obtained from the implementation of $H_a\left(z^{M_r}\right)$ as shown in Fig. 4.4, where the filter is of even order. $y^c(n)$ is the complementary output.

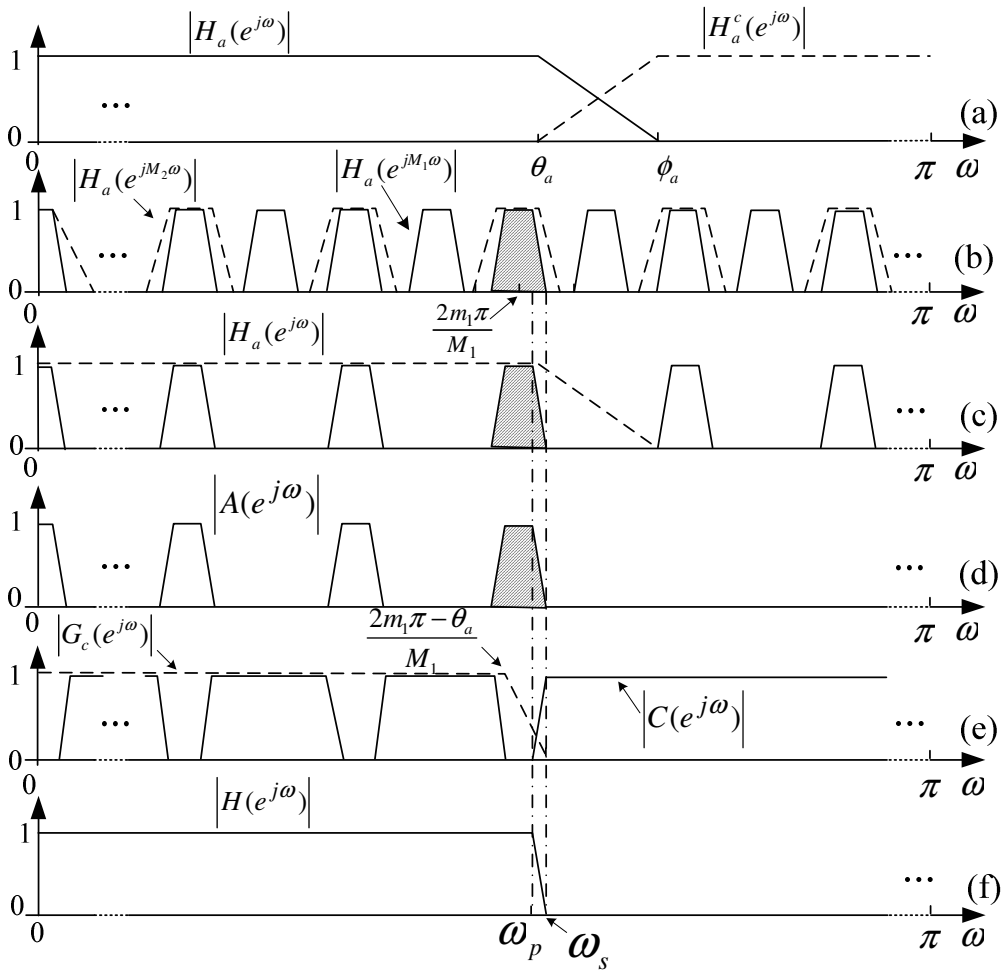

Figure 4.3 Frequency responses of subfilters and the overall filter in the new structure.

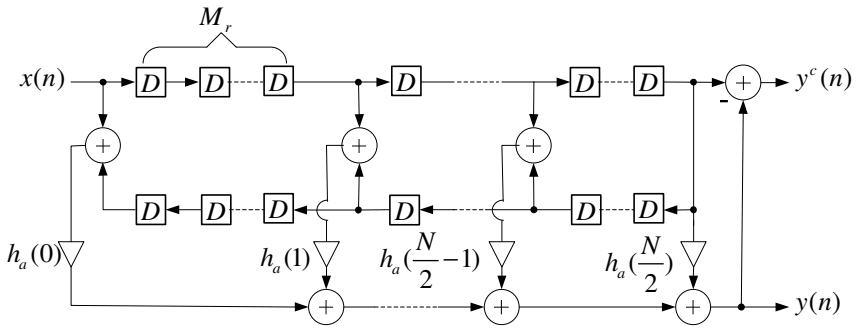

Figure 4.4 Implementation of an FIR filter with complementary output.

As a result, the transfer function of the overall filter is expressed as

$$H(z) = z^{-GD_{G_c}} \prod_{r=1}^{k} H_r(z) + \left[z^{-GD} - \prod_{r=1}^{k} H_r(z) \right] G_c(z) \tag{4.2}$$

where $H_1(z)$ is $H_a\left(z^{M_1}\right)$, $H_r(z)$ ($r \geq 2$) is either $H_a\left(z^{M_r}\right)$ or $H_a^c\left(z^{M_r}\right)$ $\left(M_1 > M_2 > ... > M_k\right)$, GD and GD_{G_c} are the numbers of group delay of $\prod_{r=1}^{k} H_r(z)$ and $G_c(z)$, respectively.

The structure in Fig. 4.2 is suitable for designing filters whose bandedges are determined by $H_a\left(z^{M_1}\right)$. This case is denoted as Case A. The case where the transition-band is determined by $H_a^c\left(z^{M_1}\right)$ is denoted as Case B and its realization structure is shown in Fig. 4.5. The transfer function for Case B is given by

$$H(z) = \left[z^{-GD} - \prod_{r=1}^{k} H_r(z) \right] G_c(z) \tag{4.3}$$

The frequency responses of subfilters in Fig. 4.5 are sketched in Fig. 4.6. In Case B, the unwanted passbands to left of the BS tooth are removed by cascading $H_r(z)$ ($r \geq 2$) to $H_a\left(z^{M_1}\right)$, as shown in Figs. 4.5, 4.6(b) and 4.6(c). The resulting filter is denoted as

$A(z)$, as shown in Fig. 4.6(d). A new bandedge shaping filter $C(z)$ is formed by taking the complement of $A(z)$, as shown in Figs. 4.5 and 4.6(e). The overall filter $H(z)$ is obtained by cascading a masking filter $G_c(z)$ to $C(z)$, as shown in Figs 4.5 and 4.6(f).

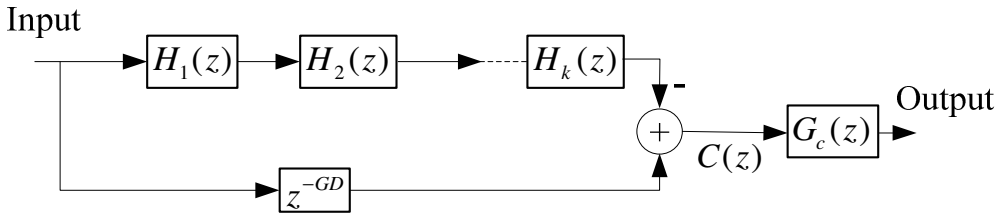

Figure 4.5 A realization structure for Case B.

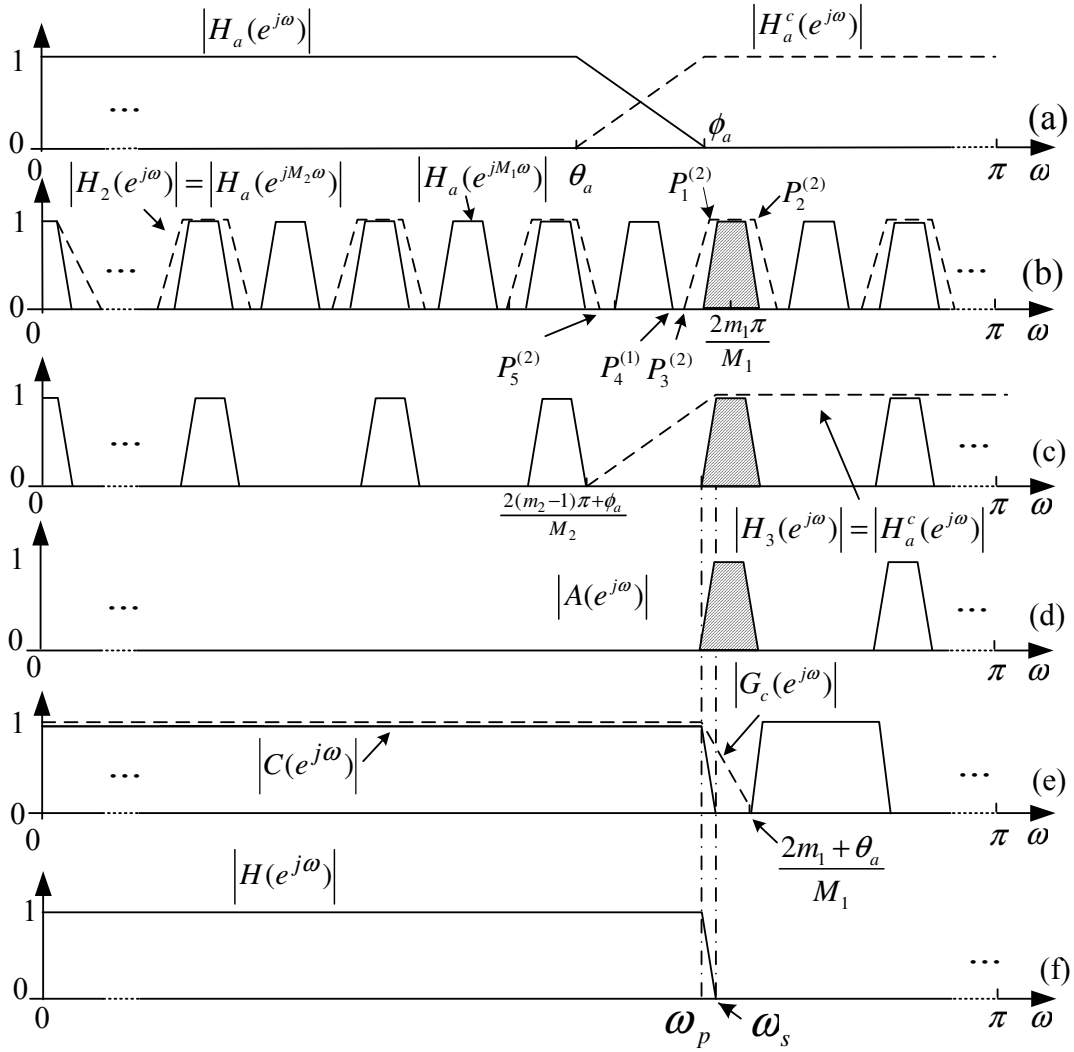

Figure 4.6 Frequency responses for Case B.

It should be noted that for a given M_1, under certain circumstances, the undesired passbands may not be removed completely by $\prod_{r=2}^{k} H_r(z)$, i.e., there is still unwanted frequency components left in the stopband (or the passband) for Case A (or Case B). In this case, a simple extra masking filter $H_e(z)$ is required to remove the rest undesired frequency components. Fig. 4.7 and Fig. 4.8 show the resulting realization structures of $H(z)$ for Case A and Case B, respectively.

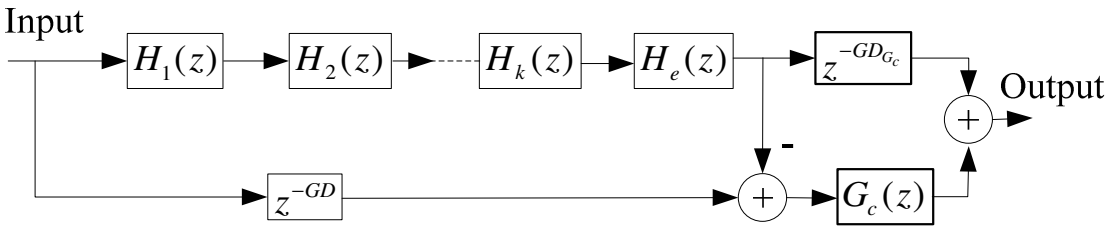

Figure 4.7 Filter structure with an extra masking filter for Case A.

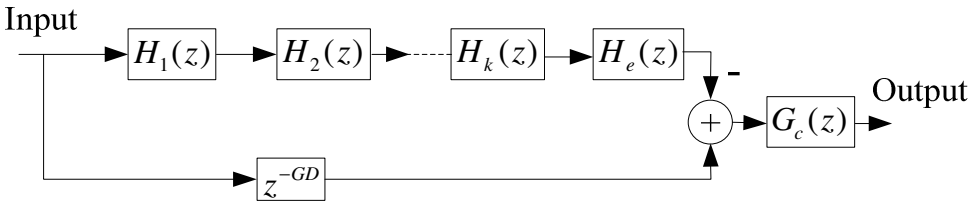

Figure 4.8 Filter structure with an extra masking filter for Case B.

4.3 Filter Design

4.3.1 Design Equations

To synthesize $H(z)$, lowpass or highpass model filters can be used to perform the bandedge shaping. In this section, equations for the design of a lowpass filter using lowpass model filters with the structures in Fig. 4.2 and 4.5 are derived. The same

procedure can be easily applied to structures in Fig. 4.7 and 4.8.

Let the passband and stopband edges of $H_a(z)$ be θ_a and ϕ_a, respectively. Let the bandedges of $G_c(z)$ be θ_{G_c} and ϕ_{G_c}, respectively. To determine the bandedges of $H_a(z)$, it can be shown that [21]

$$\omega_p = \begin{cases} \dfrac{2m_1\pi + \theta_a}{M}, & \text{for Case A} \\ \dfrac{2m_1\pi - \phi_a}{M}, & \text{for Case B} \end{cases} \tag{4.4}$$

and

$$\omega_s = \begin{cases} \dfrac{2m_1\pi + \phi_a}{M}, & \text{for Case A} \\ \dfrac{2m_1\pi - \theta_a}{M}, & \text{for Case B} \end{cases} \tag{4.5}$$

where m_1 is an integer. To ensure that (4.4) and (4.5) yield a solution with $0 < \theta_a < \phi_a < \pi$, two sets of equations are given for Case A and Case B, respectively. For Case A, we have

$$m_1 = \left\lfloor \frac{\omega_p M_1}{2\pi} \right\rfloor \tag{4.6}$$

$$\theta_a = \omega_p M_1 - 2m_1\pi \tag{4.7}$$

$$\phi_a = \omega_s M_1 - 2m_1\pi \tag{4.8}$$

where $\lfloor x \rfloor$ denotes the largest integer less than or equal to x. For Case B, we have

$$m_1 = \left\lceil \frac{\omega_s M}{2\pi} \right\rceil \tag{4.9}$$

$$\theta_a = 2m_1\pi - \omega_s M_1 \tag{4.10}$$

$$\phi_a = 2m_1\pi - \omega_p M_1 \tag{4.11}$$

where $\lceil x \rceil$ denotes the smallest integer larger than or equal to x. The bandedges of $G_c(z)$ for Case A, as shown in Fig. 4.3(e), are given by

$$\theta_{G_c} = \frac{2m_1\pi - \theta_a}{M_1} \tag{4.12}$$

$$\phi_{G_c} = \omega_s \tag{4.13}$$

For Case B, as shown in Fig. 4.6(d), we have

$$\theta_{G_c} = \omega_p \tag{4.14}$$

$$\phi_{G_c} = \frac{2m_1\pi + \theta_a}{M_1} \tag{4.15}$$

4.3.2 Determination of M_i

The computational complexity of the overall filter is determined by $H_a(z)$, $G_c(z)$ and $H_e(z)$. A cost function $C(\Delta)$ is defined to evaluate the complexity of the overall filter:

$$C(\Delta) = \begin{cases} \dfrac{1}{\Delta H_a} + \dfrac{1}{\Delta G_c}, & \text{for structures in Fig. (4.2) and (4.5)} \\ \dfrac{1}{\Delta H_a} + \dfrac{1}{\Delta G_c} + \dfrac{1}{\Delta H_e}, & \text{for structures in Fig. (4.7) and (4.8)} \end{cases} \tag{4.16}$$

where ΔH_a, ΔG_c and ΔH_e denote the transition-widths of $H_a(z)$, $G_c(z)$ and $H_e(z)$, respectively. For a given M_1, ΔH_a and ΔG_c are determined by (4.6)–(4.11) and (4.12)–(4.15), respectively. ΔH_e can be evaluated for a set of M_r (the conditions for searching M_r ($r \geq 2$) will be derived later). Therefore, an exhaustive search can be made to obtain the optimal set of M_r which minimizes (4.16).

For a given M_1, the conditions for the determination of M_r ($r \geq 2$) are proposed follows.

Case A conditions

To keep the bandedge shaping tooth undistorted and to remove the first unwanted passband beyond ω_s , there must be a "masking band" to perform the tasks as shown in Fig. 4.9, where $H_a\left(z^{M_1}\right)$ is cascaded with $H_a\left(z^{M_2}\right)$, and as shown in Fig. 4.10, where $H_a\left(z^{M_1}\right)$ is cascaded with $H_a^c\left(z^{M_2}\right)$. The bandedges of the masking band must satisfy certain conditions. Five frequency points, P_1 to P_5, as indicated in Figs. 4.9 and 4.10, are helpful in deriving the conditions. The superscript (2) for $P_1^{(2)}$ denotes that P_1 is on $\left|H_a\left(e^{jM_2\omega}\right)\right|$ (or $\left|H_a^c\left(e^{jM_2\omega}\right)\right|$). The same denotation is applied to other points, i.e., $P_n^{(i)}$ is on $\left|H_a\left(e^{jM_i\omega}\right)\right|$ (or $\left|H_a^c\left(e^{jM_i}\right)\right|$). In Fig. 4.9, $P_n^{(i)}$ ($n = 1,\ 2,\ ...,\ 5$, $i = 1,\ 2$) are defined as follows. $P_1^{(2)}$ and $P_2^{(2)}$ are the left and right passband edges of the masking band of $\left|H_a\left(e^{jM_2\omega}\right)\right|$, respectively. $P_3^{(2)}$ is the right stopband edge of the masking band. $P_4^{(1)}$ is the first stopband edge beyond ω_s. $P_5^{(2)}$ is the left stopband edge of the band next to the masking band. $P_4^{(2)}$ is the first stopband edge beyond ω_s for the cascade of $H_a\left(z^{M_1}\right)$ and $H_a\left(z^{M_2}\right)$. Similar denotations are also applied to other $P_n^{(i)}$ in the following discussion.

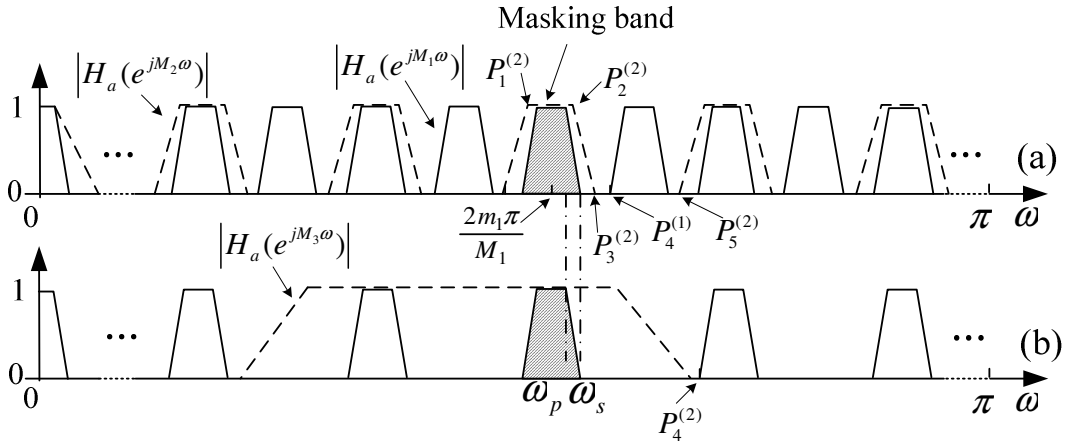

Figure 4.9 Frequency points satisfying conditions for the cascade of $H_a\left(z^{M_1}\right)$ and $H_a\left(z^{M_2}\right)$.

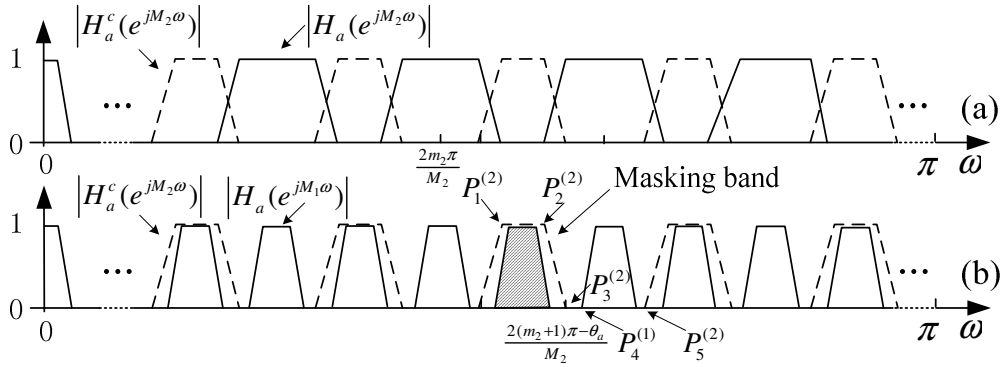

Figure 4.10 Illustration of the cascade of $H_a\left(z^{M_1}\right)$ and $H_a^c\left(z^{M_2}\right)$.

From Figs. 4.9(a) and 4.10(b), it is easy to show that

$$P_1^{(2)} \le \frac{2m_1\pi - \theta_a}{M_1} \tag{4.17}$$

and

$$\omega_p \le P_2^{(2)} \ . \tag{4.18}$$

If $P_1^{(2)}$ and $P_2^{(2)}$ are on the first passband of $\left|H_a\left(e^{jM_2\omega}\right)\right|$, $P_1^{(2)}$ in (4.17) is set to 0. In this case, (4.17) is always true. Otherwise, $P_1^{(2)}$ is given by

$$P_1^{(2)} = \begin{cases} \dfrac{2m_2\pi - \theta_a}{M_2}, \text{ for } H_a\left(z^{M_2}\right), \\ \dfrac{2m_2\pi + \phi_a}{M_2}, \text{ for } H_a^c\left(z^{M_2}\right). \end{cases} \tag{4.19}$$

where m_2 is a non-negative integer. $P_2^{(2)}$ in (4.18) is written as

$$P_2^{(2)} = \begin{cases} \dfrac{2m_2\pi + \theta_a}{M_2}, \text{ for } H_a\left(z^{M_2}\right), \\ \dfrac{2\left(m_2+1\right)\pi - \phi_a}{M_2}, \text{ for } H_a^c\left(z^{M_2}\right). \end{cases} \tag{4.20}$$

To remove the first unwanted passband, as shown in Fig. 4.9(a), we have

$$\omega_s \le P_3^{(2)} \le P_4^{(1)}. \tag{4.21}$$

$P_3^{(2)}$ is given by

$$P_3^{(2)} = \begin{cases} \dfrac{2m_2\pi + \phi_a}{M_2}, \text{ for } H_a\left(z^{M_2}\right), \\ \dfrac{2\left(m_2+1\right)\pi - \theta_a}{M_2}, \text{ for } H_a^c\left(z^{M_2}\right). \end{cases} \tag{4.22}$$

$P_4^{(1)}$ is given by

$$P_4^{(1)} = \frac{2\left(m_1+1\right)\pi - \phi_a}{M_1}. \tag{4.23}$$

M_2 is selected to satisfy (4.17), (4.18), and (4.21).

For M_r ($r > 2$), (4.17) , (4.18) and (4.21) are generalized as

$$\begin{cases} P_1^{(r)} \le \dfrac{2m_1\pi - \theta_a}{M_1} \\ P_2^{(r)} \ge \omega_p \end{cases} \tag{4.24}$$

and

$$\omega_s \le P_3^{(r)} \le P_4^{(r-1)}. \tag{4.25}$$

M_r ($r > 2$) are selected to satisfy (4.24) and (4.25). $P_1^{(r)}$, $P_2^{(r)}$, $P_3^{(r)}$ and $P_4^{(r-1)}$ ($r > 2$) in (4.24) and (4.25) are derived as follows.

$P_1^{(r)}$ equals to 0, if $P_1^{(r)}$ is on the first passband of $\left|H_a\left(e^{jM_r\omega}\right)\right|$; otherwise, $P_1^{(r)}$ is given by

$$P_1^{(r)} = \begin{cases} \dfrac{2m_i\pi - \theta_a}{M_i}, \text{ for } H_a\left(z^{M_r}\right), \\ \dfrac{2m_i\pi + \phi_a}{M_i}, \text{ for } H_a^c\left(z^{M_r}\right). \end{cases} \tag{4.26}$$

where m_i is a non-negative integer. $P_2^{(r)}$ is expressed as

$$P_2^{(r)} = \begin{cases} \dfrac{2m_i\pi + \theta_a}{M_i}, \text{ for } H_a\left(z^{M_r}\right), \\ \dfrac{2\left(m_i+1\right)\pi - \phi_a}{M_i}, \text{ for } H_a^c\left(z^{M_r}\right). \end{cases} \tag{4.27}$$

$P_3^{(r)}$ is given by

$$P_3^{(r)} = \begin{cases} \dfrac{2m_i\pi + \phi_a}{M_i}, \text{ for } H_a\left(z^{M_r}\right), \\ \dfrac{2\left(m_i+1\right)\pi - \theta_a}{M_i}, \text{ for } H_a^c\left(z^{M_r}\right). \end{cases} \tag{4.28}$$

The value of $P_4^{(r-1)}$ ($r > 2$) depends on the location of $P_5^{(r-1)}$, as shown in Figs. 4.9(b) and 4.11(b). $P_4^{(2)}$ is derived as follows.

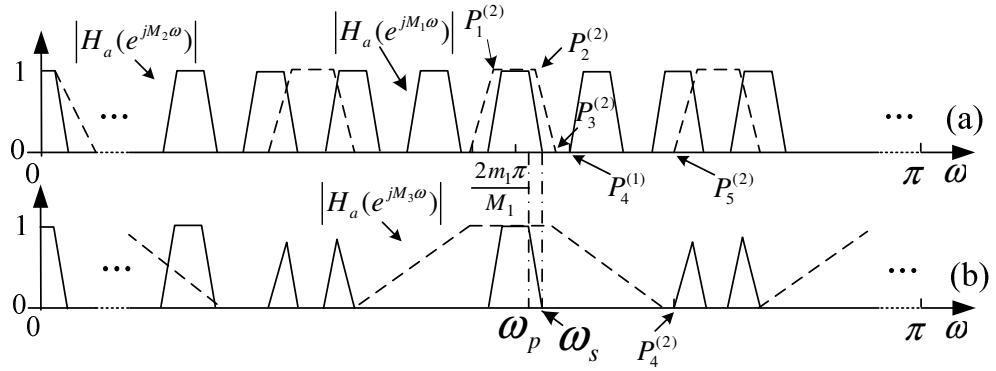

Figure 4.11 Illustration of the cascade of $H_a\left(z^{M_1}\right)$ and $H_a\left(z^{M_2}\right)$ when $P_5^{(2)}$ occurs at the passband of $H_a\left(z^{M_1}\right)$.

For the case where $H_a\left(z^{M_1}\right)$ is cascaded with $H_a\left(z^{M_r}\right)$ ($r>2$), if $P_5^{(2)}$ falls into the stopband of $H_a\left(z^{M_1}\right)$, as shown in Fig. 4.9(b), we get

$$\frac{2\left(m_1+t_1\right)\pi+\phi_a}{M_1} \le P_5^{(2)} \le \frac{2\left(m_1+t_1+1\right)\pi-\phi_a}{M_1} \ . \tag{4.29}$$

where t_1 is a non-negative integer. If the masking band is the last band of $H_a(z^{M_2})$ or $M_2=1$, $P_5^{(2)}$ is set to π. Otherwise, $P_5^{(2)}$ is given by

$$P_5^{(2)} = \frac{2\left(m_2+1\right)\pi-\phi_a}{M_2}. \tag{4.30}$$

Therefore, $P_5^{(2)}$ can be expressed as

$$P_5^{(2)} = \min\left[\frac{2\left(m_2+1\right)\pi-\phi_a}{M_2}, \pi\right]. \tag{4.31}$$

where $\min[x_1, x_2]$ denotes the minimum value among x_1 and x_2. In this case, $P_4^{(2)}$ is given by

$$P_4^{(2)} = \begin{cases} = \dfrac{2(m_1 + t_1 + 1)\pi - \phi_a}{M_1}, & \text{for } \dfrac{2(m_1 + t_1 + 1)\pi - \phi_a}{M_1} < \pi, \\ \pi, & \text{for } \dfrac{2(m_1 + t_1 + 1)\pi - \phi_a}{M_1} > \pi. \end{cases} \tag{4.32}$$

According to (4.32), $P_4^{(2)}$ can be expressed as

$$P_4^{(2)} = \min\left[\frac{2(m_1 + t_1 + 1)\pi - \phi_a}{M_1}, \pi\right]. \tag{4.33}$$

If $P_5^{(2)}$ occurs at the passband or the transition-band of $H_a\left(z^{M_1}\right)$, as shown in Fig. 4.11(a), we have

$$P_4^{(2)} = P_5^{(2)} = \min\left[\frac{2(m_2 + 1)\pi - \phi_a}{M_2}, \pi\right]. \tag{4.34}$$

Similarly, for the case where $H_a^c\left(z^{M_2}\right)$ is cascaded with $H_a\left(z^{M_1}\right)$, when $P_5^{(2)}$ falls into the stopband of $H_a\left(z^{M_1}\right)$, as shown in Fig. 4.10(b), $P_4^{(2)}$ is given by (4.33). Otherwise, we have

$$P_4^{(2)} = P_5^{(2)} = \min\left[\frac{2(m_2 + 1)\pi + \theta_a}{M_2}, \pi\right]. \tag{4.35}$$

For generalization,

a) when $H_a\left(z^{M_r}\right)$ ($r > 2$) is cascaded with $H_a\left(z^{M_1}\right)$, If $P_5^{(r-1)}$ falls into stopbands of $H_a\left(z^{M_u}\right)$ ($u \in [1, 2, ..., i-1]$) or $H_a^c\left(z^{M_u}\right)$ ($u \in [2, 3, ..., \mathrm{r}-1]$), we have

$$\begin{cases} \dfrac{2(m_u+t_u)\pi+\phi_a}{M_u} \le P_5^{(r-1)} \le \min\left[\dfrac{2(m_u+t_u+1)\pi-\phi_a}{M_u},\pi\right], \\ \text{for } H_a\left(z^{M_u}\right),\ \mathrm{u}\in[1,\ 2,\ ...,\ r-1] \\ \text{or} \\ \dfrac{2(m_u+t_u)\pi-\theta_a}{M_u} \le P_5^{(r-1)} \le \min\left[\dfrac{2(m_u+t_u)\pi+\theta_a}{M_u},\pi\right] \\ \text{for } H_a^c\left(z^{M_u}\right),\ \mathrm{u}\in[2,\ 3,\ ...,\ r-1] \end{cases} \tag{4.36}$$

where $P_5^{(r-1)} = \min\left[\dfrac{2(m_r+1)\pi-\phi_a}{M_r},\pi\right]$, m_u and t_u are non-negative integers.

Let U be a real set of the upper bounds in (4.36). We have

$$U = \left[\min\left[\frac{2(m_u+t_u+1)\pi-\phi_a}{M_u},\pi\right]\left(\text{or}\min\left[\frac{2(m_u+t_u)\pi+\theta_a}{M_u},\pi\right]\right)\right] \quad (\mathrm{u}\in[1,\ 2,\ ...,\ r-1]). \tag{4.37}$$

$P_4^{(r-1)}$ is given by

$$P_4^{(r-1)} = \max[U] \tag{4.38}$$

where $\max[x_1, x_2, ..., x_i]$ denotes the maximum value among x_1, x_2, …, x_i.

Otherwise, we have

$$P_4^{(r-1)} = P_5^{(r-1)} = \min\left[\frac{2(m_r+1)\pi-\phi_a}{M_r},\pi\right]. \tag{4.39}$$

b) when $H_a^c\left(z^{M_r}\right)$ ($r>2$) is cascaded with $H_a\left(z^{M_1}\right)$, if $P_5^{(r-1)}$ satisfies (4.36), $P_4^{(r-1)}$ is given by (4.39). Otherwise, we get

$$P_4^{(r-1)} = P_4^{(r-1)} = \min\left[\frac{2(m_r+1)\pi+\theta_a}{M_r},\pi\right]. \tag{4.40}$$

Case B conditions

For case B, similar conditions can be derived as follows. If $H_a\left(z^{M_2}\right)$ is cascaded with $H_a\left(z^{M_1}\right)$, as shown in Fig. 4.6(b), we have

$$\begin{cases} P_1^{(2)} \le \omega_s \\ P_1^{(2)} = \dfrac{2m_2\pi - \theta_a}{M_2} \end{cases} \tag{4.41}$$

where m_2 is a non-negative integer, and

$$P_2^{(2)} \ge \frac{2m_1\pi + \theta_a}{M_1}. \tag{4.42}$$

If $P_2^{(2)}$ is on the last passband (in the range of $[0,\ \pi]$) of $\left|H_a\left(e^{jM_2\omega}\right)\right|$ and M_2 is even, $P_2^{(2)}$ is set to π. Otherwise, we have

$$P_2^{(2)} = \frac{2m_2\pi + \theta_a}{M_2}. \tag{4.43}$$

To remove the unwanted passbands at the frequency lower than ω_p, we have

$$\begin{cases} \omega_p \ge P_3^{(2)} \ge P_4^{(1)} \\ P_4^{(1)} = \dfrac{2\left(m_1 - 1\right)\pi + \phi_a}{M_1} \\ P_3^{(2)} = \dfrac{2m_2\pi - \phi_a}{M_2}. \end{cases} \tag{4.44}$$

For the case where $H_a^c\left(z^{M_2}\right)$ is cascaded with $H_a\left(z^{M_1}\right)$, as shown in Fig. 4.12(b), we have

$$\begin{cases} P_1^{(2)} \le \omega_s \\ P_1^{(2)} = \dfrac{2m_2\pi + \phi_a}{M_2} \end{cases} \tag{4.45}$$

and

$$\begin{cases} P_2^{(2)} \geq \dfrac{2m_1\pi + \theta_a}{M_1} \\ P_2^{(2)} = \dfrac{2(m_2+1)\pi - \phi_a}{M_2} \end{cases} \tag{4.46}$$

where $P_2^{(2)} = \pi$, if $P_2^{(2)}$ is on the last passband of $\left|H_a^c\left(e^{jM_2\omega}\right)\right|$ and M_2 is odd. To remove the unwanted passband located to the left of ω_p, we get

$$\begin{cases} \omega_p \geq P_3^{(2)} \geq P_4^{(1)} \\ P_4^{(1)} = \dfrac{2(m_1-1)\pi + \phi_a}{M_1}. \\ P_3^{(2)} = \dfrac{2m_2\pi + \theta_a}{M_2}. \end{cases} \tag{4.47}$$

M_2 is selected to satisfy (4.41), (4.42) and (4.44) (or (4.45), (4.46) and (4.47)).

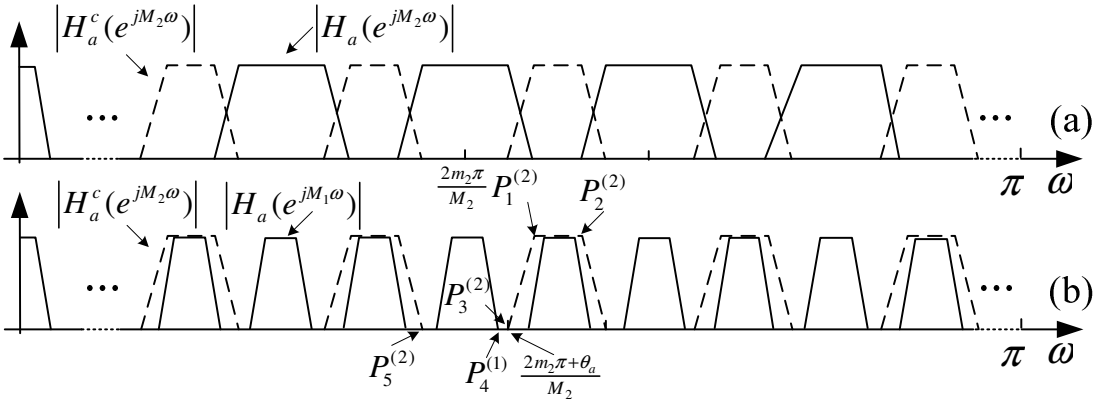

Figure 4.12 Illustration of the cascade of $H_a^c\left(z^{M_2}\right)$ and $H_a\left(z^{M_1}\right)$ for Case B.

To determine M_r ($r > 2$), by generalizing (4.41)–(4.47), we get

$$P_1^{(r)} \leq \omega_s, \tag{4.48}$$

$$P_2^{(r)} \geq \frac{2m_1\pi + \theta_a}{M_1} \tag{4.49}$$

and

$$\omega_p \geq P_3^{(r)} \geq P_4^{(r-1)}. \tag{4.50}$$

M_r ($r > 2$) are selected to satisfy (4.48), (4.49) and (4.50). $P_1^{(r)}$ in (4.48) is given by

$$P_1^{(r)} = \begin{cases} \dfrac{2m_r\pi - \theta_a}{M_r}, \text{ for } H_a\left(z^{M_r}\right), \\ \dfrac{2m_r\pi + \phi_a}{M_r}, \text{ for } H_a^c\left(z^{M_r}\right) \end{cases} \tag{4.51}$$

where m_r is a non-negative integer. $P_2^{(r)}$ in (4.49) equals to π, if it is on the last passband (in the range of $[0,\ \pi]$) of $\left|H_a\left(e^{jM_r\omega}\right)\right|$ (or $\left|H_a^c\left(e^{jM_r\omega}\right)\right|$) when M_r is even (or odd). Otherwise, we have

$$P_2^{(r)} = \begin{cases} \dfrac{2m_r\pi + \theta_a}{M_r}, \text{ for } H_a\left(z^{M_r}\right), \\ \dfrac{2\left(m_r+1\right)\pi - \phi_a}{M_r}, \text{ for } H_a^c\left(z^{M_r}\right). \end{cases} \tag{4.52}$$

$P_3^{(r)}$ in (4.50) is given by

$$P_3^{(i)} = \begin{cases} \dfrac{2m_r\pi - \phi_a}{M_r}, \text{ for } H_a\left(z^{M_r}\right), \\ \dfrac{2m_r\pi + \theta_a}{M_r}, \text{ for } H_a^c\left(z^{M_r}\right). \end{cases} \tag{4.53}$$

$P_4^{(r-1)}$ in (4.50) is determined by the location of $P_5^{(r-1)}$. If $P_5^{(r-1)}$ falls into stopbands of $H_a\left(z^{M_u}\right)$ ($u \in [1,\ 2,\ ...,\ r-2]$) or $H_a^c\left(z^{M_u}\right)$ ($u \in [2,\ 3,\ ...,\ r-2]$) as shown in Figs. 4.6(b) or 4.12 (b), respectively, we have

$$\begin{cases} \dfrac{2(m_u - t_u - 1)\pi + \phi_a}{M_u} \le P_5^{(r-1)} \le \dfrac{2(m_u - t_u)\pi - \phi_a}{M_u}, \\ \text{for } H_a\left(z^{M_u}\right),\ u \in [1,\ 2,\ ...,\ r-1] \\ \text{or} \\ \max\left[0,\ \dfrac{2(m_u - t_u)\pi - \theta_a}{M_u}\right] \le P_5^{(r-1)} \le \dfrac{2(m_u - t_u)\pi + \theta_a}{M_u}, \\ \text{for } H_a^c\left(z^{M_u}\right),\ u \in [2,\ 3,\ ...,\ r-1] \end{cases} \tag{4.54}$$

where t_u is a non-negative integer. $P_5^{(r-1)}$ is given by

$$P_5^{(r-1)} = \begin{cases} \dfrac{2(m_r - 1)\pi + \phi_a}{M_r}, \text{ for } H_a\left(z^{M_r}\right), \\ \max\left[0,\ \dfrac{2m_r\pi - \theta_a}{M_r}\right], \text{ for } H_a^c\left(z^{M_r}\right). \end{cases} \tag{4.55}$$

Let U denote a real set of the lower bounds in (4.54) . We get

$$U = \left[\frac{2(m_u - t_u - 1)\pi - \phi_a}{M_u}\left(\text{or } \max\left[0, \frac{2(m_u - t_u)\pi - \theta_a}{M_u}\right]\right)\right] \ \left(u \in [1,\ 2,\ ...,\ r-1]\right). \tag{4.56}$$

$P_4^{(r-1)}$ is given by

$$P_4^{(r-1)} = \min[U]. \tag{4.57}$$

Otherwise, we have

$$P_4^{(r-1)} = P_5^{(r-1)} = \begin{cases} \dfrac{2(m_{r-1} - 1)\pi + \phi_a}{M_{r-1}}, \text{ for } H_a\left(z^{M_{r-1}}\right), \\ \max\left[0,\ \dfrac{2m_{r-1}\pi - \theta_a}{M_{r-1}}\right], \text{ for } H_a^c\left(z^{M_{r-1}}\right). \end{cases} \tag{4.58}$$

From the above discussion, for a given M_1, M_r ($r = 2,\ 3,\ ...,\ k$) can be found to satisfy corresponding conditions. If $P_4^{(k)}$ equals to π (or 0) for Case A (or B), the unwanted frequency components can be removed successfully. Otherwise, another

masking filter $H_e(z)$ is required. The passband and stopband edges of $H_e(z)$ is given by

$$\theta_{H_e} = \begin{cases} \omega_p, \text{ for Case A} \\ \omega_s, \text{ for Case B} \end{cases} \tag{4.59}$$

and

$$\phi_{H_e} = P_4^{(k)}, \text{ for Case A and B} \ . \tag{4.60}$$

4.3.3 Ripple Analysis of Subfilters

Before embarking on the detailed design procedure, it is useful to analyze the ripple effect of each subfilter on the overall filter. The structures in Figs. 4.2 and 4.5 are analyzed. Let $F(\omega)$ and $\delta(\omega)$ denote the gain and deviation of $H(e^{j\omega})$. And the gain and deviation of $G_c(e^{j\omega})$ are $F_c(\omega)$ and $\delta_c(\omega)$, respectively. Let us consider the case where k = 3 and assume that only $H_a(z^{M_r})$ (no $H_a^c(z^{M_r})$) are adopted for Case A design. For Case B design, it is assumed that the 3 identical subfilters are $H_a(z^{M_1})$, $H_a(z^{M_2})$ and $H_a^c(z^{M_3})$. The same analysis can be applied to cases where k > 3. Let $F_a(M_r\omega)$ and $\delta_a(M_r\omega)$ denote the gain and deviation of $H_a(e^{jM_r\omega})$ (or $H_a^c(e^{jM_r\omega})$). The ripple effects of Case A and Case B are analyzed separately.

A. Case A Filter Design

From (4.2), we have

$$F(\omega)+\delta(\omega)=\left\{\prod_{r=1}^{3}\left[F_a(M_r\omega)+\delta_a(M_r\omega)\right]\right\}\left\{1-\left[F_c(\omega)+\delta_c(\omega)\right]\right\}+ F_c(\omega)+\delta_c(\omega). \tag{4.61}$$

The ripple effects of the subfilters on the overall filter are examined in the following 3 frequency ranges as shown in Fig. 4.3.

Frequency range 1: $0\le\omega<\dfrac{2m_1\pi-\theta_a}{M_1}$.

In this frequency range, $F(\omega)=F_c(\omega)=1$. (4.61) is simplified to the following form:

$$\delta(\omega)=\left\{\prod_{r=1}^{3}\left[F_a(M_r\omega)+\delta_a(M_r\omega)\right]\right\}\left[-\delta_c(\omega)\right]+\delta_c(\omega). \tag{4.62}$$

Ignoring the second order terms, we have

$$\delta(\omega)=-\delta_c(\omega)\prod_{r=1}^{3}F_a(M_r\omega)+\delta_c(\omega). \tag{4.63}$$

Depending on the value of $F_a(M_r\omega)$, the following relations are obtained.

When $F_a(M_r\omega)=0$ or $0<\prod_{r=1}^{3}F_a(M_r\omega)<1$,

$$\left|\delta(\omega)\right|\le\left|\delta_c(\omega)\right|. \tag{4.64}$$

When $\prod_{r=1}^{3}F_a(M_r\omega)=1$,

$$\delta(\omega)\approx 0. \tag{4.65}$$

Frequency range 2: $\dfrac{2m_1\pi-\theta_a}{M_1}\le\omega\le\omega_p$.

In this frequency range, $F(\omega)=F_a(M_r\omega)=1$. Ignoring the second order terms, (4.61) is simplified to

$$\delta(\omega)=\left[1-F_c(\omega)\right]\cdot\sum_{r=1}^{3}\delta_a(M_r\omega). \tag{4.66}$$

Since $F_c(\omega)$ decreases from unity to zero as ω increases, we have

$$\left|\delta(\omega)\right|\le\sum_{r=1}^{3}\left|\delta_a(M_r\omega)\right|. \tag{4.67}$$

Frequency range 3: $\omega_s\le\omega\le\pi$.

In this frequency range, $F(\omega)=F_c(\omega)=0$ and $\prod_{r=1}^{3}F_a(M_r\omega)=0$. Ignoring the second order terms, (4.61) is simplified to

$$\begin{aligned}\delta(\omega)=&F_a(M_1\omega)F_a(M_2\omega)\delta_a(M_3\omega)+F_a(M_2\omega)F_a(M_3\omega)\delta_a(M_1\omega)\\&+F_a(M_3\omega)F_a(M_1\omega)\delta_a(M_2\omega)+\delta_c(\omega).\end{aligned} \tag{4.68}$$

Let $\delta_i(\omega)=F_a(M_i\omega)F_a(M_j\omega)\delta_a(M_v\omega)$ ($i,\ j,\ v\in[1,\ 2,\ 3]$ and $i\ne j\ne v$). When $F_a(M_i\omega)F_a(M_j\omega)=1$, we have

$$\delta_i(\omega)=\delta_a(M_v\omega). \tag{4.69}$$

When $F_a(M_i\omega)F_a(M_j\omega)=0$, we get

$$\delta_i(\omega)=0. \tag{4.70}$$

When $1<F_a(M_i\omega)F_a(M_j\omega)<0$,

$$\left|\delta_i(\omega)\right|\le\left|\delta_a(M_v\omega)\right|. \tag{4.71}$$

(4.68) can be evaluated based on (4.69)–(4.71). For example, when $F_a(M_1\omega)F_a(M_2\omega)=1$ and $F_a(M_3\omega)=0$, (4.68) becomes

$$\delta(\omega) = \delta_a(M_3\omega) + \delta_c(\omega). \tag{4.72}$$

B. Case B Filter Design

From (4.3), we have

$$F(\omega) + \delta(\omega) = \left\{1 - \prod_{r=1}^{3}\left[F_a(M_r\omega) + \delta_a(M_r\omega)\right]\right\}\left[F_c(\omega) + \delta_c(\omega)\right]. \tag{4.73}$$

The ripple effects of the subfilters on the overall filter are examined in the following 3 frequency ranges, as shown in Fig. 4.6.

Frequency range 1: $0 \le \omega \le \omega_p$.

In this frequency range, $F(\omega) = F_c(\omega) = 1$. Manipulating (4.73), we get:

$$\delta(\omega) = \delta_c(\omega) - \left\{\prod_{r=1}^{3}\left[F_a(M_r\omega) + \delta_a(M_r\omega)\right]\right\}\left[1 + \delta_c(\omega)\right]. \tag{4.74}$$

Since $\prod_{r=1}^{3} F_a(M_r\omega) = 0$, ignoring the second order terms, the following relation is obtained:

$$\begin{aligned}\delta(\omega) = \delta_c(\omega) &- F_a(M_1\omega)F_a(M_2\omega)\delta_a(M_3\omega) - F_a(M_2\omega)F_a(M_3\omega)\delta_a(M_1\omega) \\ &- F_a(M_3\omega)F_a(M_1\omega)\delta_a(M_2\omega).\end{aligned} \tag{4.75}$$

Let $\delta_i(\omega) = F_a(M_i\omega)F_a(M_j\omega)\delta_a(M_v\omega)$ ($i, j, v \in [1, 2, 3]$ and $i \ne j \ne v$). When $F_a(M_i\omega)F_a(M_j\omega) = 1$, we have

$$\delta_i(\omega) = \delta_a(M_v\omega). \tag{4.76}$$

When $F_a(M_i\omega)F_a(M_j\omega) = 0$, we get

$$\delta_i(\omega) = 0. \tag{4.77}$$

When $0 < F_a(M_i\omega) F_a(M_j\omega) < 1$, we have

$$\left|\delta_i(\omega)\right| \le \left|\delta_a(M_v\omega)\right|. \tag{4.78}$$

(4.75) can be evaluated based on (4.76)–(4.78), e.g., when $0 < F_a(M_1\omega) F_a(M_2\omega) < 1$ and $F_a(M_3\omega) = 0$, (4.75) becomes

$$\left|\delta(\omega)\right| \le \left|\delta_a(M_3\omega)\right| + \left|\delta_c(\omega)\right|. \tag{4.79}$$

Frequency range 2: $\omega_s \le \omega < \dfrac{2m_1\pi + \theta_a}{M_1}$.

In this frequency range, $F(\omega) = 0$ and $F_a(M_r\omega) = 1$. By ignoring the second order terms, (4.73) is simplified to

$$\delta(\omega) = -\left[\sum_{r=1}^{3} \delta_a(M_r\omega)\right] F_c(\omega). \tag{4.80}$$

Since $F_c(\omega)$ decreases from unity to zero as ω increases, we have

$$\left|\delta(\omega)\right| \le \sum_{r=1}^{3} \left|\delta_a(M_r\omega)\right|. \tag{4.81}$$

Frequency range 3: $\dfrac{2m_1\pi + \theta_a}{M_1} < \omega \le \pi$.

In this frequency range, $F(\omega) = F_c(\omega) = 0$. Ignoring the second order terms, (4.73) is simplified to

$$\delta(\omega) = \delta_c(\omega) - \left[\prod_{r=1}^{3} F_a(M_r\omega)\right] \delta_c(\omega). \tag{4.82}$$

When $F_a(M_r\omega) = 0$ or $0 < \prod_{r=1}^{3} F_a(M_r\omega) < 1$,

$$\left|\delta(\omega)\right| \le \left|\delta_c(\omega)\right|. \tag{4.83}$$

When $\prod_{r=1}^{3} F_a(M_r\omega) = 1$,

$$\delta(\omega) \approx 0. \tag{4.84}$$

The above analysis provides a useful insight for the design of the overall filter. For Case A, it can be seen from (4.64) that in the frequency range 1, the deviation of the overall filter is determined mainly by $G_c(z)$. This corresponds to the situation in frequency range 3 for case B. In frequency range 2, $H_a(z^{M_i})$ determines the passband ripple for Case A and the stopband ripple for Case B, according to (4.67) and (4.81), respectively. Similarly, subfilters $H_a(z^{M_i})$ and $G_c(z)$ are responsible for the deviation of the overall filter in the frequency ranges 3 and 1 for Case A and Case B, respectively.

4.3.4 Design Procedures

The following design steps are recommended for the cases discussed in the previous section where 3 identical subfilters are utilized. Similar procedure can be easily applied to other cases.

Step 1. Find a set of appropriate values for M_r.

Step 2. Design $H_a(z)$ using (4.6)–(4.8) or (4.9)–(4.11) for Case A or Case B, respectively. For Case A, according to (4.67), set the passband ripple δ_{ap} of $H_a(z)$ to

be $0.9\delta_p / k$, where 10% margin is kept for the ripple compensation of $G_c(z)$. The stopband ripple δ_{as} is set to be $0.9\delta_s$. For Case B, from (4.81), we have

$$2\delta_{ap} + \delta_{as} = 0.9\delta_s \tag{4.85}$$

and

$$\max\left[\delta_{ap},\ \delta_{as}\right] \approx 0.9\delta_p . \tag{4.86}$$

Besides satisfying (4.85) and (4.86), we should maximize the value of $\delta_{ap}\delta_{as}$ to minimize the order of $H_a(z)$, e.g., if $\delta_p = \delta_s$, we may set δ_{ap} and δ_{as} to $0.9\delta_p / 4$ and $0.9\delta_p / 2$, respectively.

Step 3. Design $G_c(z)$ using $\prod_{r=1}^{3} H_a\left(z^{M_r}\right)$ as a prefilter. The zero-phase frequency response of $G_c(z)$ can be written as

$$G_c(\omega) = \sum_i G_c(n)\,\mathrm{trig}(\omega, i) \tag{4.87}$$

where $\mathrm{trig}(\omega, i)$ is a proper trigonometric function depending on the type of filter under consideration, $G_c(n)$ is the impulse response of $G_c(z)$. Similar definitions are applied to other subfilters. For Case A, in the passband, $G_c(z)$ has to satisfy the following:

$$\begin{aligned} &1-\delta_p - \prod_{i=r}^{3} H_a(M_r\omega) \le \left[G_c(n)\,\mathrm{trig}(\omega,i)\right]\left[1-\prod_{r=1}^{3} H_a(M_r\omega)\right] \le \\ &1+\delta_p - \prod_{i=r}^{3} H_a(M_r\omega). \end{aligned} \tag{4.88}$$

In the stopband, we have

$$-\delta_s - \prod_{r=1}^{3} H_a(M_r\omega) \le \left[G_c(n)\,\mathrm{trig}(\omega,i)\right]\left[1-\prod_{r=1}^{3} H_a(M_r\omega)\right] \le \delta_s - \prod_{r=1}^{3} H_a(M_r\omega). \tag{4.89}$$

For Case B, in the passband, $G_c(z)$ has to satisfy

$$1-\delta_p \le \left[G_c(n)\,\mathrm{trig}(\omega,i)\right]\left[1-\prod_{r=1}^{3} H_a(M_r\omega)\right] \le 1+\delta_p . \tag{4.90}$$

In the stopband, we have

$$-\delta_s \le \left[G_c(n)\,\mathrm{trig}(\omega,i)\right]\left[1-\prod_{r=1}^{3} H_a(M_r\omega)\right] \le \delta_s . \tag{4.91}$$

Linear programming or any other suitable techniques may be used to minimize δ_p and δ_s in (4.90) and (4.91), respectively.

Step 4. Repeat Step 2 and 3 by slightly adjusting the ripple margins of $H_a(z)$ until no improvements are obtained.

4.4 Implementation Issue

In [17], the implementation of a filter $H_a(z)$ consists of two parts: arithmetic operations and delay (storage) elements, as shown in Fig. 4.13, where S_a denotes the arithmetic operations of $H_a(z)$ and *D* denotes the delay elements or memory elements. Using the structure in Fig. 4.13 as a basic building block and applying folding transformation [81] to all identical subfilters, a structure for implementation of the cascade of identical subfilters was introduced [17], as shown in Fig. 4.14, where T is a latch used to store the internal signals. Fig. 4.15 illustrates an implementation structure for the cascade of $H_a(z^{M_1})H_a(z^{M_2})$ based on the structure in Fig. 4.14, where the length of $H_a(z)$ is 3. Therefore, all identical subfitlers can share adders and multipliers. The structure in Fig. 4.15 can be easily applied to implement filters in Fig.

4.2 or Fig. 4.5. Let N_{H_a} and N_{G_c} be the orders of $H_a(z)$ and $G_c(z)$, respectively, the total memory elements required is

$$N_{H_a}\sum_{r=1}^{k}M_r + N_{G_c} + 1 \tag{4.92}$$

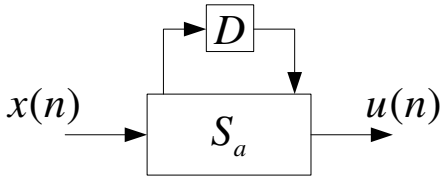

Figure 4.13 A filter is composed of the delay (storage) elements and arithmetic operations.

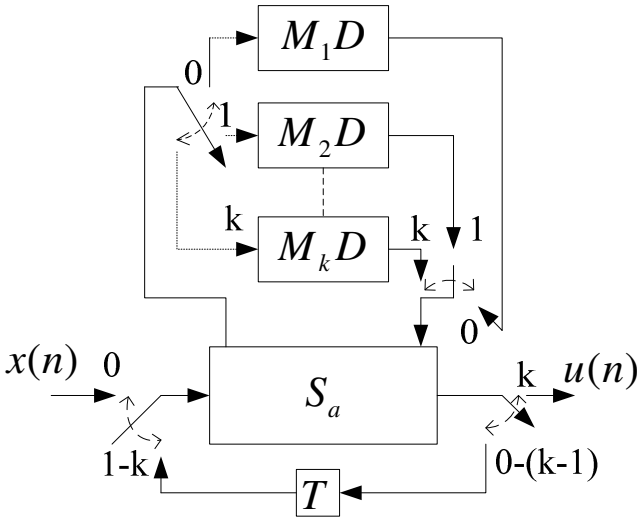

Figure 4.14 An implementation structure of the cascade of identical subfilters.

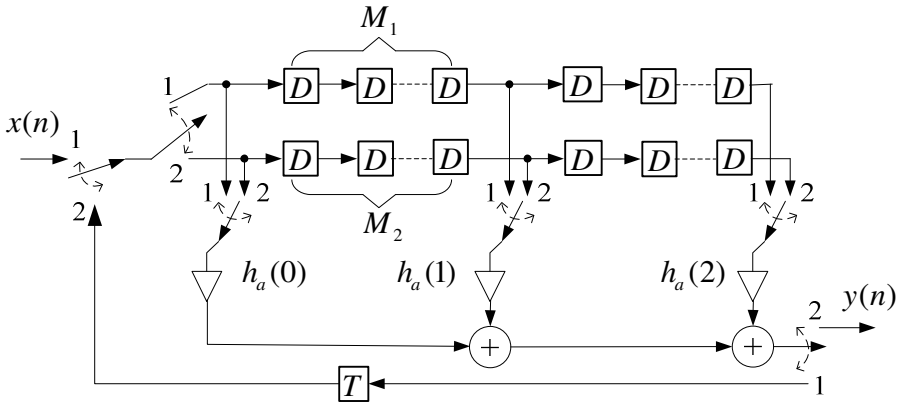

Figure 4.15 An implementation structure of $H_a\left(z^{M_1}\right)H_a\left(z^{M_2}\right)$.

4.5 FIR Filters with Varying Specifications

$H_a\left(z^{M_1}\right)$ is a multi-band filter, as shown Fig. 4.3(b). In Figs. 4.3(b) and 4.6(b), only one band is used to perform the bandedge shaping for one filter. By selecting different combinations of identical subfilters with different periods, it is interesting to note that filters with different passband and stopband cutoff frequencies can be designed by using the same model filter. Fig. 4.16 illustrates the frequency responses of $H_a\left(z^{M_1}\right)$ cascaded with different identical subfilters separately. "Band1", "Band2" and "Band3" in Fig. 4.16 can be employed to design different FIR filters. Hence, if L number of masking filters $G_{c_i}\left(z\right)$ ($i = 1, 2, ..., L$) are introduced, an FRM-based FIR filter can be designed in a single structure which has the flexibility to meet different specifications. The realization structures for Case A and Case B are illustrated in Fig. 4.17 and Fig. 4.18, respectively, where D_{C_i} ($i = 1, 2, ..., L$) are the group delays of G_{c_i}, and $S_1^{'}$, $S_2^{'}$, …, $S_L^{'}$ are switches to control which filter is to be realized. In Fig. 4.17 and Fig.

4.18, $\prod_{r=1}^{k} H_r(z)$ has different outputs by selecting different combinations of delay elements. A realization structure for $\prod_{r=1}^{k} H_r(z)$ is shown in Fig. 4.19, where by controlling "on" or "off" of different switches (s_1, s_2, …, s_k), different delay elements from $M_1 D$ to $M_k D$ are selected.

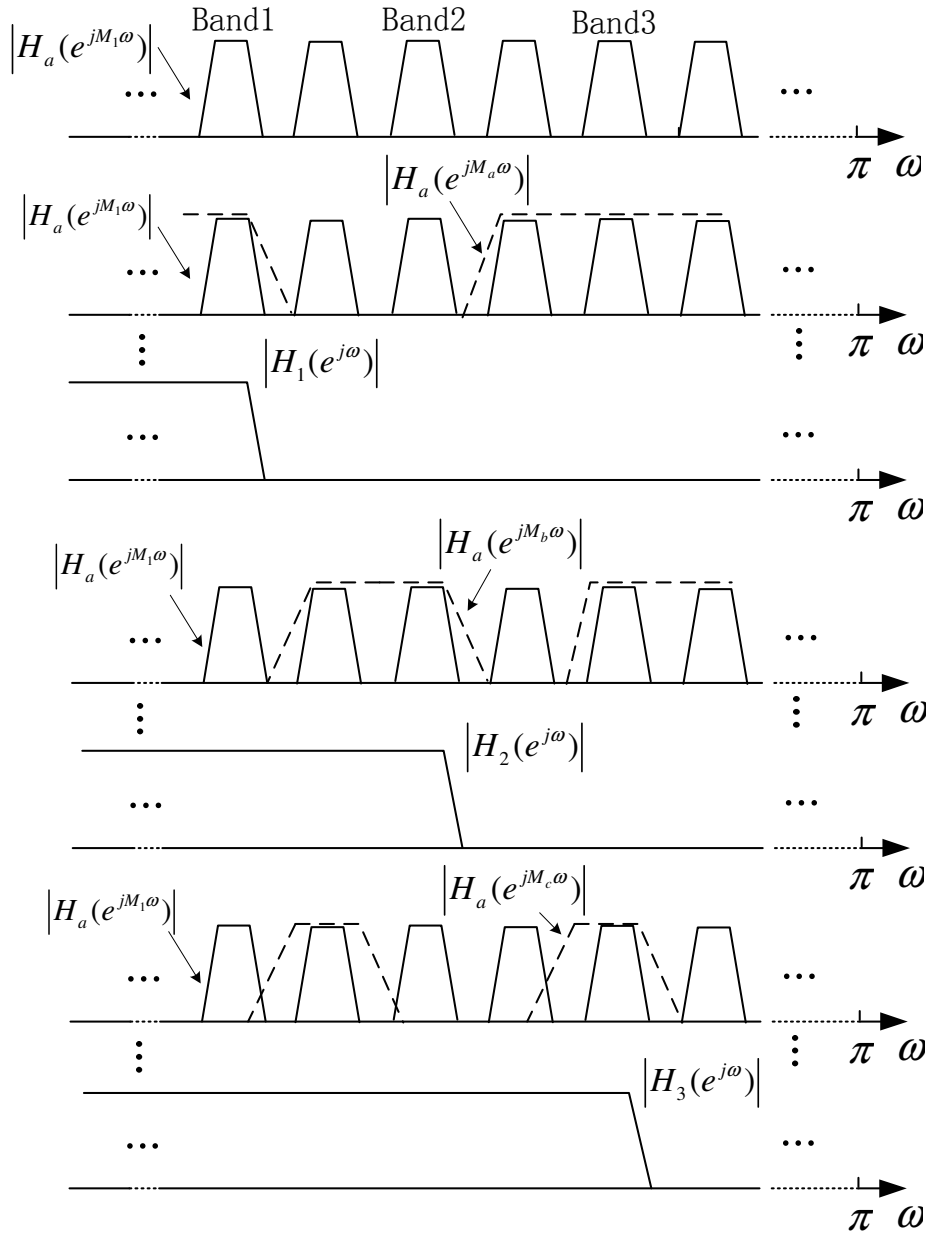

Figure 4.16 Illustration of designing different filters using one model filter.

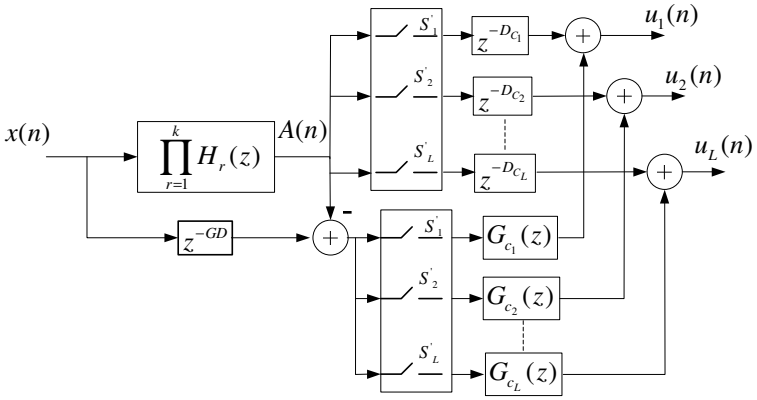

Figure 4.17 A structure for designing a FIR filter with different specifications for Case A.

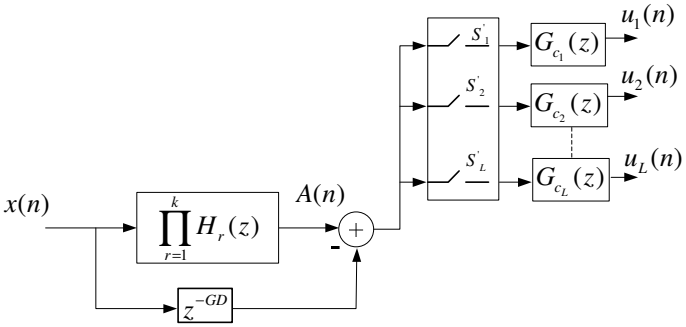

Figure 4.18 A structure for designing a FIR filter with different specifications for Case B.

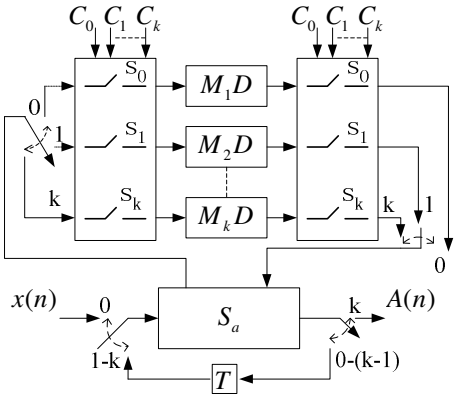

Figure 4.19 A realization structure for $\prod_{r=1}^{k} H_r(z)$.

4.6 Examples and Comparisons

***Example* 1**

To illustrate the new design approach, a lowpass filter is designed with passband edge at $\omega_p = 0.3\times 2\pi$ and stopband edge at $\omega_s = 0.301\times 2\pi$. The passband ripple is at most 0.01 and the stopband attenuation is at least 40 dB. Using the proposed method, for $M_1 = 31$, the remaining M_r are found to be 11, and 1. The lengths of $H(z)$ and $G_c(z)$ are 75 and 95, respectively. The implementation uses the structure for Case A which requires 86 multipliers, 170 adders and 3277 delay elements. If the structure for Case B is utilized, M_r are found to be 27, 14, 3, and 1. A highpass model filter is required with a length of 95. The length for $G_c(z)$ is 71. For implementation, 84 multipliers, 165 adders and 4301 delay elements are required. Figs. 4.20–4.22 show the magnitude responses of subfilters and the overall filter for $M_1 = 31$. If $G_c(z)$ is designed by the FRM approach, further reduction in the number of multipliers can be achieved. For clarity, the complexity of the overall filter is summarized in Table 4.1 in terms of multipliers, adders, and the number of delay elements using different design methods. As indicated in Table 4.1, 130 multipliers and 256 adders are required using the single-stage FRM approach. If $G_c(z)$ is designed using the FRM technique, more than 42% savings in the number of multipliers and adders can be achieved compared with the single-stage FRM technique. Indicated in Table 4.1, the proposed method also outperforms the IFIR-FRM approach and the two-stage FRM technique in terms of the required multipliers and adders.

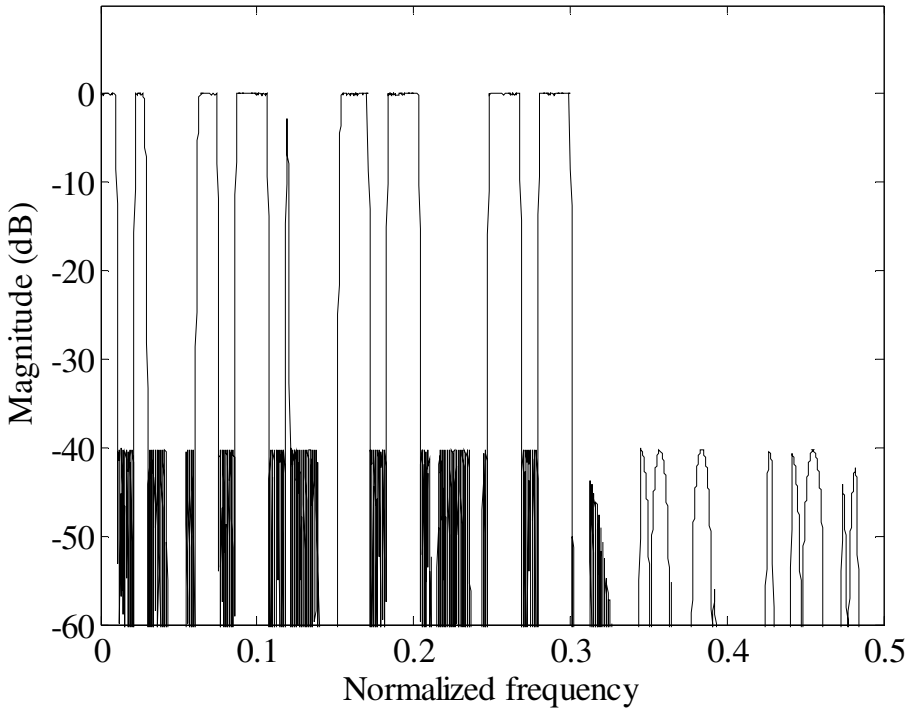

Figure 4.20 Magnitude response of $\prod_{i=1}^{3} H_a\left(z^{M_i}\right)$ in example 1 for $M_1 = 31$.

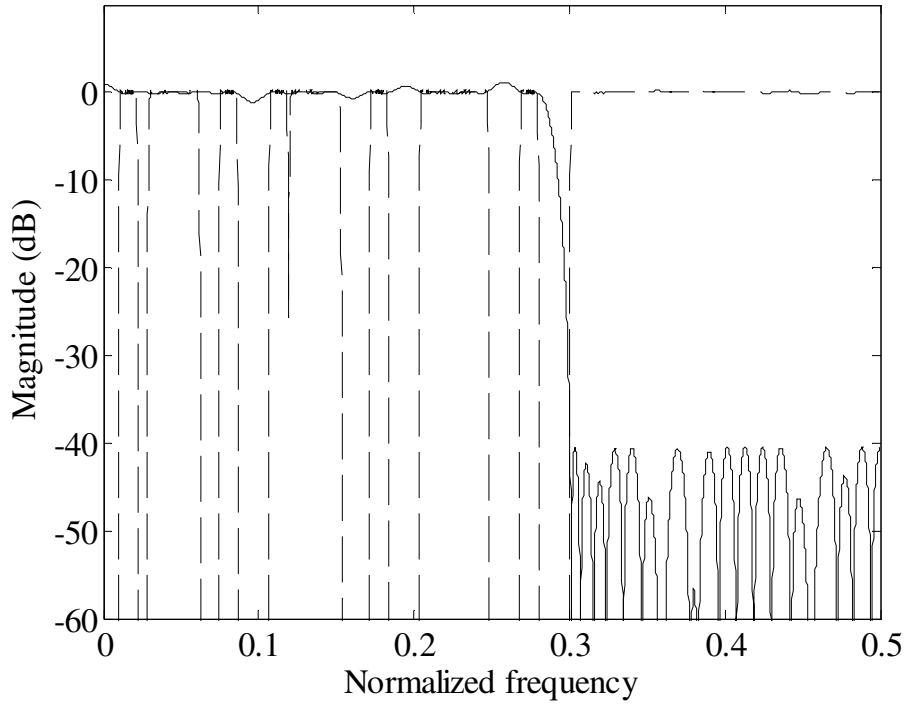

Figure 4.21 Magnitude responses of $C\left(z\right)$ (solid line) and $G_c\left(z\right)$ (dashed line) in example 1 for $M_1 = 31$.

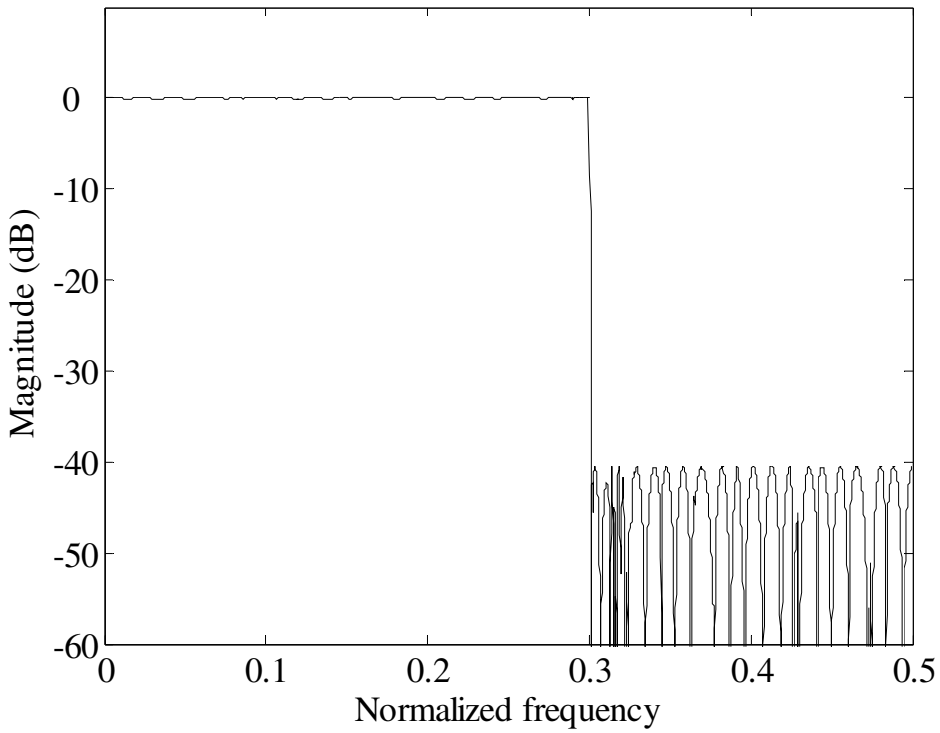

Figure 4.22 Magnitude response of the overall filter in example 1 for $M_1 = 31$.

Table 4.1 Comparison of different design methods of example 1.

Design	Multipliers	Adders	delays
Conventional	925	1850	1850
1-stage FRM	130	256	2000
2-stage FRM	92	177	2210
IFIR-FRM	104	202	2168
Proposed 1 (M_r: 31, 11, 1)	86	170	3277
Proposed 2 (M_r: 31, 11, 1)	74	144	3309
$G_c(z)$ designed by the FRM approach			
Proposed 3 (M_r: 27, 14, 3, 1)	84	165	4301

***Example* 2**

Using the structure in Fig. 4.17, the lowpass model filter in example 1 can be utilized to design filters with different passband and stopband edges having a transition-width of $0.001\times 2\pi$. For $M_1 = 31$, θ and ϕ are $0.3\times 2\pi$ and $0.331\times 2\pi$, respectively. Table 4.2 shows the bandedges of filters that can be designed by selecting appropriate M_r, where f_p and f_s denote the normalized passband and stopband edges, respectively. It should be noted that if the constraint of the transition-width ($0.001\times 2\pi$) is relaxed, the proposed structure can be used to design much more filters than those indicated in Table 4.2. In general, the transition-width may range from $0.001\times 2\pi$ to $0.331\times 2\pi$.

Table 4.2 Filters designed using the lowpass model filter in example 1.

M_i	f_p	f_s
31, 7, 4, 2, 1	0.0419	0.042
31, 4, 2, 1	0.0742	0.0743
31, 6, 2, 1	0.1065	0.1075
31, 9, 2, 1	0.1387	0.1397
31, 13, 7, 3, 1	0.1710	0.172
31, 8, 3, 1	0.2032	0.2042
31, 7, 5, 1	0.2355	0.2455
31, 12, 6, 1	0.2677	0.2777
31, 11, 1	0.3000	0.301
31, 5, 2	0.3323	0.3333
31, 9, 6, 4	0.3645	0.3655
31, 18, 4	0.3968	0.3978
31, 10, 6	0.429	0.430
31, 10	0.4613	0.4713

4.7 Summary

In this chapter, two FRM-based structures are proposed for the design of arbitrary bandwidth sharp FIR filters. The proposed approach combines the SFFM technique and the FRM method. One identical model filter (with different interpolation factors) is repeatedly cascaded with itself. The cascade of identical model filters with different interpolation factors performs both the bandedge shaping and the masking tasks. With the help of only one masking filter, the overall filter is synthesized. Arithmetic operations are greatly reduced using the proposed structures at the price of increasing delays. With simple modifications, the proposed structures can be extended to design FIR filters with varying specifications. This provides significant flexibility for the design and implementation of sharp FIR filters.

Chapter 5

Design of Computationally Efficient Narrowband and Wideband Sharp FIR Filters

5.1 Introduction

Interpolated finite impulse response (IFIR) technique [10] is one of the most computationally efficient approaches to realize narrowband and wideband FIR filters. The frequency responses for a lowpass IFIR filter are shown in Fig. 5.1. The design starts with a lowpass model filter $H_M(z)$ shown in Fig. 5.1(a). By replacing each delay element of $H_M(z)$ with M delay elements, a bandedge shaping filter $H_M(z^M)$ is formed which has periodic frequency response with a period of $\frac{2\pi}{M}$, as shown in Fig. 5.1(b). To synthesize the overall filter $H(z)$, a masking filter $G(z)$ is required to remove the undesired frequency components in the stopband, as shown in Figs. 5.1(b)

and 5.1(c). $H(z)$ has a narrow transition-width which is $\frac{1}{M}$ of $H_M(z)$. The transfer function of $H(z)$ is written as

$$H(z) = H_M(z^M)G(z). \tag{5.1}$$

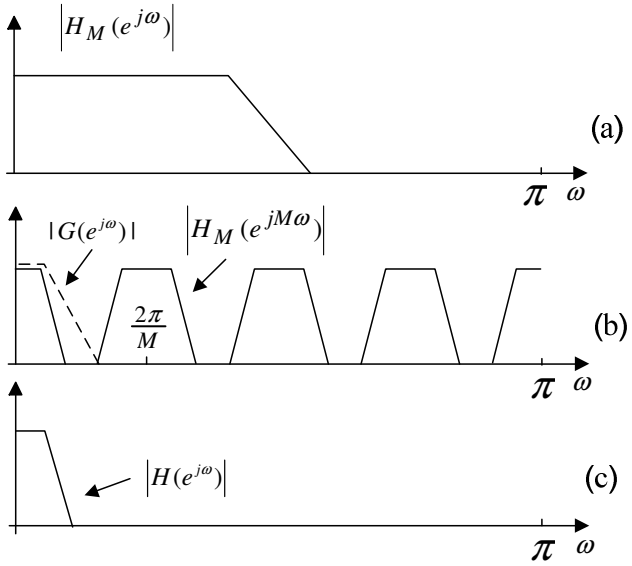

Figure 5.1 Frequency responses for a lowpass IFIR filter.

A wideband highpass (lowpass) filter is a complement of the corresponding narrowband lowpass (highpass) IFIR filter. A realization structure for wideband IFIR filters is shown in Fig. 5.2 and the corresponding *z*-transform transfer function is given by

$$H(z) = z^{-GD} - H_M(z^M)G(z) \tag{5.2}$$

where *GD* is the total number of group delay of $H_M(z^M)$ and $G(z)$. The frequency response of each subfilter for a lowpass (highpass) wideband filter is illustrated in Fig. 5.3. To design a narrowband highpass or a wideband lowpass filter using a lowpass model filter, *M* must be even to include π in the passband, as shown in Figs. 5.3(b) and

5.3(d). Otherwise, M must be odd as shown in Fig. 5.3(e), if a highpass model filter is used.

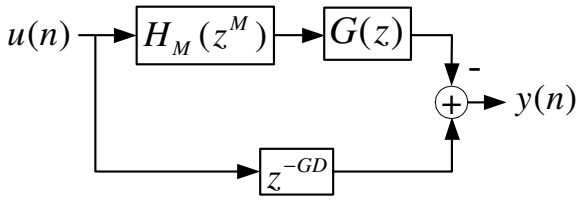

Figure 5.2 Wideband IFIR filters.

The complexities of $H_M(z)$ and $G(z)$ are interrelated: increasing the value of M will reduce the complexity of $H_M(z)$ while increasing the order of $G(z)$. With an appropriate choice of M, the number of the overall orders of $H_M(z)$ and $G(z)$ can be reduced significantly. Therefore, there exists an optimal decomposition of an IFIR filter which usually leads to multi-stage IFIR filters when a large M is adopted [12]. The drawbacks of multi-stage IFIR filters are the relatively high complexity associated with the design of each subfilter and the increased number of delay elements.

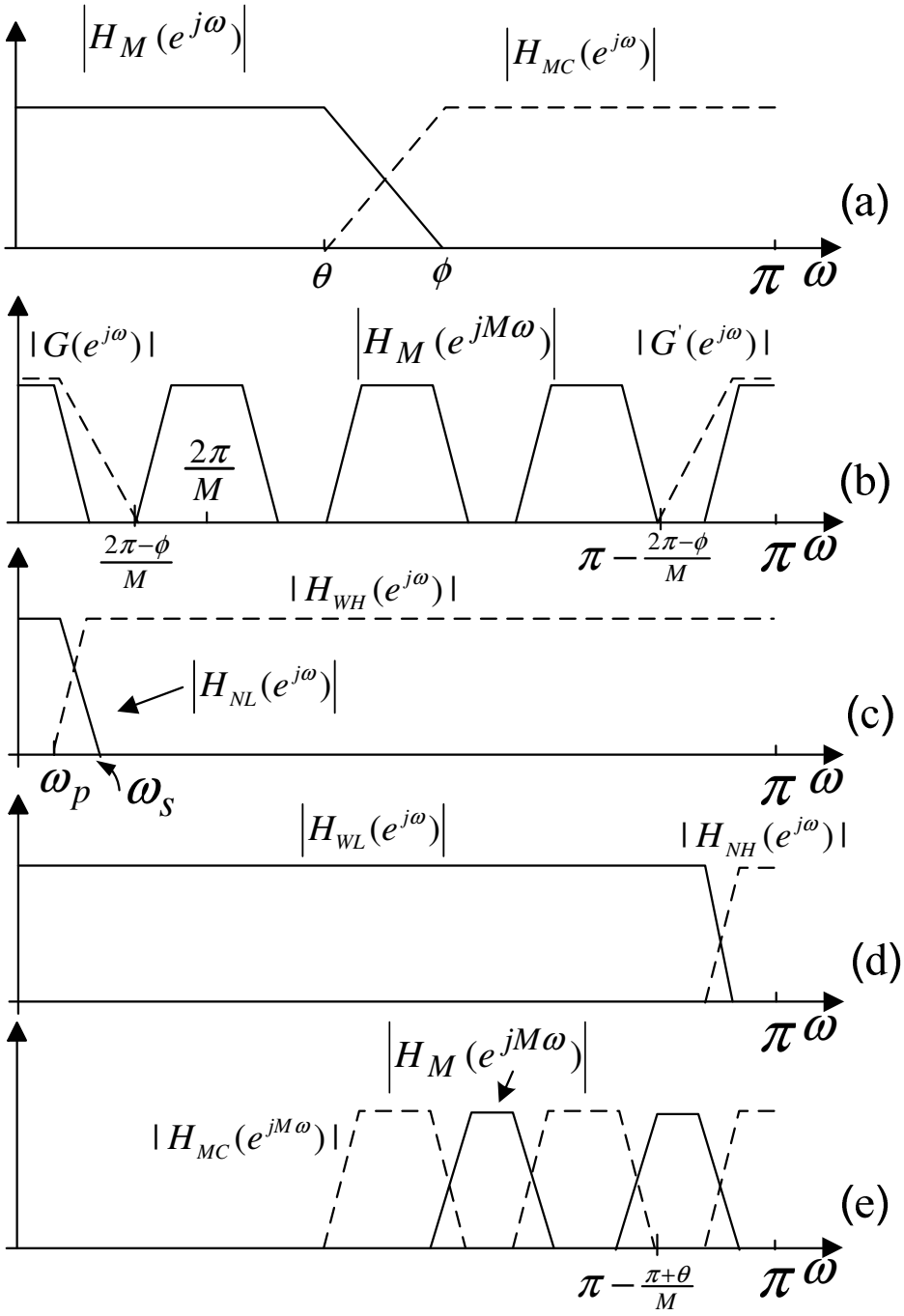

Figure 5.3 Frequency responses of subfilters in the IFIR technique. *M* is even in (b) and odd in (e).

Several improvements to the IFIR filters were proposed [12–14] by using efficient methods to design the masking filters. In this chapter, a new class of masking filter structures is proposed to design narrowband lowpass, highpass and bandpass IFIR filters, respectively. Wideband lowpass (highpass) IFIR filters can be easily obtained from the

corresponding narrowband IFIR filters. The proposed masking filters can also be used as a prefilter in the "prefilter plus equalizer" technique. Examples show that the new masking filters can achieve great savings in terms of arithmetic operations compared with the original IFIR filters. Meanwhile, the required delay elements are decreased compared with other equivalent computationally efficient filters.

The organization of this chapter is as follows. New masking filter structures for the design of lowpass, highpass, and bandpass IFIR filters are developed in Section 5.2. In Section 5.3, design procedures are discussed thoroughly. Implementation consideration is introduced in Section 5.4. Design examples and comparison are illustrated in Section 5.5. Section 5.6 summarizes this chapter.

5.2 New Masking Filters

5.2.1 For Lowpass FIR Filter Design

In Chapter 3, a multiplication-free FIR filter is developed with the transfer function given by (3.10), i.e.,

$$P_{Lc}(N,L,K,z)=\frac{1}{8^L\cdot 3^K}\left[\left(1+z^{-N}\right)^2\left(1+z^{-2N}\right)\right]^L\left(1+z^{-N}+z^{-2N}\right)^K \tag{5.3}$$

where N is a positive integer, L and K are called sharpening factors for the purpose of providing enough stopband attenuation. By selecting different values of L and K, different stopband attenuations are obtained. $P_{Lc}(z)$ has periodic frequency response with a period of $\frac{2\pi}{N}$ and is monotonically decreasing in $\omega\in\left[0,\ \frac{\pi}{2\mathrm{N}}\right]$. To utilize $P_{Lc}(z)$

as the masking filter for IFIR filters, the aliasing bands beyond $\frac{\pi}{2N}$ must be removed. It is noted that reducing the value of *N*, the number of aliasing bands is reduced too. Therefore, using $P_{Lc}(z)$ as a basic building block, a new masking filter $P_L(z)$ is obtained. The transfer function is defined as

$$P_L(z) = \prod_{i=1}^{r} \left[P_{L4}\left(z^{N_i}\right) \right]^{L_i} \left[P_{L2}\left(z^{N_i}\right) \right]^{K_i} \tag{5.4}$$

where N_i are positive integers and $N_1 > N_2 > ... > N_r$, $P_{L4}(z^{N_i})$ and $P_{L2}(z^{N_i})$ are given by

$$P_{L4}\left(z^{N_i}\right) = \frac{1}{8}\left(1 + z^{-N_i}\right)^2 \left(1 + z^{-2N_i}\right) \tag{5.5}$$

and

$$P_{L2}\left(z^{N_i}\right) = \frac{1}{3}\left(1 + z^{-N_i} + z^{-2N_i}\right), \tag{5.6}$$

respectively. The magnitude response of $P_L(z)$ is expressed as

$$\left|P_L(e^{j\omega})\right| = \prod_{i=1}^{r} \frac{1}{2^{L_i} \cdot 3^{K_i}} \left[\cos\left(N_i\omega\right) + \cos^2\left(N_i\omega\right) \right]^{L_i} \left[1 + 2\cos\left(N_i\omega\right) \right]^{K_i}. \tag{5.7}$$

The selection of N_i will be discussed in later sections. It should be noted that if L_i or K_i equals to 0, the corresponding subfilter $P_{L4}(z)$ or $P_{L2}(z)$ is in fact not used to construct $P_L(z)$.

5.2.2 For Highpass FIR Filter Design

Applying the transformation: $z^{-1} \to -z^{-1}$ in (5.3), a highpass version $P_{Hc}(z)$ is formed which is suitable for the design of highpass IFIR filters. The transfer function and the magnitude response are written as

$$P_{Hc}\left(N,L,K,z\right)=\frac{1}{8^{L}\cdot 3^{K}}\left[\left(1-z^{-N}\right)^{2}\left(1+z^{-2N}\right)\right]^{L}\left(1-z^{-N}+z^{-2N}\right)^{K} \tag{5.8}$$

and

$$\left|P_{Hc}(e^{j\omega})\right|=\frac{1}{2^{L}\cdot 3^{K}}\left[\cos^{2}(N\omega)-\cos(N\omega)\right]^{L}\left[1-2\cos(N\omega)\right]^{K} \tag{5.9}$$

where N must be odd to include π in the passband. By combining different $P_{Lc}(z)$ and $P_{Hc}(z)$ together, a new masking filter for highpass IFIR filters is obtained with the transfer function written as

$$P_{H}\left(z\right)=\prod_{i=1}^{r}P_{Lc}\left(N_{1i},L_{1i},K_{1i},z\right)P_{Hc}\left(N_{2i},L_{2i},K_{2i},z\right) \tag{5.10}$$

where N_{1i} ($N_{11}>N_{12}...>N_{1k}$) are even integers, and N_{2i} ($N_{21}>N_{22}...>N_{2k}$) are odd integers.

5.2.3 For Bandpass Filter Design

$P_{Lc}(N,L,K,z)$ has periodic frequency response with main lobes centered at $\frac{2\pi n}{N}$, where $n=0,\ 1,\ ...,\ N-1$. Similarly, $P_{Hc}(N,L,K,z)$ has periodic frequency response with main lobes centered at $\frac{2\pi\left(0.5+n\right)}{N}$. The main lobes of $P_{Lc}(N,L,K,z)$ or $P_{Hc}(N,L,K,z)$ can be used to design IFIR bandpass filters. A new masking filter $P_{B}(z)$ is obtained by cascading r sections of $P_{Lc}(z)$ and/or $P_{Hc}(z)$ with different N, K, L. The transfer function of $P_{B}(z)$ is given by

$$P_{B}\left(z\right)=\prod_{i=1}^{r}P_{LH}\left(N_{i},L_{i},K_{i},z\right) \tag{5.11}$$

where $P_{LH}(N_i, L_i, K_i, z)$ is chosen from [$P_{Lc}(N_i, L_i, K_i, z), P_{Hc}(N_i, L_i, K_i, z)$]. N_1 is the largest integer among N_i. N_i ($i \geq 2$) should be chosen in such a way that the nulls of $P_{LH}(N_i, L_i, K_i, z)$ should cancel the undesired lobes of $P_{LH}(N_1, L_1, K_1, z)$ and should keep the desired lobe of $P_{LH}(N_1, L_1, K_1, z)$ undistorted. Fig. 5.4 shows the magnitude response of $P_B(z)$, when N_i are $9^{(L)}$, $6^{(L)}$, $3^{(L)}$, and $2^{(H)}$, where the superscript "(L)" or "(H)" corresponds to $P_{Lc}(N_i, L_i, K_i, z)$ or $P_{Hc}(N_i, L_i, K_i, z)$, respectively. L_i for all i are 1. K_i are 1, 0, 1, and 0. $P_B(z)$ can serve as a masking filter in IFIR filters or a prefilter in the prefitler-equalizer approach (this will be illustrated in Section 5.5.) The passband degradation of $P_B(z)$ can be easily compensated by a bandedge shaping filter or an equalizer.

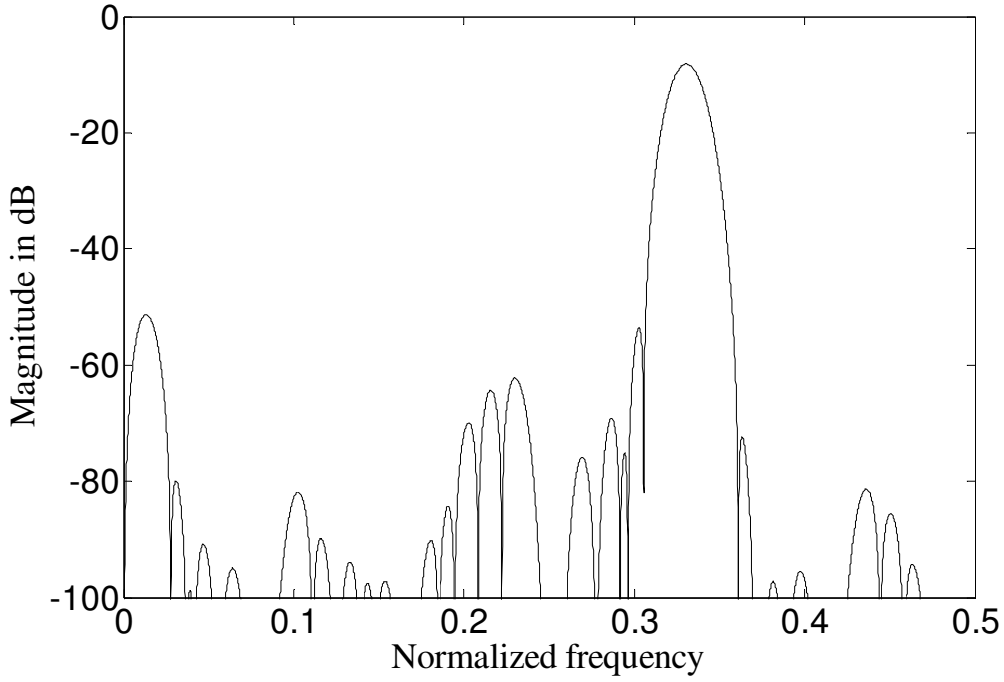

Figure 5.4 Magnitude response of $P_B(z)$ for $N_i = 9,\ 6,\ 3,\ 2$, $L_i = 1$ and $K_i = 1,\ 0,\ 1,\ 1$, ($i = 1,\ 2,\ 3,\ 4$).

5.3 Filter Design

5.3.1 Lowpass Filter Design

In this section, the design for narrowband lowpass filter is discussed. Similar results can be easily obtained for highpass cases. Let the desired passband and stopband edges are ω_p and ω_s, respectively. The passband and stopband edges of $H_M(z)$ are given by

$$\theta = M\omega_p \tag{5.12}$$

and

$$\phi = M\omega_s, \tag{5.13}$$

respectively. To remove the aliasing bands of $H_M(z^M)$, $P_L(z)$ should meet the following requirement:

$$\left|P_L\left(e^{j\omega}\right)\right| < \delta_s, \text{ for } \omega \in \left[\frac{2\pi-\phi}{M},\ \pi\right] \tag{5.14}$$

where δ_s is the required stopband ripple. For a given M, a set of N_i, K_i and L_i ($i = 1,\ 2,\ ...,\ k$) should be found to meet (5.14). N_1 is selected as follows. From (5.7), the first null ω_{null}^1 of $P_L(z)$ is given by

$$\omega_{null}^1 = \frac{\pi}{2N_1} \tag{5.15}$$

ω_{null}^1 should be chosen in such a way that it falls into the interval $\left[\omega_s,\ \frac{2\pi - \phi}{M}\right]$ and it should be as close to $\frac{2\pi - \phi}{M}$ as possible, as shown in Fig. 5.3(b). Hence, we get

$$\frac{\pi}{2N_1} \le \frac{2\pi-\phi}{M} \tag{5.16}$$

Solve (5.16), we have

$$N_1 \geq \text{round}\left[\frac{M\pi}{2(2\pi-\phi)}\right] \tag{5.17}$$

where round[x] rounds x to the nearest integer. After N_1 is determined, a search program can be made to find a set of N_i , K_i and L_i ($i = 1, 2, ..., k$) satisfying (5.14) and leading to the minimum number of delays of $P_L(z)$.

For the design of $H_M(z)$, we have

$$\begin{cases} -\delta_p \leq \left|H_M\left(e^{jM\omega}\right)P_L\left(e^{j\omega}\right)\right| - 1 \leq \delta_p, \text{ for } \omega \in \left[0,\ \omega_p\right] \\ \left|H_M\left(e^{jM\omega}\right)P_L\left(e^{j\omega}\right)\right| \leq \delta_s, \text{ for } \omega \in \left[\omega_s,\ \pi\right] \end{cases} \tag{5.18}$$

where δ_p is the required passband ripple. Given $P_L(e^{j\omega})$, an optimal $H_M(e^{j\omega})$ minimizing δ_p and δ_s in the passband and stopband, respectively, can be obtained using well-known filter design tools, such as the modified Parks-McClellan method [79] and linear programming [78].

5.3.2 Bandpass Filter Design

Let a lowpass filter $H_a(z)$ be used as the model filter. Fig. 5.5 shows the frequency response of each subfilter for the design of a bandpass filter $H(z)$. The passband and stopband cutoff frequencies of $H_a(z)$ are θ_a and ϕ_a, respectively, as shown in Fig. 5.5(a). The passband center frequency is given by

$$\omega_o = \frac{2\pi m}{M} \tag{5.19}$$

where *m* is an integer. Let $\Delta\omega_1$ denote the required passband width and $\Delta\omega_2$ denote the transition-width. For a given *M*, we have

$$\begin{cases} \theta_a = \dfrac{M\Delta\omega_1}{2} \\ \phi_a = M\left(\dfrac{\Delta\omega_1}{2} + \Delta\omega_2\right) \end{cases} \tag{5.20}$$

When M is specified, the masking filter $P_B(z)$ can be designed. Assume that $P_{LH}(N_1, L_1, K_1, z)$ is $P_{Lc}(N_1, L_1, K_1, z)$. The center frequency of one of the main lobes of $P_{LH}(N_1, L_1, K_1, z)$ should be as close to ω_o as possible. Therefore, we have

$$\frac{2\pi n_1}{N_1} \approx \frac{2\pi m}{M} \tag{5.21}$$

where n_1 is a positive integer.

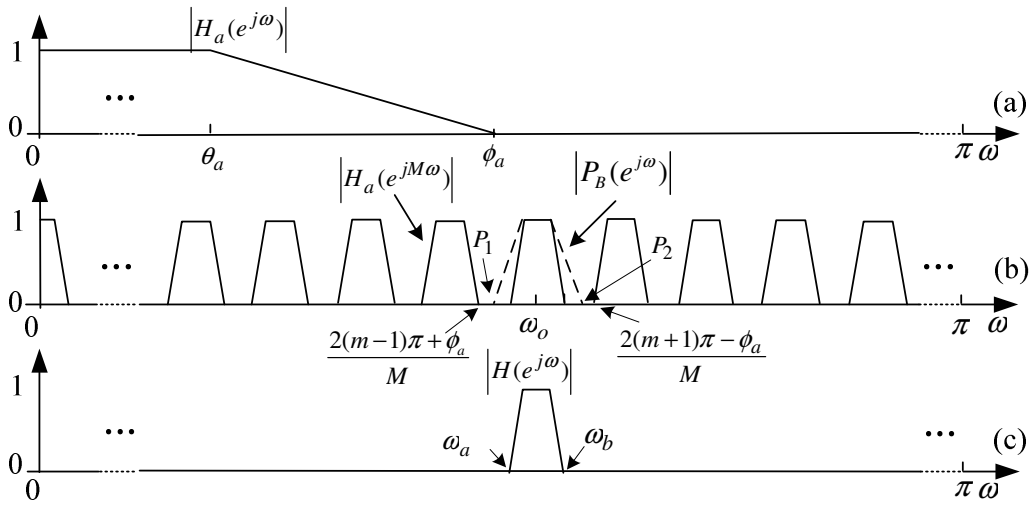

Figure 5.5 Frequency responses for the design of bandpass IFIR filters.

As shown in Fig. 5.5(b), the nulls P_1 and P_2 of $P_{Lc}(N_1, L_1, K_1, z)$ should meet the conditions:

$$\omega_{P_1} < \omega_a \tag{5.22}$$

and

$$\omega_{P_2} > \omega_b \tag{5.23}$$

where ω_a and ω_b denote the required lower and upper stopband edges, respectively. ω_{P_1} and ω_{P_2} are given by

$$\begin{cases} \omega_{P_1} = \dfrac{(2q_1+1)\pi}{2N_1} \\ \omega_{P_2} = \dfrac{(2q_1+3)\pi}{2N_1} \end{cases} \tag{5.24}$$

where q_1 is an integer. N_1 can be found using (5.21)–(5.23). Similar to (5.14), $P_B(z)$ needs to satisfy the following:

$$\left|P_B\left(e^{j\omega}\right)\right| < \delta_s, \text{ for } \omega \in \left[0,\ \frac{2\pi(m-1)+\phi_a}{M}\right] \cup \left[\frac{2\pi(m+1)-\phi_a}{M},\ \pi\right]. \tag{5.25}$$

An exhaustive search should be preformed to determine N_i, L_i and K_i based on (5.21) –(5.25) for a given *M*. The selected set of N_i, L_i and K_i should produce low hardware cost for the overall filter in terms of multiplications, additions and delays. When $P_B(z)$ is determined, $H_a(z)$ can be designed in a similar way as for lowpass cases.

In case that (5.25) can not be satisfied thoroughly in some frequency ranges, an additional simple masking filter is required to perform the task which leads to a modified IFIR structure as shown in Fig. 5.6. The frequency response of each subfilter in Fig. 5.6 is sketched in Fig. 5.7. In Fig. 5.6, the cascade of $G(z)$ and $P_B(z)$ removes all unwanted passbands of $H_a(z^M)$ as shown in Figs. 5.7(b) and 5.7(c).

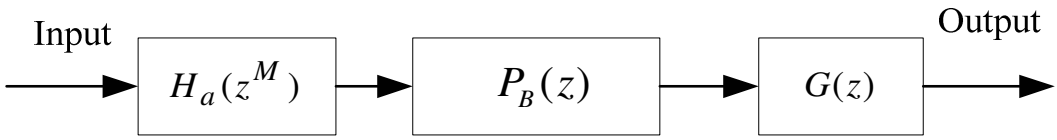

Figure 5.6 A modified IFIR structure.

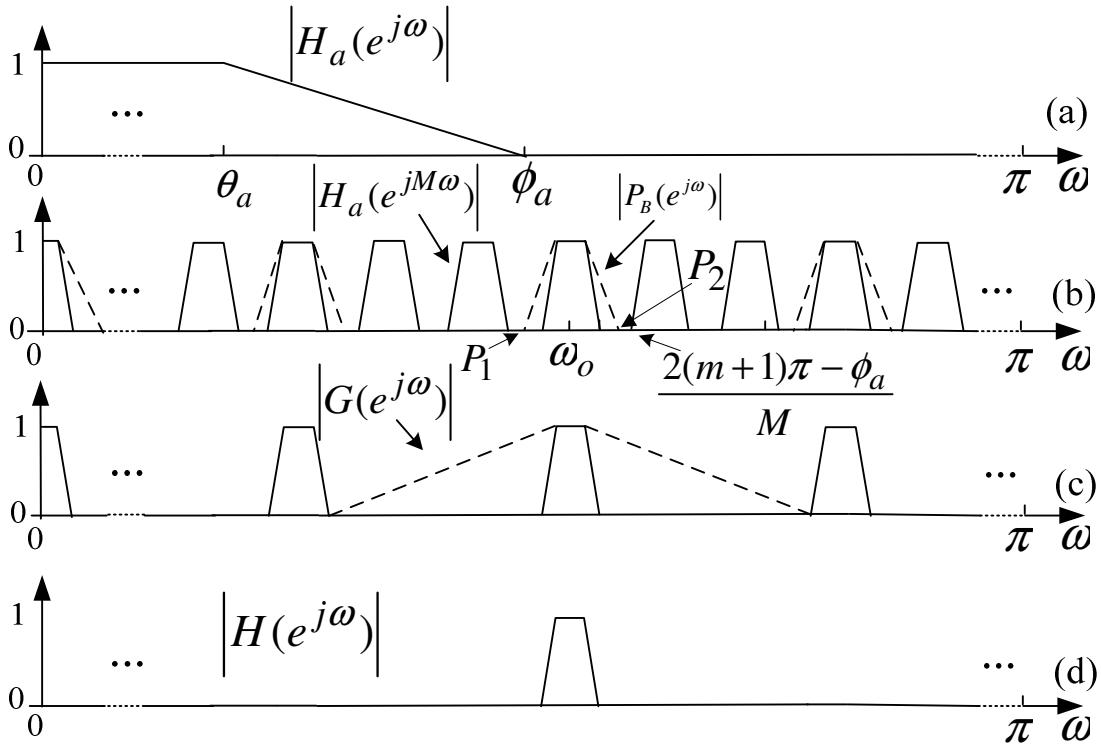

Figure 5.7 Frequency responses for the filters in Fig. 5.6.

If the structure in Fig. 5.6 is used, (5.25) can be relaxed to

$$\begin{cases} \left|P_B\left(e^{j\omega_1}\right)\right| \le \delta_s \\ \left|P_B\left(e^{j\omega_2}\right)\right| \le \delta_s \end{cases} \tag{5.26}$$

where ω_1 and ω_2 are given by

$$\begin{cases} \omega_1 = \dfrac{2\pi(m-1)+\phi_a}{M} \\ \omega_2 = \dfrac{2\pi(m+1)-\phi_a}{M} \end{cases} \tag{5.27}$$

In this case, $P_B(z)$ is used as prefilter and $H_a(z)$ is designed in such a way that $H_a(z)P_B(z)$ meet the overall passband and transition-band specifications. The role of $G(z)$ is to achieve the overall specification.

5.4 Implementation Issue

The proposed masking filters are combinations of identical subfilters with different periods. By folding transformation [81], identical subfilters may be mapped to a single hardware structure [17]. Fig. 5.8 shows an implementation structure for $P_{L2}(z^{N_1})P_{L2}(z^{N_2})$ by applying the concept in [17], where T is a latch for the purpose of storing previous signals for the next operation. A loop is introduced in Fig. 5.8 which is only significant for the view of implementation and will not affect such features as stability and linear-phase for the overall filter. Therefore, adders can be shared between identical subfilters with different periods.

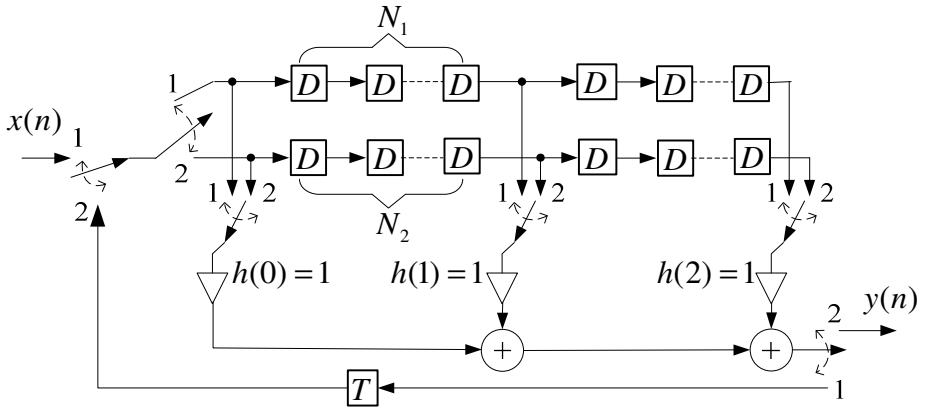

Figure 5.8 An implementation structure for $P_{L2}(z^{N_1})P_{L2}(z^{N_2})$.

5.5 Design Examples and Comparison

5.5.1 Narrowband Lowpass Filters

Two lowpass filters are designed to illustrate the proposed method. Let us consider the first filter with the specifications taken from [12]: $\omega_p = 0.05\pi$, $\omega_s = 0.1\pi$ and $\delta_p = 0.01$, $\delta_s = 0.001$. To design such a filter, different sets of N_i , L_i , and K_i ($i = 1,\ 2,\ ...,\ r$) can be found for different *M*. Using the proposed method, for $M = 9$, N_i are 5, 3, 2, 1. L_i and K_i for all i equal to 1. The length for $H_M(z)$ is 9. To implement the overall filter, 5 multipliers and 13 adders are required; the total number of delay elements is 140. In [12], the optimal IFIR design requires 15 multipliers with 127 delay elements. The proposed approach can achieve more than 66% savings in the number of multipliers. The designed filter is also more efficient than the one in [15], in which 5 multiplier and 170 delay elements are required.

The second example is also taken from [12], which have the passband and stopband edges located at $\omega_p = 0.01\pi,$ and $\omega_s = 0.02\pi,$ respectively. The passband ripple is 0.01 and the stopband ripple is 0.001. With the proposed method, *M* is chosen to be 30, $r = 5$ and N_1 to N_5 in ascending order are 17, 12, 4, 2, 1. L_i for all i are 1. And the values of K_1 to K_5 in ascending order are 1, 1, 1, 0, 0. The length for the model filter $H_M(z)$ is 15. The hardware cost is 8 multipliers, 19 adders and 632 delay elements. Considerable computational savings have been achieved compared with the design in [12] which requires 21 multipliers, 35 adders and 640 delay elements. The results using different design methods are summarized in Table 5.1. The magnitude responses for example 1

and 2 are shown in Figs. 5.9–5.12, respectively. Coefficients for $H_M(z)$ in example 1 and 2 are shown in Appendix A.

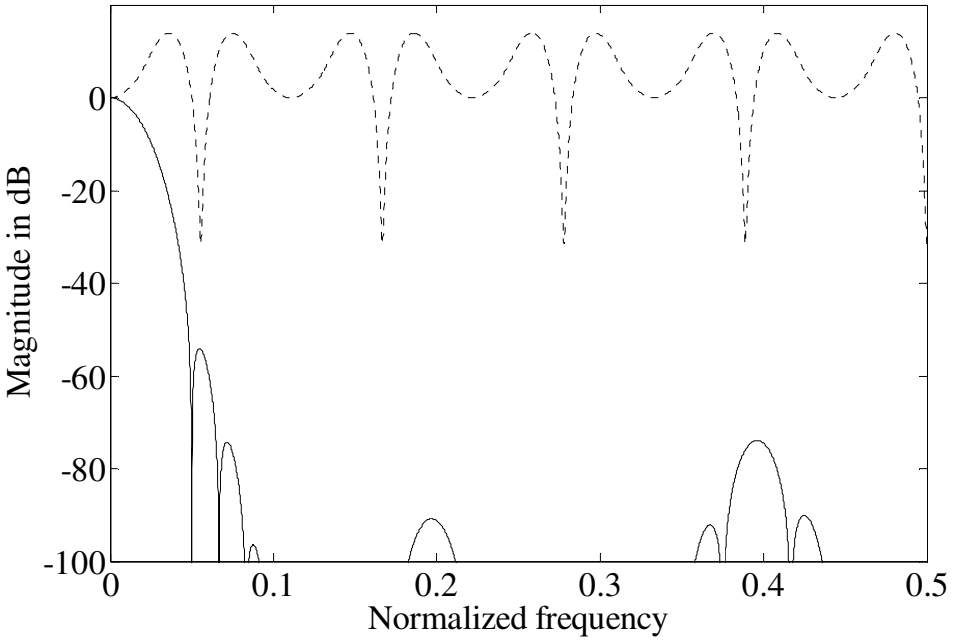

Figure 5.9 Magnitude responses of $P_L(z)$ (solid line) and $H_M(z^M)$ (dotted line) in example 1 (lowpass filter).

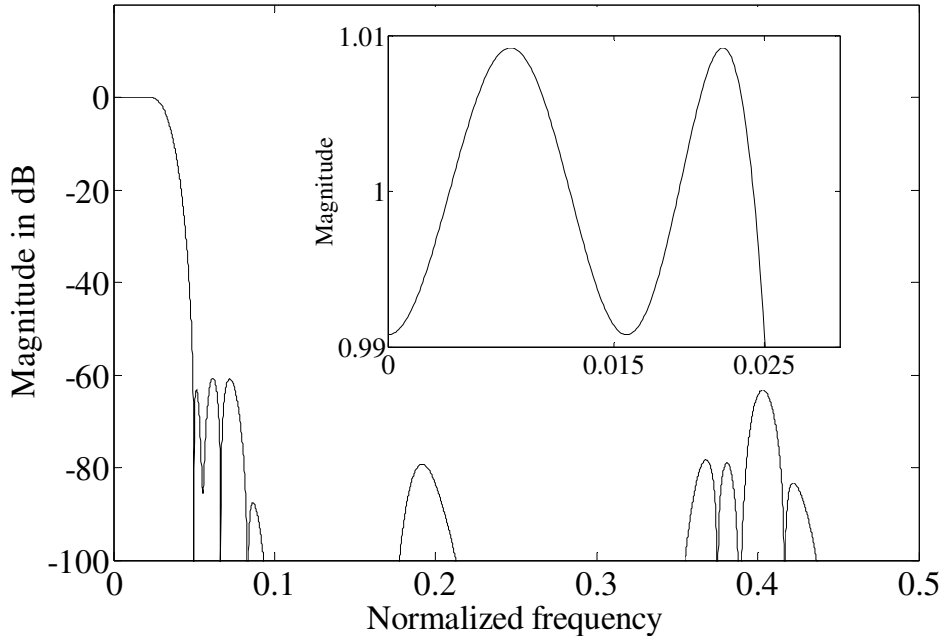

Figure 5.10 Magnitude response of $H(z)$ in example 1 (lowpass filter).

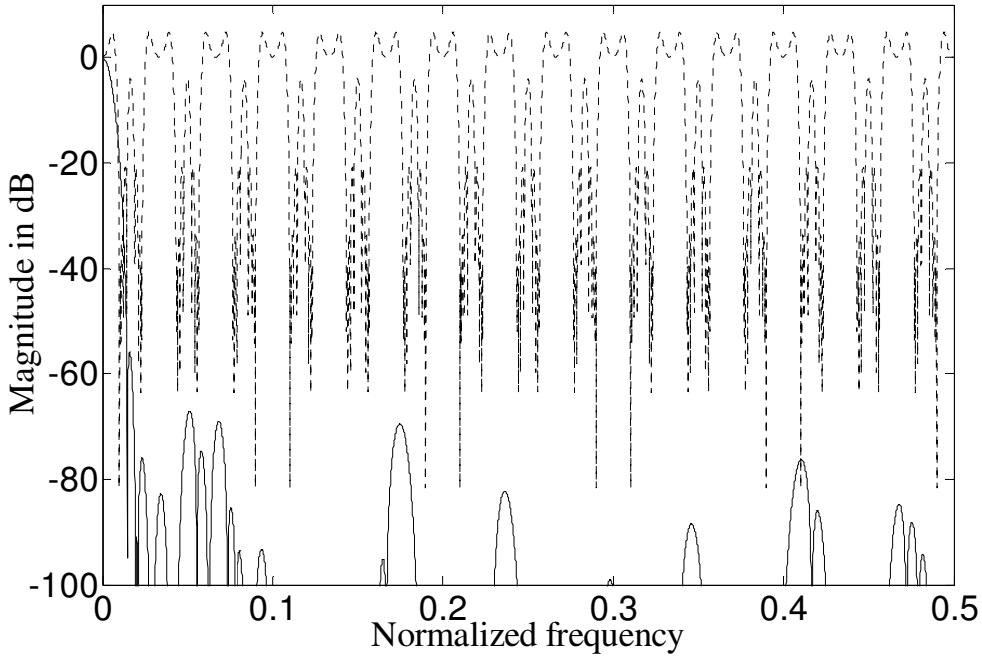

Figure 5.11 Magnitude responses of $P_L(z)$ (solid line) and $H_M(z^M)$ (dotted line) in example 2 (lowpass filter).

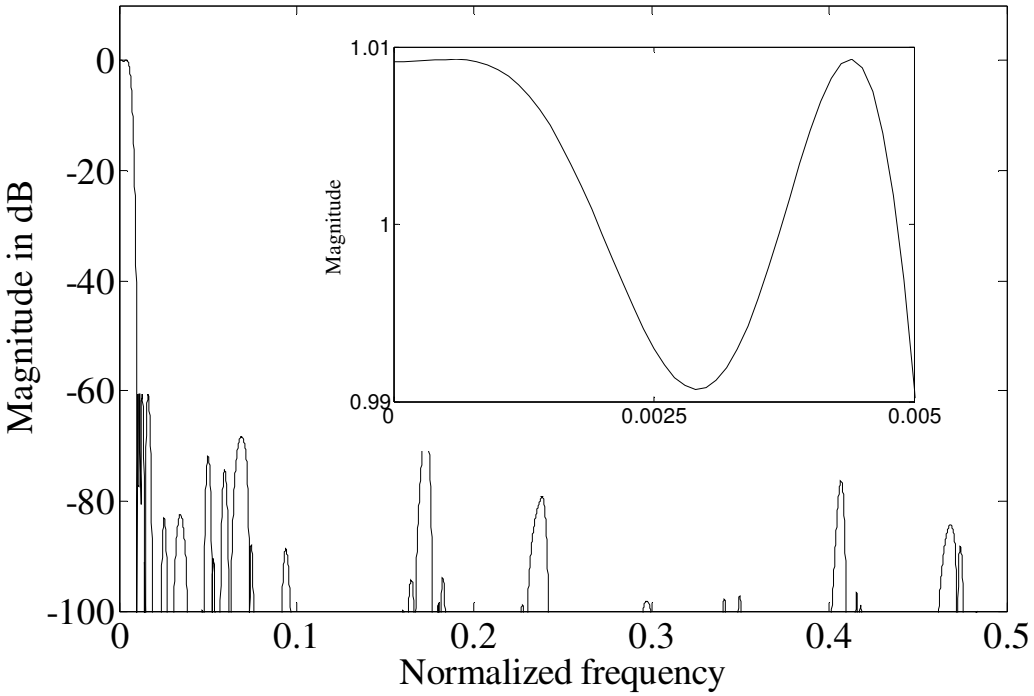

Figure 5.12 Magnitude response of $H(z)$ in example 2 (lowpass filter).

Table 5.1 Results of designing narrowband lowpass filters using different methods.

	Design method	Multipliers	Adders	Delays
Example 1	Conventional	55	108	108
	3-stage IFIR [12]	15	24	127
	SFFM [18]	10	18	181
	Design of [15]	5	19	170
	Proposed: $M = 9$	5	13	140
Example 2	Conventional	270	538	538
	3-stage IFIR [12]	21	35	640
	SFFM [18]	9	16	913
	Proposed: $M = 30$	8	19	632

5.5.2 Wideband Lowpass Filter

This example is a wideband lowpass filter taken from [19] with passband edge and stopband edge at 0.9π and 0.91π, respectively. The passband and stopband ripples are 0.05 and 0.01, respectively. A narrowband highpass filter is designed firstly with the passband and stopband edges at 0.91π and 0.9π, respectively. The overall filter is the complement of the highpass filter. Using the proposed method, for $M = 8$, only the filter type of $P_{Hc}(z)$ is required to form the masking filter. r is found to be 2. N_{21} and N_{22} are 3 and 1, respectively. L_{21} and L_{22} are 2 and 1, respectively. K_{21} and K_{22} are 1 and 2, respectively. The length for the model filter $H_M(z)$ is 57. The implementation of the overall filter requires 29 multipliers, 62 adders and 488 delay elements. Using the single filter frequency masking (SFFM) technique [19], the best design required 37 multipliers, 72 adders and 720 delay elements. Compared with IFIR filters in [10], the proposed

method achieves considerable arithmetic savings with less delay elements, as summarized in Table 5.2. Figs. 5.13–5.15 show the magnitude responses for this example.

Table 5.2 Results of designing the wideband lowpass filter using different methods.

Design method	Multipliers	Adders	Delays
Conventional	217	432	432
One stage IFIR [10]	58	115	512
SFFM [19]	37	72	720
Proposed: $M = 8$	29	62	488

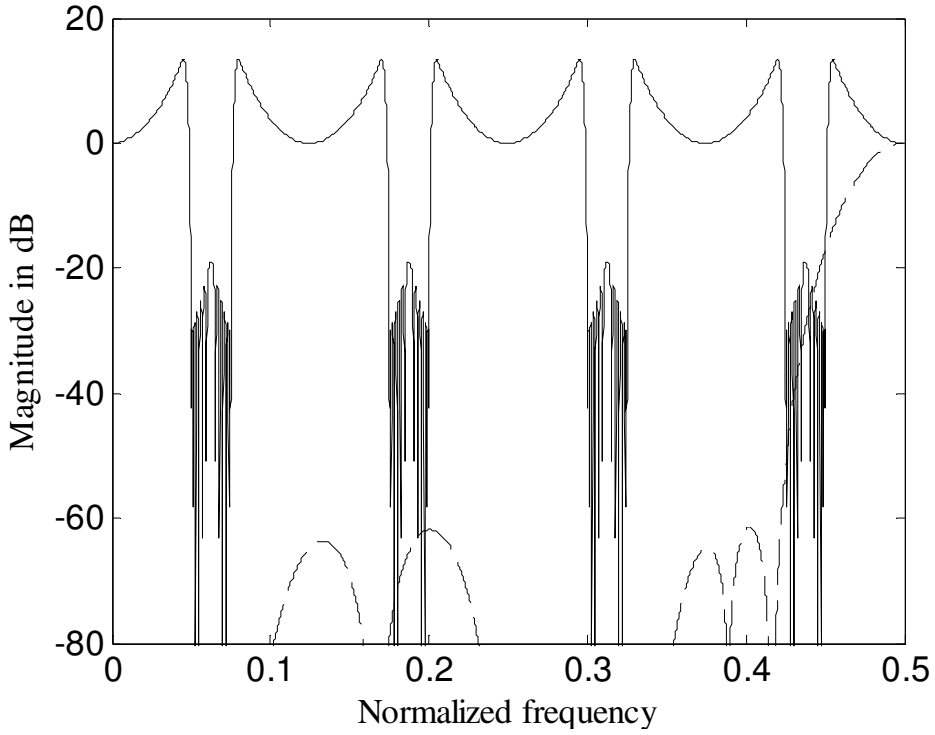

Figure 5.13 Magnitude responses of $P_H(z)$ (dashed line) and $H_M(z^M)$ (solid line) for the wideband lowpass filter.

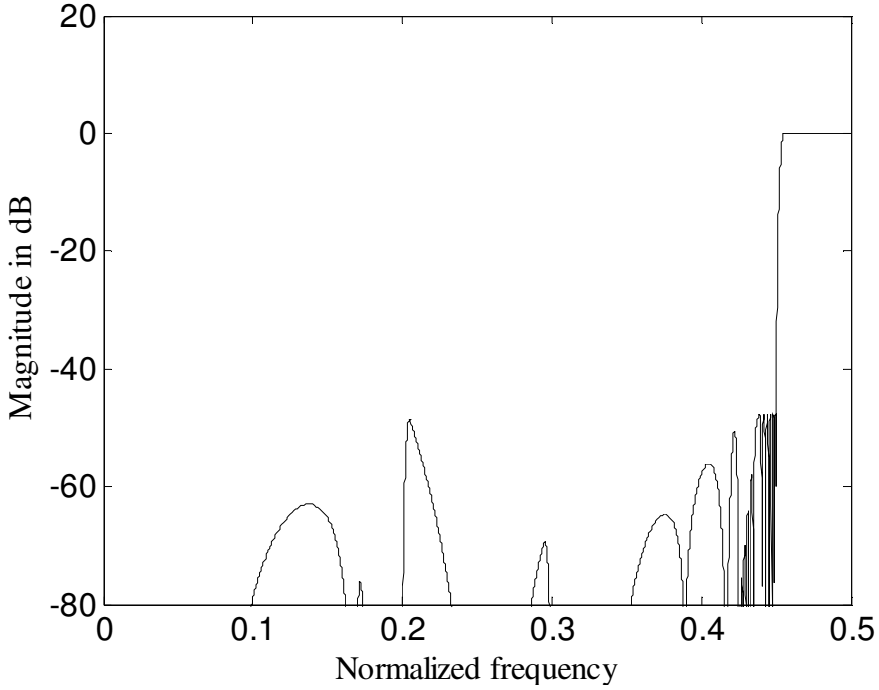

Figure 5.14 Magnitude response of $P_H(z)H_M(z^M)$ for the wideband lowpass filter.

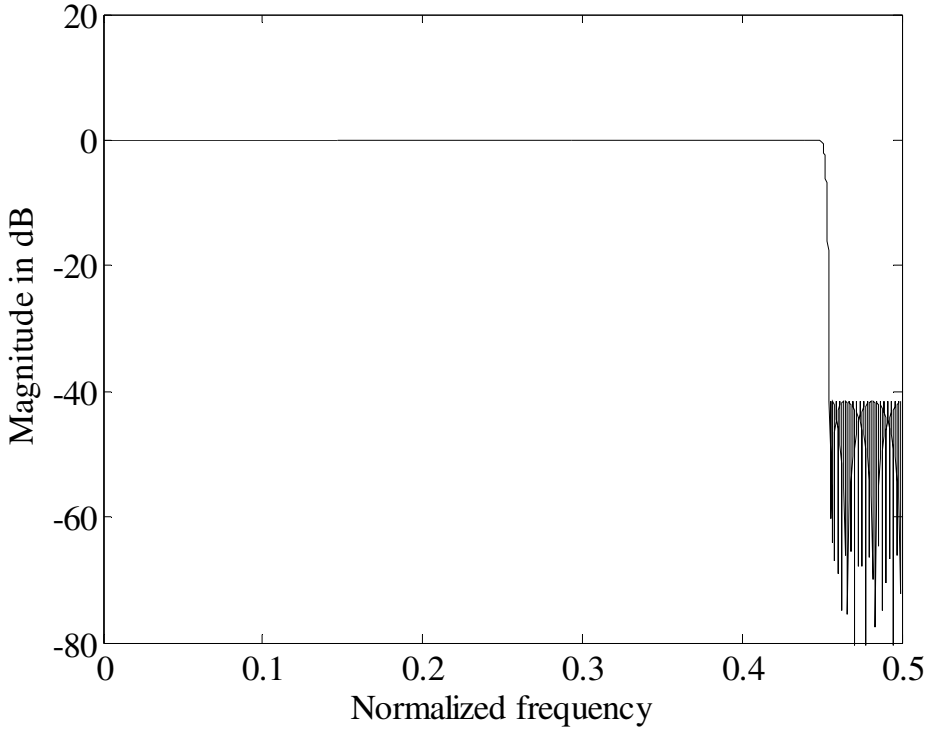

Figure 5.15 Magnitude response of $H(z)$ for the wideband lowpass filter.

5.5.3 Bandpass Filters

Three bandpass filters are designed using the proposed filter $P_B(z)$ given by (5.11). When designing the first filter, $P_B(z)$ is a masking filter. For the design of the other two filters, $P_B(z)$ is a prefilter.

Let us consider the first narrowband bandpass filter with the specifications given by

$$\omega_{p_1} = 0.24\times 2\pi, \quad \omega_{p_2} = 0.26\times 2\pi \quad \text{(passband edges)}$$

$$\omega_{s_1} = 0.239\times 2\pi, \quad \omega_{s_2} = 0.261\times 2\pi \quad \text{(stopband edges)}$$

Maximum passband ripple: 0.01.

Minimum stopband attenuation: 40 dB.

For $M = 24$, N_i are found to be $8^{(L)}$, $4^{(L)}$, and $2^{(H)}$, respectively. L_i for all i are 1. K_i are 1, 0 and 0. The length of the model filter is 82. The implementation of this filter requires 41 multipliers, 89 adders and 2018 delay elements. The estimated filter length of the conventional design is about 1850. Using the original IFIR approach, the optimal interpolation factor is 20. The lengths of the corresponding model filter and masking filter are 99 and 81, respectively. This corresponds to 91 multipliers, 178 adders, and 2040 delay elements. Compared with the original IFIR approach the overall savings in the number of multipliers and adders are about 55.4% and 50%, respectively. Moreover, the implementation using the proposed method requires less delay elements than the original IFIR approach. The computational cost of different design methods is summarized in Table 5.3. Figs. 5.16 and 5.17 show the magnitude responses for this example.

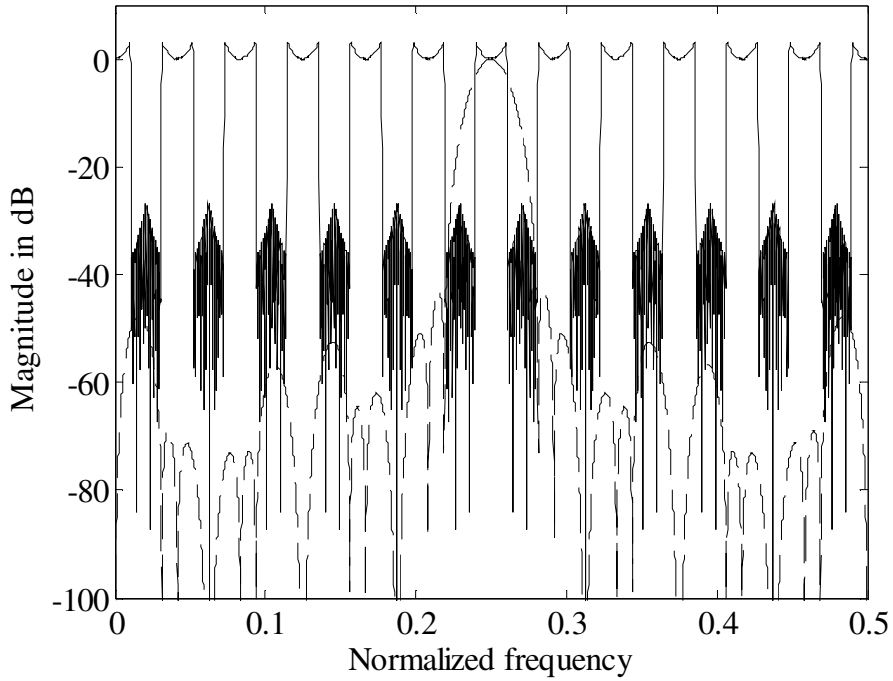

Figure 5.16 Magnitude responses of $P_B(z)$ (dashed line) and $H_M(z^M)$ (solid line) in example 1(bandpass filter).

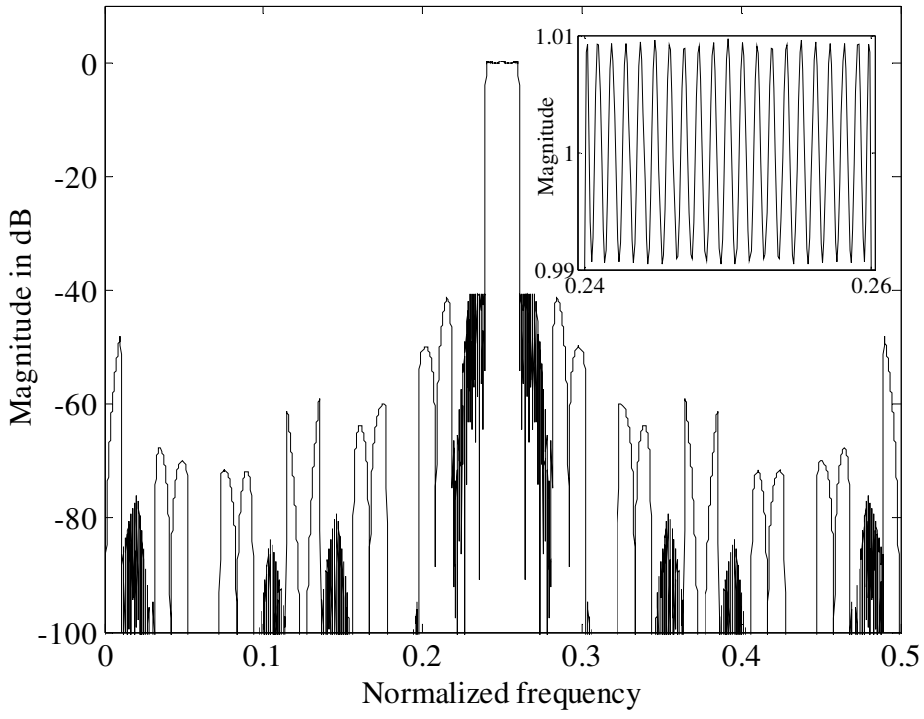

Figure 5.17 Magnitude response of $H(z)$ in example 1 (bandpass filter).

The second filter is taken from [15]. The center frequency of the passband of the filter is located at $\omega_o = 0.251 \times 2\pi$. The passband width and the transition-width are 0.02π and 0.04π, respectively. The passband ripple is at most ±0.045 dB and the stopband attenuation is at least 30 dB. The implementation of this filter using the method in [15] requires 5 multipliers, 12 adders and 120 delay elements. Using the proposed approach, $P_B(z)$ serves as a prefilter. $P_B(z)$ is constructed by $P_{Lc}(z)$ only. N_i are found to be 8, 4 and 2. L_i are 1 for $i = 1,\ 2,\ 3$. K_1 to K_3 are 1, 0, and 0. The length of the interpolated equalizer is 5 with an interpolation filter factor of 12. The design corresponds to 3 multipliers, 9 adders and 121 delay elements. In [13], 18 multipliers, 27 adders and 111 delay elements are required to implement this filter. Clearly, the proposed method achieves significant savings in terms of arithmetic operations compared with the techniques in [13] and [15]. The magnitude responses of subfilters designed in this example are illustrated in Figs. 5.18 and 5.19. The computational cost of different design methods is also summarized in Table 5.3.

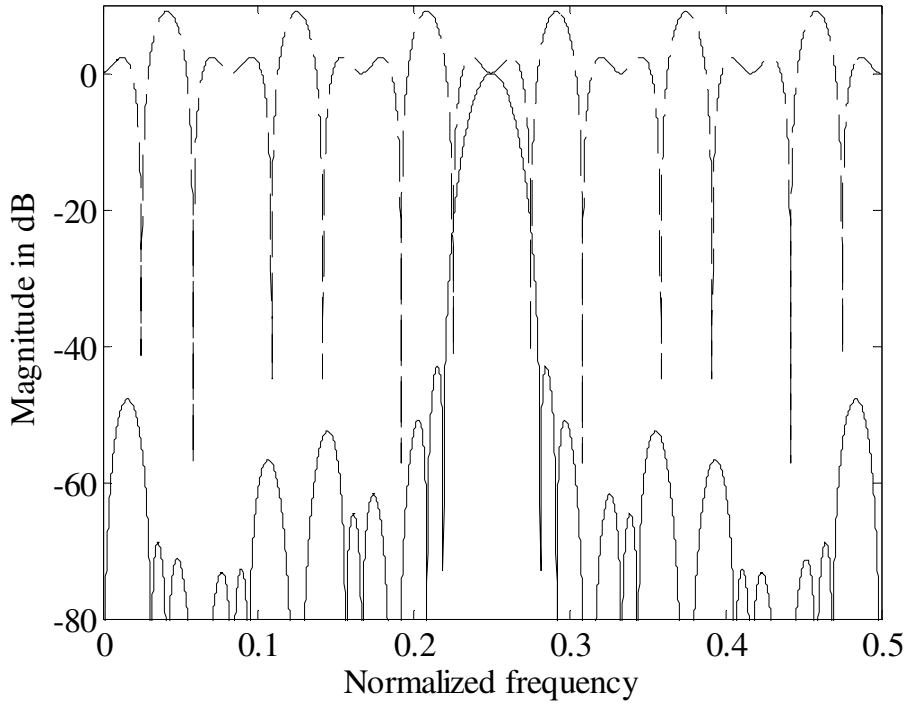

Figure 5.18 Magnitude responses of $P_B(z)$ (solid line) and $H_M(z^M)$ (dashed line) in example 2 (bandpass filter).

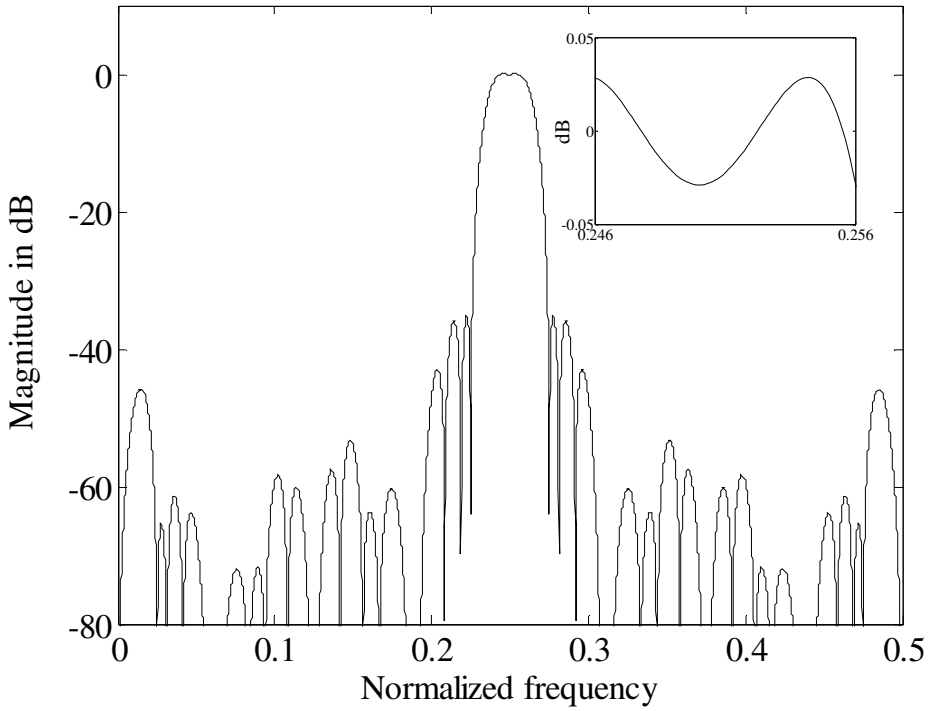

Figure 5.19 Magnitude response of $H(z)$ in example 2 (bandpass filter).

The last example is a bandpass filter taken from [15] with the center frequency of the passband located at $\omega_o = 0.2 \times 2\pi$. The passband width and the transition-width are 0.044π and 0.042π, respectively. The passband ripple is at most ±0.5 dB and the stopband attenuation is at least 60 dB. Using the prefilter-equalizer [4] design method, 43 multiplier, 163 adders and 162 delay elements are required to implement this filter. In [15], the hardware cost is 7 multipliers, 48 adders and 217 delay elements. Using the proposed design, 4 sections of $P_{LH}(N_i)$ are cascaded to form the prefilter $P_B(z)$. N_i are found to be $10^{(L)}$, $5^{(L)}$, $3^{(H)}$ and $2^{(H)}$. L_i for all i are 1. K_1 to K_4 are 1, 1, 1, and 2. The length of the interpolated equalizer is 7 with an interpolation factor of 15. The implementation requires 4 multipliers, 16 adders and 218 delay elements. Table 5.3 summarizes the design results of different design methods. If a larger interpolation factor is adopted for the equalizer, more savings in terms of multipliers can be achieved at the price of increasing the number of delay elements as shown in Table 5.3. Compared with other computationally efficient FIR design methods, the proposed approach can greatly decrease the required number of multipliers and adders in implementation, as shown in Table 5.3. The magnitude responses for this example for $M = 15$ are plotted in Figs. 5.20 and 5.21. Coefficients for $H_M(z)$ in example 2 and 3 are shown in Appendix B.

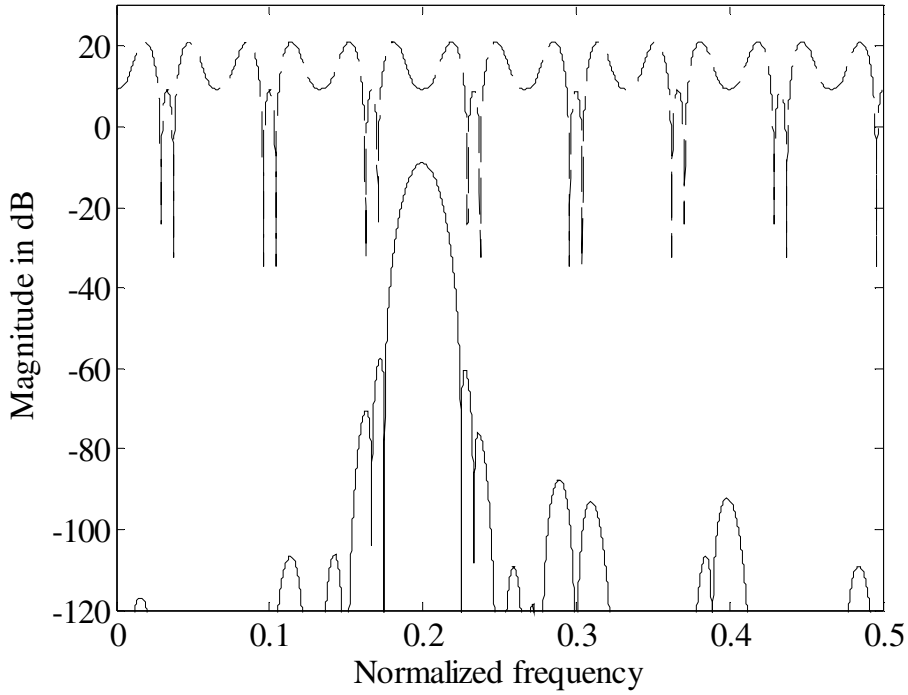

Figure 5.20 Magnitude responses of $P_B(z)$ (solid line) and $H_M(z^M)$ (dashed line) in example 3 (bandpass filter).

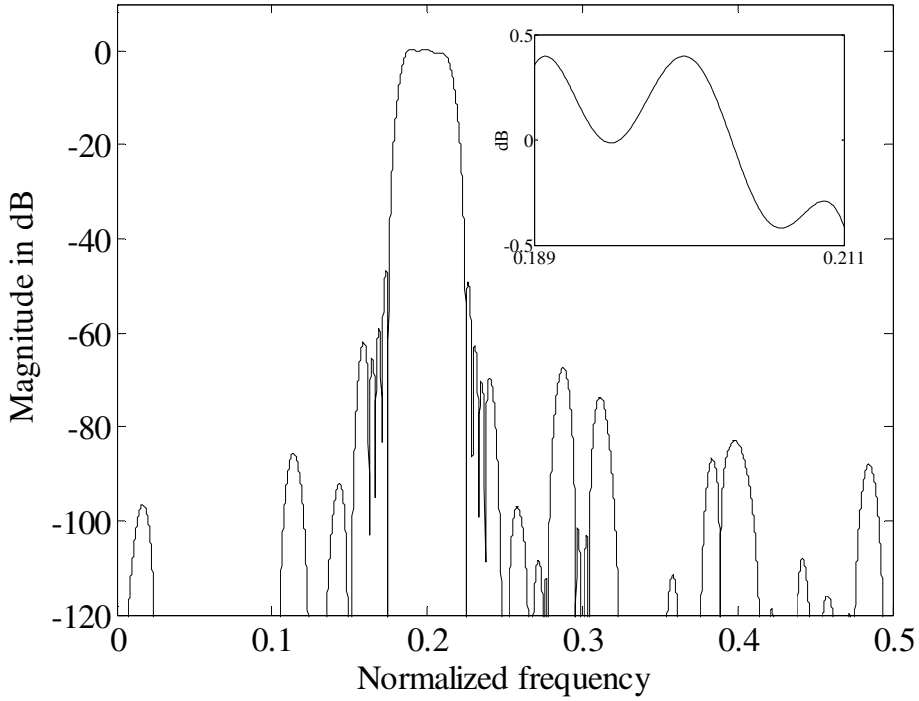

Figure 5.21 Magnitude response of $H(z)$ in example 3 (bandpass filter).

Table 5.3 Results of designing narrowband bandpass filters using different methods.

	Design method	Multipliers	Adders	Delays
Filter 1	Conventional	925	1849	1849
	One stage IFIR filter	91	178	2040
	Proposed: $M = 9$	41	89	2018
Filter 2	Conventional	48	94	94
	Design of [13]	18	27	111
	Design of [15]	5	12	120
	Proposed: $M = 12$	3	9	121
Filter 3	Conventional	61	120	120
	Prefilter-equalizer [4]	43	163	162
	Design of [15]	7	48	217
	Proposed: $M = 15$	4	16	218
	Proposed: $M = 30$	3	14	238

5.6 Summary

In this chapter, a new class of multiplication-free masking filters is proposed for the design of narrowband lowpass, highpass and bandpass IFIR filters. Wideband filters can be easily obtained from the corresponding narrowband IFIR filters. Using the proposed method significant savings in arithmetic operations can be achieved compared with other efficient design methods. The advantage of the new approach is that the required number of multipliers and adders is reduced greatly while keeping the number of the delay elements in check. Moreover, the proposed filter structures are simple and can be easily realized with VLSI technology.

Chapter 6

Novel Digital Filter Banks for Digital Audio Applications

6.1 Introduction

Digital audio systems have many advantages in the quality of sound reproduction, such as reduced distortions. The rapid development in CMOS technology has made it possible to implement sophisticated digital algorithms on-chip. This helps to push the audio signal processing which is currently done in the analog domain into the digital domain. Digital filter banks are desirable in high-fidelity audio applications, where an audio signal is split into *n* adjacent frequency bands for processing, as shown in Fig. 6.1.

Various ways [82–87] have been proposed to design digital filter banks for audio applications. However, there exist some disadvantages among those methods such as phase distortion [82], limited frequency bands (normally less than 4) and dynamic

range [83–85], uniform subbands [86], and relatively high computationally cost [87]. In this chapter, the FRM technique is extended for the design of non-uniform linear-phase filter banks. The proposed filter banks are not multi-rate systems. Therefore, equalization for each subband can be easily performed. Moreover, the multi-complementary concept is employed in the new filter banks, leading to perfect reconstruction of signals.

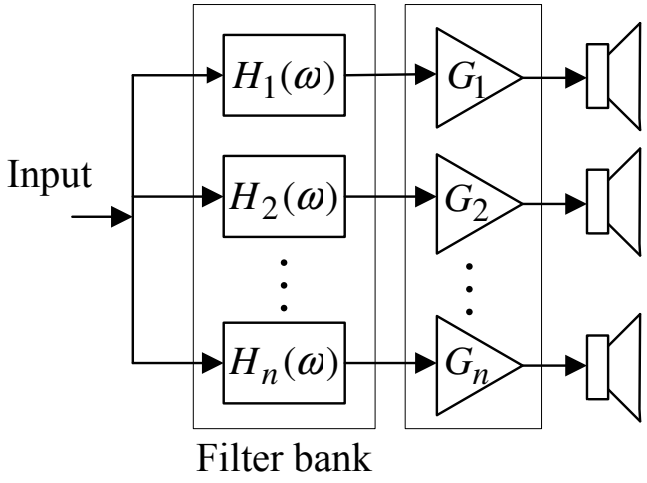

Figure 6.1 An *n*-way digital audio system.

This chapter is organized as follows. A new structure for a 3-way non-uniform filter bank is presented in Section 6.2. Design equations are given in Section 6.3. A generalized structure for the digital filter banks is presented in Section 6.4, and the design examples are provided in Section 6.5. A summary is given in Section 6.6.

6.2 A New Non-uniform 3-way Filter Bank

In the FRM approach, a bandedge shaping filter $H_a(z^L)$ has periodic frequency response. The multiple passbands of $H_a(z^L)$ can be used to form a non-uniform filter

bank if the delayed-complementary concept in the FRM technique is applied. Fig. 6.2 shows one of such non-uniform filter bank structures, where N_a is filter length of $H_a(z)$ and N_m is the length of the longer filter among two masking filters $F_1(z)$ and $F_2(z)$. N_3 is the filter length of $F_3(z)$. The frequency responses of the various subfilters in the 3-way filter bank are shown in Figs. 6.3(a)–6.3(i).

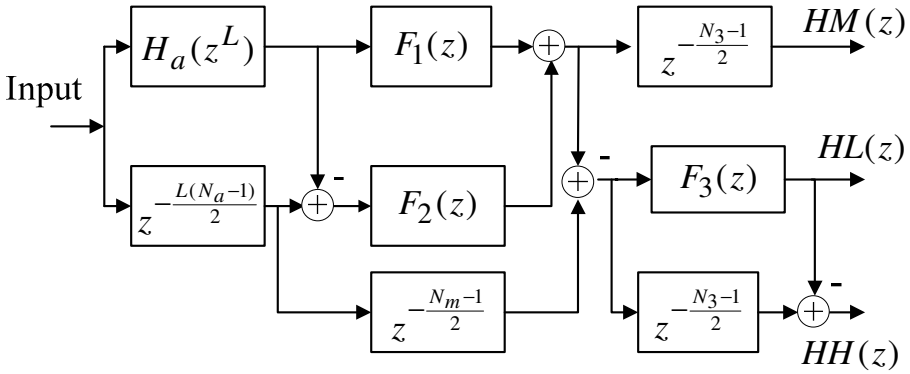

Figure 6.2 A realization structure for the 3-way filter bank.

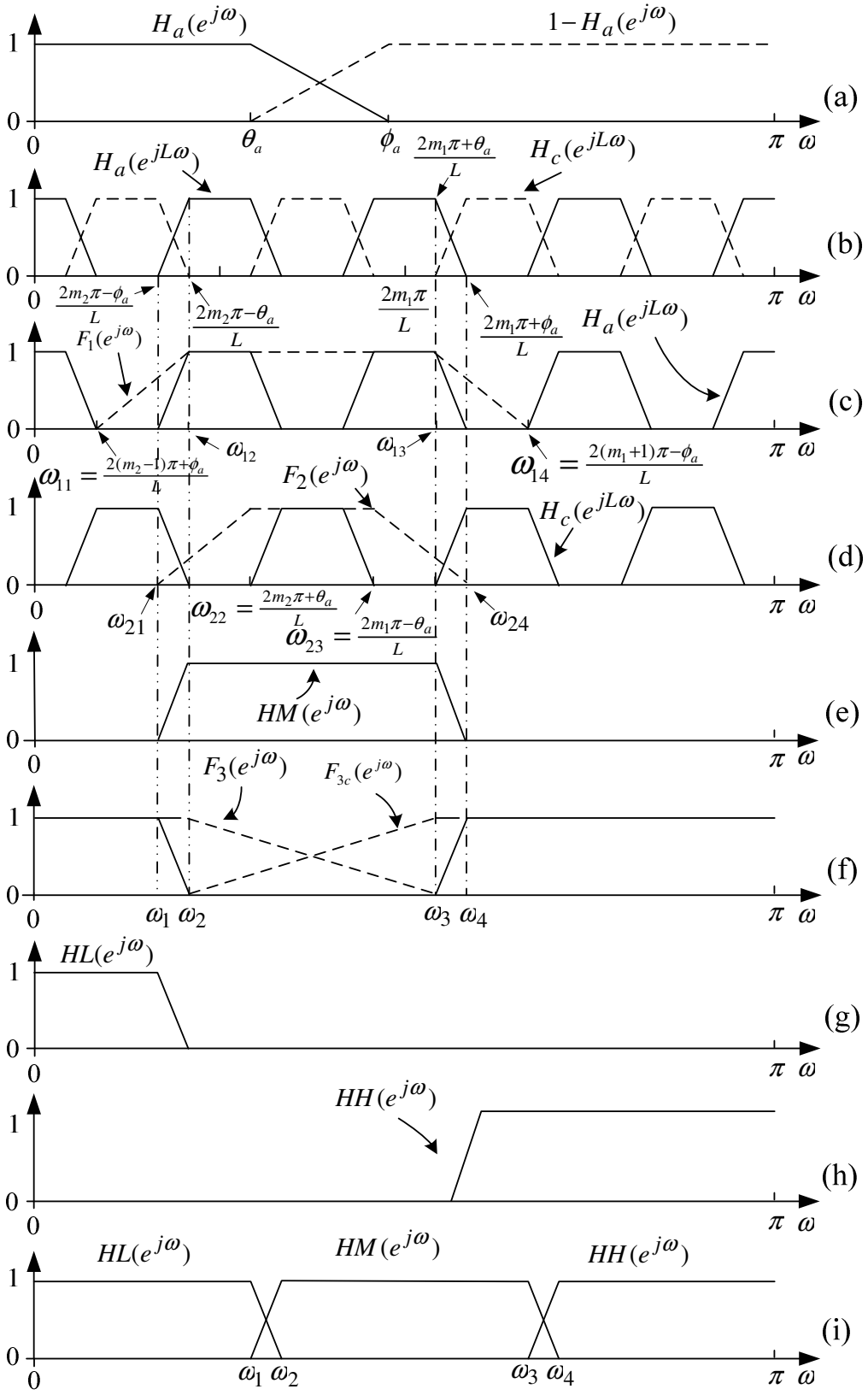

Figure 6.3 Frequency responses of the subfilters of the 3-way filter bank.

In Fig. 6.3(a), $H_a(z)$ is a prototype lowpass filter with passband and stopband edges at θ_a and ϕ_a, respectively. Replacing each delay element of $H_a(z)$ with *L* delay elements, the frequency response of $H_a(z)$ is compressed by a factor of *L*, as shown in Fig. 6.3(b). $H_c(z^L)$ is the complement of $H_a(z^L)$. Two masking filters $F_1(z)$ and $F_2(z)$, as shown in Figs. 6.3(c) and 6.3(d), are cascaded to $H_a(z^L)$ and $H_c(z^L)$, respectively, to form the middle frequency band $HM(z)$ as shown in Figs. 6.2 and 6.3(e). Cascading the complement of $HM(z)$ with another lowpass masking filter $F_3(z)$ and $F_{3c}(z)$, respectively, where $F_{3c}(z)$ refers to the complement of $F_3(z)$ as shown in Fig. 6.3(f), we get the lower frequency band $HL(z)$ and the upper frequency band $HH(z)$ with their frequency responses shown in Figs. 6.3(g) and 6.3(h), respectively. The case where the bandedges of $HM(z)$ are determined by $H_a(z^L)$ is denoted as Case AA as shown in Fig. 6.3(e), and the case where the bandedges of $HM(z)$ are determined by $H_c(z^L)$ is denoted as Case BB as shown in Fig. 6.3(i). If the transition-bands of $HM(z)$ are determined by $H_c(z^L)$ and $H_a(z^L)$, respectively, it refers to Case BA. Similarly, Case AB refers to the case where the transition-bands of $HM(z)$ are determined by $H_a(z^L)$ and $H_c(z^L)$, respectively.

6.3 Design Equations

To synthesize the 3-way non-uniform filter bank introduced in Section 6.2, four subfilters need to be designed, namely, $H_a(z)$, $F_1(z)$, $F_2(z)$, and $F_3(z)$. In this section, the design equations are derived using a lowpass prototype filter. The main issue here is how to select a proper prototype filter $H_a(z)$ and the interpolation factor *L* such that

the middle frequency bandpass filter $HM(z)$ meets the given specifications. Let us denote ω_1, ω_2, ω_3 and ω_4 as the bandedge specifications of the overall filter as shown in Figs. 6.3(f) and 6.3(i).

In case AA and BA the right-side transition-band of $HM(z)$ is determined by $H_a(z^L)$, as shown in Figs. 6.3(b) and 6.3(e), we have

$$\begin{cases} \omega_3 = \dfrac{2m_1\pi + \theta_a}{L} \\ \omega_4 = \dfrac{2m_1\pi + \phi_a}{L} \end{cases} \tag{6.1}$$

where m_1 is an integer. To ensure that (6.1) yields a solution with $0 < \theta_a < \phi_a < \pi$, we have

$$m_1 = \left\lfloor \frac{\omega_3 L}{2\pi} \right\rfloor \tag{6.2}$$

$$\theta_a = \omega_3 L - 2m_1\pi \tag{6.3}$$

$$\phi_a = \omega_4 L - 2m_1\pi \tag{6.4}$$

where $\lfloor x \rfloor$ denotes the largest integer less than or equal to *x*.

Similarly, in Case AB and Case BB the right-side transition-band of $HM(z)$ is determined by $H_c(z^L)$, and the following design equations are obtained:

$$\begin{cases} \omega_3 = \dfrac{2m_1\pi - \phi_a}{L} \\ \omega_4 = \dfrac{2m_1\pi - \theta_a}{L} \end{cases} \tag{6.5}$$

$$m_1 = \left\lceil \frac{\omega_4 L}{2\pi} \right\rceil \tag{6.6}$$

$$\theta_a = 2m_1\pi - \omega_4 L \tag{6.7}$$

$$\phi_a = 2m_1\pi - \omega_3 L \tag{6.8}$$

where $\lceil x \rceil$ denotes the least integer larger than or equal to x.

To meet the requirement of the left-side transition-band of $HM(z)$, L must satisfy the following conditions:

$$\begin{cases} \omega_1 = \dfrac{2m_2\pi - \phi_a}{L} \\ \omega_2 = \dfrac{2m_2\pi - \theta_a}{L} \end{cases}, \text{ for Case A} \bullet \tag{6.9}$$

and

$$\begin{cases} \omega_1 = \dfrac{2m_2\pi + \theta_a}{L} \\ \omega_2 = \dfrac{2m_2\pi + \phi_a}{L} \end{cases}, \text{ for Case B} \bullet \tag{6.10}$$

where m_2 is an integer less than m_1, and "$\bullet$" denotes "A" or "B". (6.1)–(6.10) are used to determine the bandedges of the prototype filter $H_a(z)$ and the interpolation factor L. The value of L minimizing the overall filter complexity can be found using an exhaustive search program.

When the bandedges of $H_a(z)$ are determined, it is easy to derive the bandedges of the other subfilters. Let ω_{11}, ω_{12}, ω_{13} and ω_{14} be the bandedges of $F_1(z)$, as shown in Fig. 6.3(c). Similar notations are applied to $F_2(z)$, as shown in Fig. 6.3(d). For case AA, we have

$$\omega_{11} = \frac{2(m_2 - 1)\pi + \phi_a}{L} \tag{6.11}$$

$$\omega_{12} = \omega_2 \tag{6.12}$$

$$\omega_{13} = \omega_3 \tag{6.13}$$

$$\omega_{14} = \frac{2(m_1 + 1)\pi - \phi_a}{L} \tag{6.14}$$

$$\omega_{21} = \omega_1 \tag{6.15}$$

$$\omega_{22} = \frac{2m_2\pi + \theta_a}{L} \tag{6.16}$$

$$\omega_{23} = \frac{2m_1\pi - \theta_a}{L} \tag{6.17}$$

$$\omega_{24} = \omega_4 \tag{6.18}$$

For case BB, the bandedges of $F_1(z)$ and $F_2(z)$ are given by

$$\omega_{11} = \omega_1 \tag{6.19}$$

$$\omega_{12} = \frac{2(m_2 + 1)\pi - \phi_a}{L} \tag{6.20}$$

$$\omega_{13} = \frac{2(m_1 - 1)\pi + \phi_a}{L} \tag{6.21}$$

$$\omega_{14} = \omega_4 \tag{6.22}$$

$$\omega_{21} = \frac{2m_2\pi - \theta_a}{L} \tag{6.23}$$

$$\omega_{22} = \omega_2 \tag{6.24}$$

$$\omega_{23} = \omega_3 \tag{6.25}$$

$$\omega_{24} = \frac{2m_1\pi + \theta_a}{L} \tag{6.26}$$

$F_3(z)$ is a lowpass filter with the passband and stopband edges located at ω_2 and ω_3, respectively, as shown in Fig. 6.3(f).

The same procedures can be employed to calculate the bandedges of each subfilter for Case AB and Case BA. For convenience, Table 6.1 lists the design equations of $F_1(z)$ and $F_2(z)$ for Case AB and Case BA, respectively.

Table 6.1 Design equations of $F_1(z)$ and $F_2(z)$ for Case AB and Case BA.

	$F_1(z)$	$F_2(z)$
Case AB	$\omega_{11} = [2(m_2 - 1)\pi + \phi_a]/L$ $\omega_{12} = \omega_2$ $\omega_{13} = [2(m_1 - 1)\pi + \phi_a]/L$ $\omega_{14} = \omega_4$	$\omega_{21} = \omega_1$ $\omega_{22} = (2m_2\pi + \theta_a)/L$ $\omega_{23} = \omega_3$ $\omega_{24} = (2m_1\pi + \theta_a)/L$
Case BA	$\omega_{11} = \omega_1$ $\omega_{12} = [2(m_2 + 1)\pi - \phi_a]/L$ $\omega_{13} = \omega_3$ $\omega_{14} = [2(m_1 + 1)\pi - \phi_a)]/L$	$\omega_{21} = (2m_2\pi - \theta_a)/L$ $\omega_{22} = \omega_2$ $\omega_{23} = (2m_1\pi - \theta_a)/L$ $\omega_{24} = \omega_4$

6.4 A Generalized Structure

The structure in Fig. 6.2 is able to synthesize most of non-uniform filter banks. In some cases, it is difficult to find a suitable L and a prototype filter that produce an overall filter satisfying the given bandedge specifications. A generalized structure of the filter bank, as shown in Fig. 6.4, can be employed. The frequency responses of the various subfilters in Fig. 6.4 are sketched in Fig. 6.5. $H_1(z)$ is a lowpass filter used to produce the lower-band output. Its complement is cascaded with another lowpass filter $H_2(z)$ to form the middle-band output. The higher-band output can be derived from

$H_{1c}(z)$ and $H_{2c}(z)$, which are the complements of $H_1(z)$ and $H_2(z)$, respectively. G_1 and G_2 are the group delays of $H_1(z)$ and $H_2(z)$, respectively.

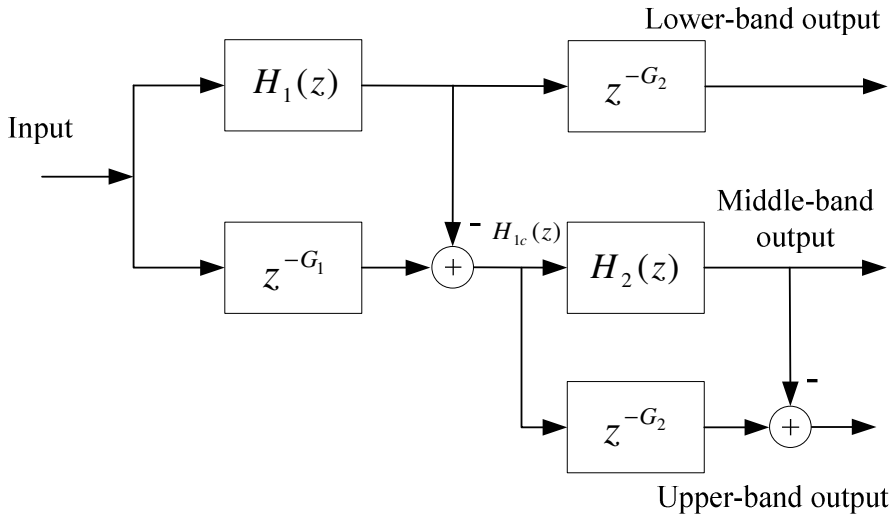

Figure 6.4 A generalized structure for the 3-way filter bank.

The structure of Fig. 6.4 is able to synthesize any non-uniform filter bank with given specifications. However, the computational complexity is normally higher than the one in Fig. 6.2. In practical implementation, $H_1(z)$ is a narrowband filter which can be realized by interpolated finite impulse response (IFIR) filters or filter structures introduced in Chapter 5 in order to minimize the computational complexity. Whereas, $H_2(z)$ can be designed using the FRM technique to reduce the hardware cost.

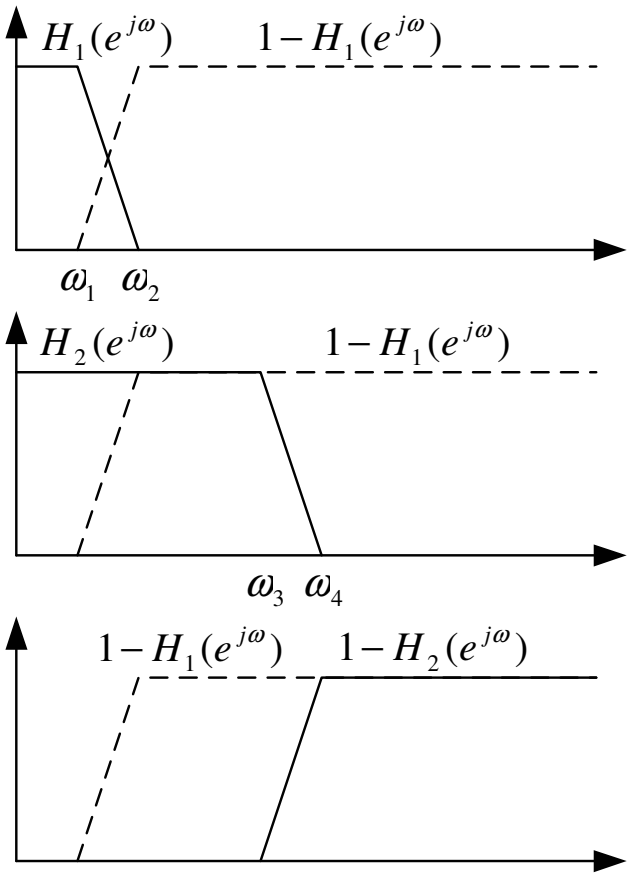

Figure 6.5 Frequency responses of the subfilters in Fig. 6.4.

6.5 Examples

***Example* 1**

To illustrate the new method, a 3-way digital filter bank is designed with the same specifications as in the example of [87], namely, $\omega_1 = 0.12\pi$, $\omega_2 = 0.2\pi$, $\omega_3 = 0.4\pi$, and $\omega_4 = 0.48\pi$. The maximum passband ripple and the minimum stopband attenuation for each subband are 0.0001 and 80 dB, respectively. The generalized structure in Fig. 6.4 is used to synthesize this filter bank. The lengths for $H_1(z)$ and $H_2(z)$ are 45 and 107, respectively. In [87], three subfilters were used with a total length of 195. The proposed approach requires a total length of 152 which corresponds

to more than 20% savings in the number of arithmetic operations compared with the method in [87]. The magnitude responses of the three subfilters are shown in Fig. 6.6 (a). The peak-to-peak deviation for the magnitude-summed frequency responses of all subband filters is less than 5×10^{-15} dB as shown in Figs. 6.6 and 6.7.

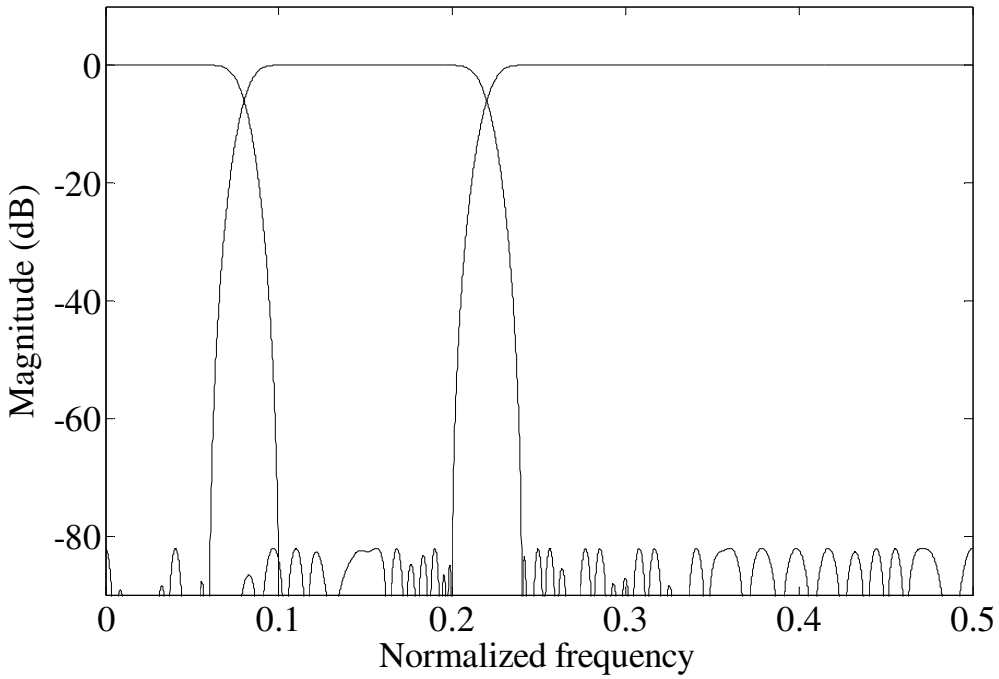

Figure 6.6 Magnitude responses of three subbands in example 1.

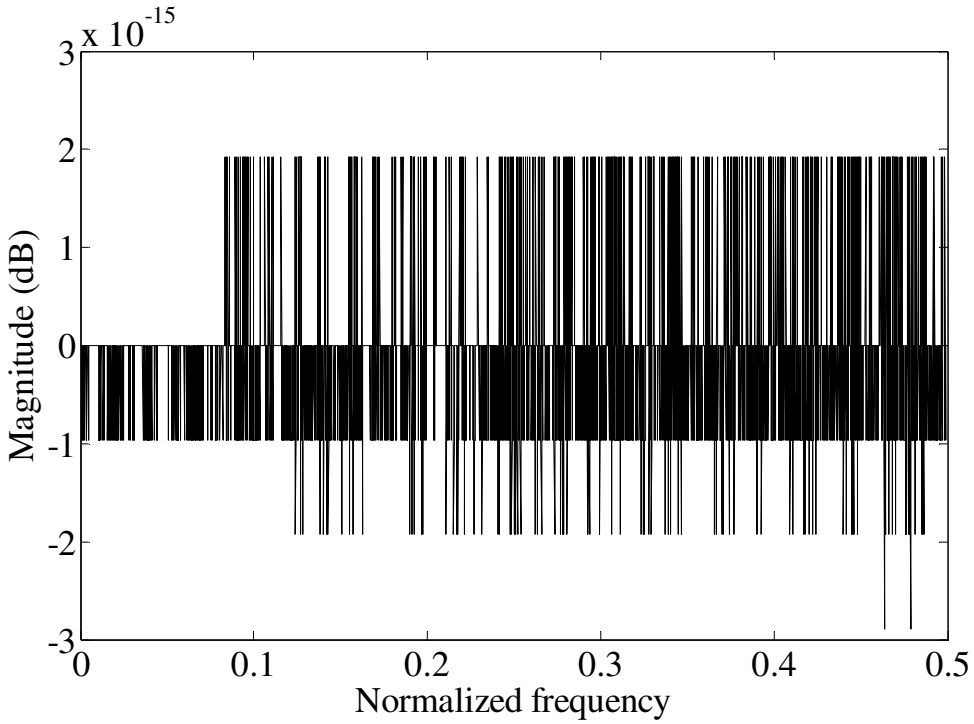

Figure 6.7 The summered magnitude response in example 1.

***Example* 2**

In this example, another 3-way crossover system is designed with the following specifications: $\omega_1 = 0.08\pi$, $\omega_2 = 0.16\pi$, $\omega_3 = 0.34\pi$, and $\omega_4 = 0.42\pi$. The filter has the same transition-width and ripple requirements as in example 1. For this filter bank, the structure in Fig. 6.2 is used. The interpolation factor for $H_a(z)$ is 4, for this reason, $HM(z)$ can be obtained from the complement of $H_a(z^4)$. As a result, $F_1(z)$ is omitted. The lengths of $H_a(z)$, $F_2(z)$, and $F_3(z)$ are 29, 35, and 53, respectively. The total length is 117. The magnitude responses of subfilters are shown in Fig. 6.8. Clearly, this design is more computationally efficient than example 1 and the one in [87].

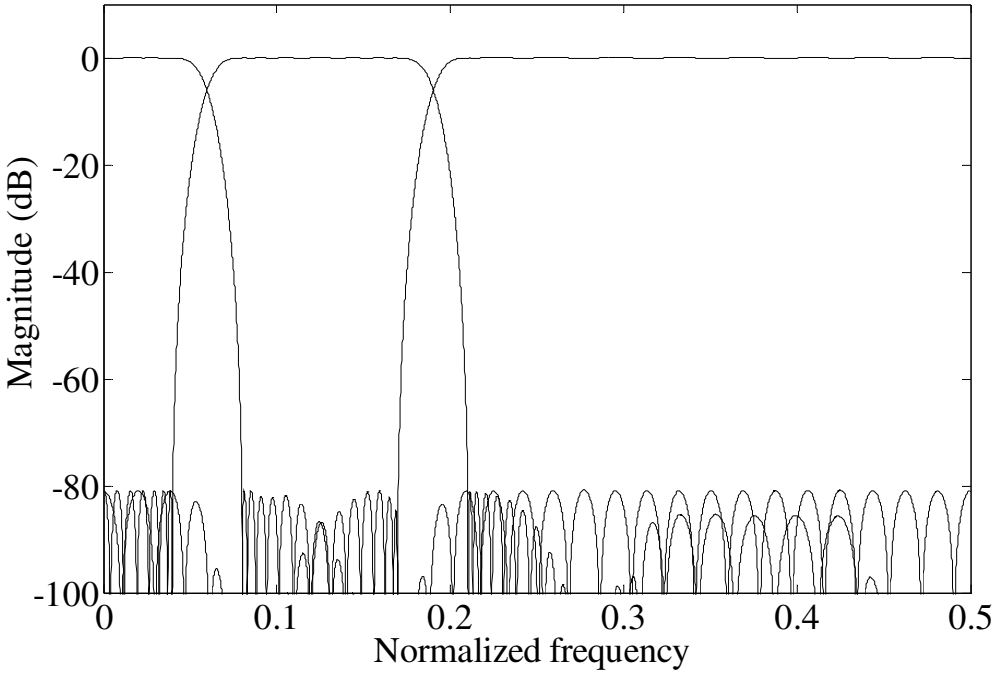

Figure 6.8 Magnitude responses of subbands in example 2.

6.6 Summary

Two structures have been presented for the design of the FRM based non-uniform linear-phase digital filter banks. The proposed filter banks yield considerable savings in terms of arithmetic operations. The design procedure is simple and standard filter design algorithms can be used to design the proposed filter banks.

Chapter 7

Conclusions

There are three main techniques to design computationally efficient FIR filters: the "prefilter plus equalizer" approach, the IFIR approach and the FRM technique. A common feature among these techniques is to design a filter using several subfilters with low complexities. The IFIR and FRM techniques are closely related. The IFIR filters can be treated as a special case of the FRM filters. Both methods share a common concept in which a low order FIR filter is interpolated to yield the narrow transition-width. The resulting interpolated filter has very sparse coefficients which lowers the complexity of the overall filter significantly. In the thesis, significant improvements and developments have been made to the FRM and IFIR techniques as well as the prefilter-equalizer method.

In the FRM technique, there is a correlation between the transition-widths of the two masking filters and the bandedge shaping filter. A new structure was proposed in Chapter 2 to decouple the masking filters from the bandedge shaping filter. The proposed structure generalizes the IFIR-FRM approach. As a result, more flexibility is

obtained in selection of the interpolation factors for the bandedge shaping filter and the masking filters. A decoupling stage is inserted between the bandedge shaping filter and the masking filters which lowers the complexity of the long masking filter in the IFIR-FRM approach. The two masking filters in the new structure have much wider transition-widths than those of the masking filters in the FRM technique and consequently have little correlation with the bandedge shaping filter. Examples showed that the proposed structure achieves up to 40% computational savings compared with the FRM technique.

In Chapter 3, a new method to design sharp FIR filters was presented. Two modified FRM structures were developed in which a prefilter-equalizer is combined with a bandedge shaping filter to perform the tasks of the bandedge shaping filter and one masking filter in the original FRM approach. The other masking filter can be designed using the FRM approach if required. New multiplication-free prefilters were developed for the design of the prefilter-equalizer. Results indicated that the proposed method reduces the number of multipliers and adders in implementation of sharp FIR filters considerably. Moreover, the group delay of the overall filter is relatively short compared to other computationally efficient FRM filters.

To further reduce the arithmetic operations of sharp FIR filters, a new structure combining the single filter frequency masking filter and the FRM technique was proposed in Chapter 4. This approach utilizes one model filter and a masking filter to design arbitrary bandwidth FIR filters. By the cascade of several identical model filters with different periods, new bandedge shaping filter is formed. With the help of the masking filter, the specification of the overall filter can be satisfied. The example

showed that more than 42% savings in the number of multipliers can be achieved compared with the FRM technique. Simple modifications to the proposed structure allow it to design FIR filters with different specifications, which is desirable in many practical applications.

Besides the developments to the FRM filters, new masking filters for the design of narrowband and wideband lowpass/highpass IFIR filters as well as narrowband bandpass IFIR filters were proposed in Chapter 5. The masking filters are multiplication free and provide good stopband attenuation. The proposed filter structures can also serve as prefilters if they are used in the prefilter-equalizer method. It was illustrated by examples that the proposed method can reduce the number of multipliers and adders of IFIR filters significantly. Meanwhile, the required delay elements are decreased compared with other computationally efficient narrowband FIR filters.

Using the FRM technique, new linear-phase digital filter banks for audio applications were proposed in Chapter 6. The filter banks have non-uniform subbands with narrow transition-band. Equalization for each band can be easily realized. Perfect reconstruction of signals can be achieved using the proposed filter banks. Furthermore, the implementation of the digital filter banks requires low hardware cost.

Among the proposed computationally efficient methods for the design of sharp FIR filters in the thesis, linear programming was the main optimization algorithm adopted in designing the examples which is a sub-optimized method. It is interesting to note that the algorithms introduced in [33-36] can be utilized to optimize subfilters in the

proposed structures to achieve more computational savings. Therefore, future research works may investigate some other non-linear optimization algorithms to design the proposed filters to achieve better results. Besides the optimization algorithm, the real VLSI implementation for the proposed filters is an interesting field to explore which may include finite wordlength effect, maximizing speed and low power consumption. Another interesting work is to realize the proposed digital filter banks in real high fidelity audio playback system to achieve high quality sound effects.

Appendix A

Coefficient values for $H_M(z)$ in example 1 (Narrowband lowpass filter)

$H_M(z)$
H(0) = -0.1674314239 = H(8)
H(1) = 0.6086136831 = H(7)
H(2) = -0.7901437373 = H(6)
H(3) = -0.3676139013 = H(5)
H(4) = 2.4239401918

Coefficient values for $H_M(z)$ in example 2 (Narrowband lowpass filter)

$H_M(z)$
H(0) = -0.0464258108 = H(14)
H(1) = 0.0685611252 = H(13)
H(2) = 0.0446615854 = H(12)
H(3) = 0.0085200157 = H(11)
H(4) = -0.2530002261 = H(10)
H(5) = -0.0237502730 = H(9)
H(6) = 0.3498438613 = H(8)
H(7) = 0.7123327259

Appendix B

Coefficient values for $H_M(z)$ in example 2 (Narrowband bandpass filter)

$H_M(z)$
H(0) = -0.4416197687 = H(4)
H(1) = -1.0000000000 = H(3)
H(2) = -0.1028481760

Coefficient values for $H_M(z)$ in example 3 (Narrowband bandpass filter)

$H_M(z)$
H(0) = 0.3448723992 = H(4)
H(1) = -1.4212786873 = H(3)
H(2) = 5.0592890742

Bibliography

[1] J. F. Kaiser, "Nonrecursive digital filter design using i_0-sinh window function," in *Proc. 1974 IEEE Int. Symp. Circuits Syst*., pp. 20–23, April 1974.

[2] J. W. Adams and A. N. Willson, "A new approach to FIR digital filters with fewer multipliers and reduced sensitivity," *IEEE Trans. Circuits Syst.,* vol. CAS-30, pp. 277–283, May 1983.

[3] J. W. Adams and A. N. Willson, "Some efficient digital prefilter structures," *IEEE Trans. Circuits Syst.,* vol. CAS-31, pp. 260–265, March. 1984.

[4] J. W. Adams and A. N. Willson, "A novel approach to the design of efficient FIR digital bandpass filters," in *Proc. IEEE Int. Symp. Circuits Syst*., vol.1. pp. 28–32, Montreal, Canada, May 1984.

[5] P. P. Vaidyanathan and G. Beitman, "On prefilters for digital FIR filter design," *IEEE Trans. Circuits Syst.,* vol. CAS-32, pp. 494–499, May 1985.

[6] H. Kikuchi, Y. Abe, H. Watanabe and T. Yanagisawa, "Efficient prefiltering for FIR digital filters," *Trans. IEICE* (*Japan*), vol. E70, pp. 918–927, Oct. 1987.

[7] Y. L. Tai and T. P. Lin, "Design of FIR digital filters with novel prefilter structures," *Int. J. Electron.*, vol. 70, No. 3, pp. 573–590, 1991.

[8] J. C. Liu and T. P. Lin, "Recursive Hartley filter – a new efficient digital-prefilter structure," *IEE Proceedings-G*, vol. 139, No. 4, pp. 438–444, Aug. 1992.

[9] Y. Lian and Y. C. Lim, "New prefilter structure for designing of FIR filters," *IEE Electron. Letters*, vol. 29, pp. 1034–1036, May 1993.

[10] Y. Neuvo, C. Y. Dong and S. K. Mitra, "Interpolated finite impulse response filters," *IEEE Trans. Acoust. Speech, Signal Processing*, vol. ASSP-32, pp. 563–570, June 1984.

[11] T. Saramäki, Y. Neuvo and S. K. Mitra, "Efficient interpolated FIR filters," in *Proc. IEEE Int. Symp. Circuits Syst*., pp. 1145–1148, Kyoto, Japan, July 1985.

[12] T. Saramäki, Y. Neuvo and S. K. Mitra, "Design of computationally efficient interpolated FIR filters," *IEEE Trans. Circuits Syst.,* vol. CAS-35, pp. 70–88, Jan. 1988.

[13] Y. Neuvo, G. Rajan and S. K. Mitra, "Design of Narrow-band FIR bandpass digital filters with reduced arithmetic complexity," *IEEE Trans. Circuits Syst.,* vol. CAS-34, pp. 409–419, April 1987.

[14] H. Kikuchi, Y. Abe, H. Watanabe and T. Yanagisawa, "Interpolated FIR filters based on the cyclotomic polynomials," *Trans. IEICE* (*Japan*), vol. E70, pp. 928–937, Oct. 1987.

[15] J. C. E. Cabezas and P. S. R. Diniz, "FIR filters using interpolated prefilters and equalizers," *IEEE Trans. Circuits Syst.,* vol. CAS-37, pp. 17–23, Jan. 1990.

[16] Z. Jing and A. T. Fam, "A new structure for narrow transition band, lowpass digital filter design," *IEEE Trans. Acoust.*, *Speech*, *Signal Processing*, vol, ASSP-32, pp. 362–370, April 1984.

[17] O. Gustafsson, H. Johansson, and L. Wanhammar, "Design and efficient implementation of narrow-band single filter frequency masking FIR filters," in *Proc. X European Signal Processing Conf.*, vol. 1,Tampere, Finland, Sept. 4-8, 2000.

[18] O. Gustafsson, H. Johansson, and L. Wanhammar, "Design and efficient implementation of single filter frequency masking FIR filters," in *Proc. IEEE Int. Symp. Intelligent Signal Processing Communication Systems*, vol. 1, pp. 135–140, Hawaii, USA, Nov. 5-8, 2000.

[19] O. Gustafsson, H. Johansson, and L. Wanhammar, "Narrow-band and wide-band single filter frequency masking FIR filters," in *Proc. IEEE Int. Symp. Circuits Syst.*, *ISCAS 2001*, vol. 2, pp. 181–184, Sydney, Australia, May 6-9, 2001.

[20] Y. Lian and Y. C. Lim, "Reducing the complexity of FIR filters by using parallel structures," in *Proc. IEEE Int. Symp. Circuits Syst*., *ISCAS 1993*, vol. 1, pp. 100–103, Chicago, Illinois, USA, May 3-6, 1993.

[21] Y. C. Lim, "Frequency-response masking approach for the synthesis of sharp linear phase digital filters," *IEEE Trans. Circuits Syst.,* vol. CAS-33, pp. 357–364, April 1986.

[22] R. Yang, B. Liu and Y. C. Lim, "A new structure of sharp transition FIR filters using frequency-response masking," *IEEE Circuits Syst.,* vol. CAS-35, pp. 955–966, Aug. 1988.

[23] Y. C. Lim and Y. Lian, "The optimal design of one- and two- dimensional FIR filters using the frequency response masking technique," *IEEE Trans. Circuits Syst.*, *Part 2.,* vol. 40, pp. 88–95, Feb. 1993.

[24] Y. C. Lim and Y. Lian, "Frequency response masking approach for digital filter design: complexity reduction via masking filter factorization," *IEEE Trans. Circuits Syst.,* part2, vol. 41, pp. 518–525, Aug. 1994.

[25] Y. Lian and Y. C. Lim, "Reducing the complexity of frequency-response masking filters using half band filters," *Signal Processing*, Vol. 42, No. 3, pp. 227–230, March 1995.

[26] T. Saramäki and Y. C. Lim, "Use of the Remez algorithm for designing FIR filters utilizing the frequency-response masking approach," in *Proc. IEEE Int. Symp. Circuits Syst*., *ISCAS 1999*, vol. 3, pp. 449–455, Orlando, USA, May 1999.

[27] L. Zhang, Y. Lian and C. C. Ko, "A new approach for design sharp FIR filters using frequency-response masking technique," in *Proc. 9th IEEE DSP Workshop,* Texas, USA, Oct. 2000.

[28] Y. Lian, L. Zhang, and C.C. Ko, "An improved frequency response masking approach designing sharp FIR filters," *Signal Processing*, 81, pp. 2573–2581, Dec., 2001.

[29] T. Saramäki and Johansson, "Optimization of FIR filters using the frequency-response masking approach," in *Proc. IEEE Int. Symp. Circuits Syst*., *ISCAS 2001*, vol. II, pp. 177–180, Sydney, Australia, May 6-9, 2001.

[30] Y. Lian, "A new frequency response masking structure with reduced complexity for FIR filter design," in *Proc. IEEE Int. Symp. Circuits Syst*., *ISCAS 2001*, vol. II, pp. 609–612, Sydney, Australia, May 6-9, 2001.

[31] Y. Lian, "Reducing the complexity of the masking filter in a frequency-response masking approach," in *Proc. 3rd Int. Conf. Info., Communication, Signal Processing*, pp. 2E34, Singapore, Oct. 2001.

[32] L. C. R. Barcellos, S. L. Netto and P. S. R. Diniz, "Design of FIR filters combining the frequency-response masking and the WLS-Chebyshev approaches," in *Proc. IEEE Int. Symp. Circuits Syst.*, *ISCAS 2001*, vol. II, pp. 613–616, Sydney, Australia, May 6-9, 2001.

[33] T. Saramäki and J. Yli-Kaakinen, "Optimization of frequency-response-masking based FIR filters with reduced complexity," in *Proc. IEEE Int. Symp. Circuits Syst*., *ISCAS 2002*, vol. 3, pp. 225-228, Phoenix, USA, May 26–29, 2002.

[34] W-S. Lu and T. Hinamoto, "Optimal design of frequency-response-masking filters using semidefinite programming," *IEEE Trans. Circuits Syst*., *I*: *Fundamental Theory and Applications*, vol. 50, pp. 557–568, April 2003.

[35] W-S. Lu and T. Hinamoto, "Optimal design of FIR frequency-response-masking filters uses second-order cone programming," in *Proc. IEEE Int. Symp. Circuits Syst*., *ISCAS 2003*, vol. 3, pp. 878–881, Bangkok, Thailand, May 25-28, 2003.

[36] Y. J. Yu, T. Saramäki and Y. C. Lim, "An iterative method for optimizing FIR filters synthesized using the two-stage frequency-response masking technique," in *Proc. IEEE Int. Symp. Circuits Syst*., *ISCAS 2003*, vol. 3, pp. 874–877, Bangkok, Thailand, May 25-28, 2003.

[37] W. R. Lee, V. Rehbock, K. L. Teo and Caccetta, "A weighted least-square-based approach to FIR filter design using the frequency-response masking technique," *IEEE Signal Processing Letters*, vol. 11, pp. 593-596, July 2004.

[38] T. Saramäki, Y. C. Lim and R. Yang, "The synthesis of half-band filter using frequency-response masking technique," *IEEE Trans. Circuits Syst*., *II*: *Analog and digital signal processing,* vol. 42, pp. 58–60, Jan. 1995.

[39] Y. Lian, "The optimum design of half-band filter using multi-stage frequency-response masking technique," *Signal Processing*, Vol.44, No.7, pp. 369–372, July 1995.

[40] G. Rajan, Y. Neuvo, and S. K. Mitra, "On the design of sharp cutoff wide-band FIR filters with reduced arithmetic complexity," *IEEE Trans. Circuits Syst.*, Vol. 35, No.11, pp. 1447–1454, Nov. 1988.

[41] R. Yang, Y. C. Lim and M. Bellanger, "Design of sharp FIR bandstop filters using quadrature masking filters," *Proc. IEEE Int. Conf. Acoustics, Speech, Signal*, *ICASSP 1997*, vol.3, pp. 2193–2196, 1997.

[42] R. Yang, Y. C. Lim and S. R. Parker, "Design of sharp linear-phase FIR bandstop filters using frequency-response masking filters," *Circuit, Syst*, *Signal Processing, Parker Memorial Issue,* 1998.

[43] H. Johansson and L. Wanhammar, "Filter structures composed of all-pass and FIR filters for interpolation and decimation by a factor of two," *IEEE Trans. Circuits Syst.* II: *Analog and digital signal processing,* vol. 46, pp. 896–905, July. 1999.

[44] H. Johansson, "New classes of frequency-response masking FIR filters," in *Proc. IEEE Int. Symp. Circuits Syst.*, *ISCAS 2000*, vol. 3, pp. 81–84, Geneva, Switzerland, May 28-31, 2000.

[45] H. Johansson, "Efficient FIR filter structures based on the frequency-response masking approach for interpolation and decimation by a factor of two," in *Proc. Second Int. Workshop Spectral Methods Multirate Signal Processing*, Toulouse, France, Sept. 7-8, 2002.

[46] Y. C. Lim and R. Yang, "The synthesis of linear-phase multirate frequency-response masking filters," *Proc. IEEE Int. Symp. Circuits Syst.,* vol.4, pp.2341–2344, Hong Kong, China, June 9-12, 1997.

[47] Y. C. Lim and B. Farhang-Boroujeny, "Fast Filter Bank (FFB)," *IEEE Trans. Circuits and Systems II*, vol. 39, pp.316–318, May 1992.

[48] H. Johansson and T. Saramäki, "Two-channel FIR filter banks based on the frequency-response masking approach," in *Proc. Second Int. Workshop Transforms Filter Banks*, Brandenburg an der Havel, Germany, Mar. 5-7, 1999.

[49] P. S. R. Diniz, L. C. R. Barcellos and S. L. Netto, "Design of cosine-modulated filter bank prototype filters using the frequency-response masking approach," in *Proc. IEEE Int. Conf. Acoustics, Speech, Signal*, *ICASSP 2001*, vol.6, pp. 3621–3624, Salt Lake City, USA, May 2001.

[50] S. L. Netto, P. S. R. Diniz and L. C. R. Barcellos, "Efficient implementation for cosine-modulated filter banks using the frequency response masking approach," in *Proc. IEEE Int. Symp. Circuits Syst*., *ISCAS 2002*, vol. 3, pp. 229–232, Phoenix, USA, May 26-29, 2002.

[51] J. W. Lee and Y. C. Lim, "Efficient implementation of real filter banks using frequency response masking techniques," in *Proc. IEEE Asia-Pacific Conf. Circuits Syst.*, *APCCAS'02*, vol. I, pp. 69–72, Oct. 28-31, 2002.

[52] L. Rosenbaum, P. Lowenborg, and M. Johansson, "Cosine and sine modulated FIR filter banks utilizing the frequency-response masking approach," in *Proc. IEEE Int. Symp. Circuits Syst*., *ISCAS 2003*, vol. 3, pp. 882–885, Bangkok, Thailand, May 25-28, 2003.

[53] C-S. Lin and C. Kyriakakis, "Frequency response masking approach for designing filter banks with rational sampling factors," *IEEE Workshop*

Applications of Signal Processing to Audio and Acoustics, pp. 99–102, New York, USA, Oct. 19-22, 2003.

[54] M. B. Jr. Furtado, P. S. R. Diniz and S. L. Netto, "Optimization techniques for cosine-modulated filter banks based on the frequency-response masking approach," in *Proc. IEEE Int. Symp. Circuits Syst*., *ISCAS 2003*, vol. 3, pp. 890–893, Bangkok, Thailand, May 25-28, 2003.

[55] S. H. Low and Y. C. Lim, "Synthesis of sharp 2-D filters using the frequency response masking technique," in *Proc*. *IEEE Int. Symp. Circuits Syst.*, *ISCAS 1997*, vol. 4, pp. 2445–2448, Hong Kong, China, June 9-12, 1997.

[56] Y. C. Lim and S. H. Low, "Frequency-response masking approach for the synthesis of sharp two-dimensional diamond-shaped filters," *IEEE Trans. Circuits Syst.*, II: *Analog and digital signal processing,* vol. 45, pp. 1573–1584, Dec. 1998.

[57] S. H. Low and Y. C. Lim, "Synthesis of 2-D half-band filters using the frequency response masking technique," in *Proc*. *IEEE Int. Symp. Circuits Syst.*, *ISCAS 1998*, vol. 5, pp. 57–60, , Monterey, USA, May 31 - June 3, 1998.

[58] S. H. Low and Y. C. Lim, "Multi-stage approach for the design of 2-D half-band filters using the frequency response masking technique," in *Proc*. *IEEE Int. Symp. Circuits Syst.*, *ISCAS 2001*, vol. II, pp. 557–560, Sydney, Australia, May 6-9, 2001.

[59] H. Johansson and L. Wanhammar, "High-speed recursive filtering using the frequency response masking approach," in *Proc. IEEE Int. Symp. Circuits Syst.*, *ISCAS 1997*, vol. IV, pp. 2208–2211, Hong Kong, China, June 9-12, 1997.

[60] H. Johansson and L. Wanhammar, "A filter structure based on the frequency-response masking approach for high-speed recursive filtering," in

Proc. IEEE Nordic Signal Processing Symp., pp. 165–168, Denmark, June 8-11, 1998.

[61] H. Johansson, "A class of high-speed approximately linear-phase recursive digital filters based on the frequency-response masking approach," in *Proc. Midwest Symp. Circuits Syst.*, vol. 1, pp. 397–400, Las Cruces, New Mexico, USA, Aug. 1999.

[62] H. Johansson and L. Wanhammar, "High-speed recursive digital filters based on frequency masking techniques," in *Proc. National Conf. Radio Science (RVK)* , vol. 1, pp. 357–361, Karlskrona, Sweden, June 14-17, 1999.

[63] H. Johansson, "A class of high-speed wide-band frequency masking recursive digital filters with approximately linear phase," in *Proc. IEEE Nordic Signal Processing Symp.* , pp. 319–322, Kolmarden, Norr-koping, Sweden, June 13-15, 2000.

[64] H. Johansson and L. Wanhammar, "High-speed recursive digital filters based on the frequency-response masking approach," *IEEE Trans. Circuits Syst.* II: *Analog and digital signal processing,* vol. 47, pp. 48–61, Jan. 2000.

[65] O. Gustafsson, H. Johansson, and L. Wanhammar, "Design and efficient implementation of high-speed narrow-band recursive digital filters using single filter frequency masking techniques," in *Proc. IEEE Int. Symp. Circuits Syst*., vol. 3, pp. 359-362, Geneva, Switzerland, May 28-31, 2000.

[66] O. Gustafsson, H. Johansson, and L. Wanhammar, "Narrow-band and wide-band high-speed recursive digital filters using single filter frequency masking techniques," in *Proc. IEEE Int. Symp. Signal Processing, Applications*, vol. 1, pp. 36–39, Kuala-Lumpur, Malaysia, Aug. 13-16, 2001.

[67] M. D. Lutovac and L. D. Milic, "IIR filters based on frequency-response masking approach**,"** *5th Int. Conf. Telecommunications in Modern Satellite, Cable and Broadcasting Service* (TELSIKS 2001), vol: 1, Page(s): 163–170, Nis, Yugoslavia, Sept. 19-21, 2001.

[68] W-S. Lu and T. Hinamoto, "Optimal design of IIR frequency-response-masking filters using second-order cone programming," *IEEE Trans. Circuits Syst. II*: *Fundamental Theory and Applications*, vol. 50, pp. 1401–1412, Nov. 2003.

[69] L. Svensson and H. Johansson, "Frequency-response masking FIR filters with short delay," in *Proc. IEEE Int. Symp. Circuits Syst.*, *ISCAS 2002*, vol. 3, pp. 233–236, Phoenix, USA, May 26-29, 2002.

[70] L. Svensson and H. Johansson, "Narrow-band and wide-band frequency masking FIR filters with short delay," in *Proc. National Conf. Radio Science (RVK)*, Stockholm, Sweden, June 10-13, 2002.

[71] M. G. Bellanger, "Improved design of long FIR filters using the frequency masking technique," in *Proc. IEEE Int. Conf. Acoust. Speech, Signal Processing,* pp. 1272– 1275, Atlanta, USA, May 7-10, 1996.

[72] Y. Lian, "Design of discrete valued coefficient FIR filters using frequency-response masking technique," in *Proc. 6th IEEE Conf. Electronics, Circuits & Systems*, Paphos, Cyprus, Sept., 1999.

[73] Y. Lian, "FPGA implementation of high speed multiplierless frequency response masking FIR filters," in *Proc. IEEE workshop Signal Processing Syst.*: *Design & Implementation*, Lafayette, USA, 2000.

[74] Y. C. Lim, Y. J. Yu, H. Q. Zheng and S. W. Foo, "FPGA implementation of digital filters synthesized using the frequency-response masking technique," in

Proc. IEEE Int. Symp. Circuits Syst., *ISCAS 2001*, Vol. 2, pp. 173–176, Sydney, Australia, May 6-9, 2001.

[75] Y. C. Lim and S. R. Parker, "Discrete coefficient FIR digital filter design based upon on LMS criteria," *IEEE Trans. Circuits Syst.,* vol. CAS-30, pp. 723–739, Oct. 1983.

[76] Y. C. Lim and S. R. Parker, "FIR filter design over a discrete powers-of-two coefficient space," *IEEE Trans. Acoust. Speech, Signal Processing*, vol. ASSP-31, pp. 583–591, June 1983.

[77] Y. C. Lim and S. R. Parker, and A. G. Constantinides, "Finite word-length FIR filter design using integer programming over a discrete coefficient space," *IEEE Trans. Acoust. Speech, Signal Processing*, vol. ASSP-30, pp. 661–664, Aug. 1982.

[78] L. R. Rabiner, " Linear program design of finite impulse response (FIR) digital filters,"*IEEE Trans. Audio Electroacoust*., vol AU-20, pp. 280–288, Oct. 1972.

[79] J. H. McCellan, T. W. Parks, and L. R. Rabiner, "A computer program for designing optimum FIR linear phase digital filters," *IEEE Trans. Audio Electroacoust*., vol AU-21, pp. 506–526, Dec. 1973.

[80] J. F. Kaiser and R. W. Hamming, "Sharpening the response of a symmetric non-recursive filter by multiple use of the same filter," *IEEE Trans Acoust. Speech, Signal Processing*, vol. ASSP-25, pp. 415–422, Otc. 1977.

[81] K. K. Parhi, C.-Y. Wang, and A. P. Brown, "Synthesis of control circuits in folded pipelined DSP architectures," *IEEE J. Solid-State Circuits*, vol. 27, pp. 29–43, Jan. 1992.

[82] P.J. Berkhout and L. D. J. Eggermont, "Digital audio systems," *IEEE Acoust. Speech, Signal Processing Mag.*, pp. 45–67, Oct.1985.

[83] Y. C. Lim, "Linear-Phase digital audio tone control," *J. Audio Eng. Soc.* (Engineering Reports), vol. 35, pp. 38–40, Jan./Feb. 1987.

[84] R. H. Yang, "Linear-phase digital audio tone control using dual RRS structure," *Electron. Lett.,* vol. 25, pp. 360–362, March 1989.

[85] Y. Lian and Y. C. Lim, "Linear-phase digital audio tone control using multiplication-free FIR filter," *J. Audio Eng. Soc.* (Engineering Reports), vol. 41, pp. 791–794, October. 1993.

[86] Y. C. Lim, "A digital filter bank for digital audio systems," *IEEE Trans. Circuits Syst.*, vol. CAS-33, No. 8, pp. 848–849, April 1986.

[87] K. C. Haddad, H. Stark and N. P. Galatsanos, "Design of digital linear-phase FIR crossover systems for loudspeakers by the method of vector space projections," *IEEE Trans. Signal processing*, vol. 47, No. 11, pp. 3058–3066, November 1999.

[88] J. G. Proakis and D. G. Manolakis, Digital Signal Processing: Principles, Algorithms, and Applications, pp. 620-623, Third Edition, New Jersey: Pretice-Hall Int., 1996